Dissertation
submitted to the
Combined Faculties for the Natural Sciences
and for Mathematics
of the Ruperto-Carola University of Heidelberg, Germany
for the degree of
Doctor of Natural Sciences.

presented by
Chiara Redaelli, Master of Science
born in Lecco, Italy

Date of oral examination:

Functional roles of
the Aryl Hydrocarbon Receptor
in Experimental Autoimmune Encephalomyelitis

Referees: Prof. Dr. Stefan Wiemann

Prof. Dr. Michael Platten

Table of contents

Table of Figures

Summary

Multiple sclerosis (MS) is an autoimmune and neurodegenerative disease, which affects around three million people worldwide and is the main cause of disability in young adults in the US and western Europe. It is characterised by lymphocytic infiltration into the central nervous system (CNS) and destruction of oligodendrocytes, followed by neuronal cell death. The definite cause of the disease is unknown, but most likely consists of an interplay of genetic and environmental factors. Epidemiological studies have demonstrated that the incidence and severity of MS is inversely correlated with exposure to UV light. Recent evidence has raised doubt for the UV-mediated production of vitamin D as the sole responsible factor for the protective effect of UV light. The aryl hydrocarbon receptor (AhR) is a key regulator of immune responses in neuro-inflammation and can be activated by UV photoproducts of tryptophan. We therefore investigated the role of UVB-mediated AhR activation in experimental autoimmune encephalomyelitis, the mouse model of MS. Animals lacking the AhR did not get any benefit from UVB irradiation, while the irradiation of specific AhR-reporter mice showed an increased bioluminescence signal in the skin, which reflected an AhR activation upon UV treatment. Furthermore, we identified inosine as a potent activator of the AhR accumulating in skin of irradiated mice. Antigen presenting cells homed from the skin to the draining lymph nodes due to UVB irradiation and AhR activation, where they were able to induce regulatory T-cells, the so-called UV-T_{regs}. In addition to its effects on the immune system, the AhR is widely studied as an important mediator of toxicity for xenobiotics. While we could not prove that the immunosuppressive effect of Teriflunomide, a newly approved drug for MS treatment, could be in part mediated by AhR activation, we identified the AhR as the main mediator of its gastrointestinal toxicity. AhR deficient animals treated with Teriflunomide died due to gastroenteritis, intestinal bleeding and liver toxicity. Our data showed that, in the mouse model of MS, the AhR is a key molecule in mediating the immunosuppressive effect of UVB light and the metabolisation of the MS drug Teriflunomide. Pharmacological targeting of the AhR could enhance the beneficial effects of UVB light. Genetic polymorphisms of the AhR in MS patients could explain the increased side effects of Teriflunomide.

Zusammenfassung

Multiple Sklerose (MS) ist eine Autoimmun- und neurodegenerative Erkrankung, von der circa drei Millionen Menschen weltweit betroffen sind und die Hauptursache von Behinderungen bei jungen Erwachsenen in den USA und Europa ist. MS ist charakterisiert durch lymphatische Infiltrationen ins zentrale Nervensystem (ZNS) und die Zerstörung von Oligodendrozyten, gefolgt von neuronalem Zelltod. Die Ursache dieser Krankheit ist unbekannt, beinhaltet aber höchstwahrscheinlich das Zusammenspiel genetischer und umweltbedingter Faktoren. Epidemiologische Studien haben gezeigt, dass die Inzidenz und Schwere der MS invers mit der Exposition gegenüber UV-Licht ist. Neueste Evidenzen haben Zweifel an der UV-vermittelten Vitamin D Produktion als alleiniger verantwortlicher Faktor für den protektiven Effekt von UV-Licht geweckt. Der Arylhydrokarbon-Rezeptor (AhR) ist ein Schlüsselregulator der Immunantworten während Neuroinflammation und kann durch Tryptophanderivate, die durch UV-Licht entstehen, aktiviert werden. Daher haben wir die Rolle der UVB-vermittelten AhR-Aktivierung in der Experimentellen Autoimmun-Encephalomyelitis, dem Mausmodell der MS, untersucht. AhR defiziente Tiere profitierten nicht von UVB-Bestrahlung, während die Bestrahlung von spezifischen AhR-Reporter-Mäusen zu erhöhter Biolumineszenz in der Haut, was die AhR-Aktivierung durch UV-Behandlung widerspiegelt. Weiterhin haben wir Inosin als einen potenten AhR-Aktivator identifiziert, der in der Haut bestrahlter Mäuse akkumulierte. Antigen-präsentierende Zellen migrierten aufgrund von UVB-Bestrahlung und AhR Aktivierung aus der Haut zu drainierenden Lymphknoten , wo sie regulatorische T-Zellen induzierten, sogenannte UV-T_{regs}. Zusätzlich zu diesen Effekten auf das Immunsystem wird der AhR weitgehend als ein wichtiger Mediator der Toxizität von Xenobiotika untersucht. Wir konnten zeigen, dass die immunsuppresiven Effekte von Teriflunomid, einer neuen zugelassenen Medikation für MS, nicht durch die AhR-Aktivierung vermittelt werden; allerdings identifizierten wir den AhR als den Hauptmediator der gastrointestinalen Toxizität von Teriflunomid. AhR defiziente Tiere, die mit Teriflunomid behandelt wurden, entwickelten tötliche Gastroenteritis, intestinale Blutungen und Lebertoxizität.

Unsere Daten zeigen, dass der AhR im Mausmodell der MS ein Schlüsselmolekül ist, das die immunsuppressiven Effekte von UVB-Licht sowie den Metabolismus des zugelassenen MS-Medikaments Teriflunomid vermittelt. Pharmakologisches Abzielen auf den AhR könnte die günstigen Effekte von UVB-Licht verstärken. Genetische Polymorphismen des AhR in MS-Patienten könnten die erhöhten Nebenwirkungen von Teriflunomid erklären.

Acknowledgments

The following thesis has been conducted at the German Cancer Research Centre (DKFZ) in Heidelberg, in the laboratory of Neuroimmunology and Brain Tumor Immunology.

First of all, I want to thank Prof. Michael Platten for the chance he offered me to work in Heidelberg, no matter via DKFZ or HBIGS, and his support and supervision in these years.

Many thanks also to Prof. Stefan Wiemann, my first supervisor who supported me a lot during this thesis preparation and during my TAC meetings. I am also grateful to Prof. Petra Kioschis for her enthusiasm and feedbacks during TAC meetings. I want to acknowledge my thesis referees, Prof. Rüdiger Hell and Prof. Aurelio Teleman, that kindly agreed to join the thesis defence committee.

I am totally thankful to all the scientists from DKFZ and the University Campus, which spend time to help me and solve issues together, especially Gernot Poschet, Maik Brune, Ece Gaffarogullari, Damir Krunic and Prof. Gröne with his group members.

I also want to thank all the G160/ G370/ G161 lab members for the atmosphere in and outside work. Many thanks to Caroline Pilz, challenged medical student who joined me in the UVB project and Tobias Lanz for the manuscript work. I am also grateful to colleagues that are not in the lab any more, like Aysegul Ilahn-Mutlu for the helpful brain storming talks and the nice lunch times with Yungxian Liao. Special thanks go to the “Augustins” for their smiles, suggestions, great help and for the “A190-membership” *ad honorem*.

This PhD would have not been the same without all the wonderful friends I met here via DKFZ as well as HBIGS. Thanks for the amazing time together, the support and the chance to always share amazing food, especially with my cooking sister Karin Mössenböck.

Last but not least, I wish to express my deepest gratitude to my lovely family, who keep believing in me and to my boyfriend Mattia, who even managed to follow me in Heidelberg and join me in this adventure.

1. Introduction

1.1 Multiple sclerosis

Multiple sclerosis (MS) is a chronic neuro-degenerative disease, described for the first time in 1868 by the French neurologist Dr. Jean-Martin Charcot . It occurs due to an abnormal response of the immune system against the central nervous system (CNS), where T cells and macrophages are attaching and destroying the myelin shields surrounding the nerves. Myelin is a lipids-rich substance that normally insulates the axons and helps speed nerve transmission but, once damaged, it forms a harder scar tissue (1), that distorts or interrupts nerve impulses from the brain and the spinal cord. This results in a wide variety of neurological symptoms, but it can also lead to cognitive and physical disability, with loss of muscle control, balance and vision (2). Fatigue occurs in 90% of patients and is the most common work-related disability associated with MS. More than 30% of MS patients have moderate-to severe spasticity, mostly in the legs. They often suffer of sensory disturbances, like paresthesias (numbness and tingling), dysesthesias (burning and “pins and needles”), diplopia, ataxia or vertigo (3). It can be a unilateral numbness affecting one leg, but it can also spread to the other leg and rises to the pelvis, abdomen, or thorax and even evolve in chronic neuropathic pain. Another common sign of MS is optic neuritis, highlighted by complete or partial loss of vision. Some organs can also be involved, causing for example bladder dysfunctions or sexual problems.

Four disease courses have been identified among MS patients and each of them can be mild, moderate or severe. Relapsing-remitting MS (RRMS) is the most common form, where 85% of patients are initially diagnosed. It is characterized by specific neurologic attacks, so called relapses, followed by partial or complete recovery periods (remissions), during which there is a partial or even complete improvement of the symptoms and no apparent progression of the disease. During these inflammatory attacks, activated immune cells cause small, localized areas of damage and this induces MS symptoms like numbness, vision problems, spasticity or stiffness, bowel and bladder problems, and problems with cognition. Even if the

damage locations can vary a lot, magnetic resonance imaging scans (MRI) proved that RRMS patients tend to have more lesions on the brain. Secondary-progressive MS (SPMS) usually follows the first course, since most of the people diagnosed as RRMS will reach this phase. Relapsing moments are becoming rarer and the disease progressively gets steadier, here the inflammatory process leaves space to the nerves damaging phase. The third course, the primary-progressive MS (PPMS), has not remitting phases anymore, but the worsening of neurologic functioning is continuous. In this course, that affects about 10% of patients, lesions are more on the spinal cord side and this usually corresponds to gradually worsening problems with walking and mobility. Progressive-relapsing MS (PRMS) is the least common of the four disease courses, characterized by progressing disease from the beginning and occasional exacerbations along the way. Sometimes a patient is initially diagnosed as PPMS and then the diagnosis can be modified when the first relapse occurs. Although this disease course is progressive from the outset, each person's symptoms and rate of progression will be different.

In order to make a proper diagnosis, focusing on the predictive value of the early clinical course of MS might not be enough. But it is also true that individuals are often diagnosed in early adulthood and therefore encounter a variety of common experiences that must be managed within the context of their chronic illness. Since there is not a specific diagnostic test for MS, the diagnosis is based on evidences and clinical findings obtained from magnetic resonance imaging (MRI) of the brain and examination of the cerebrospinal fluid (CSF). Three parameters are usually considered: the attack rate, the first inter-attack interval and the rate at which disability develops in the early years of the disease, referring to the chronic inflammation of the CNS, as determined by analysis of the CSF (3, 4) .

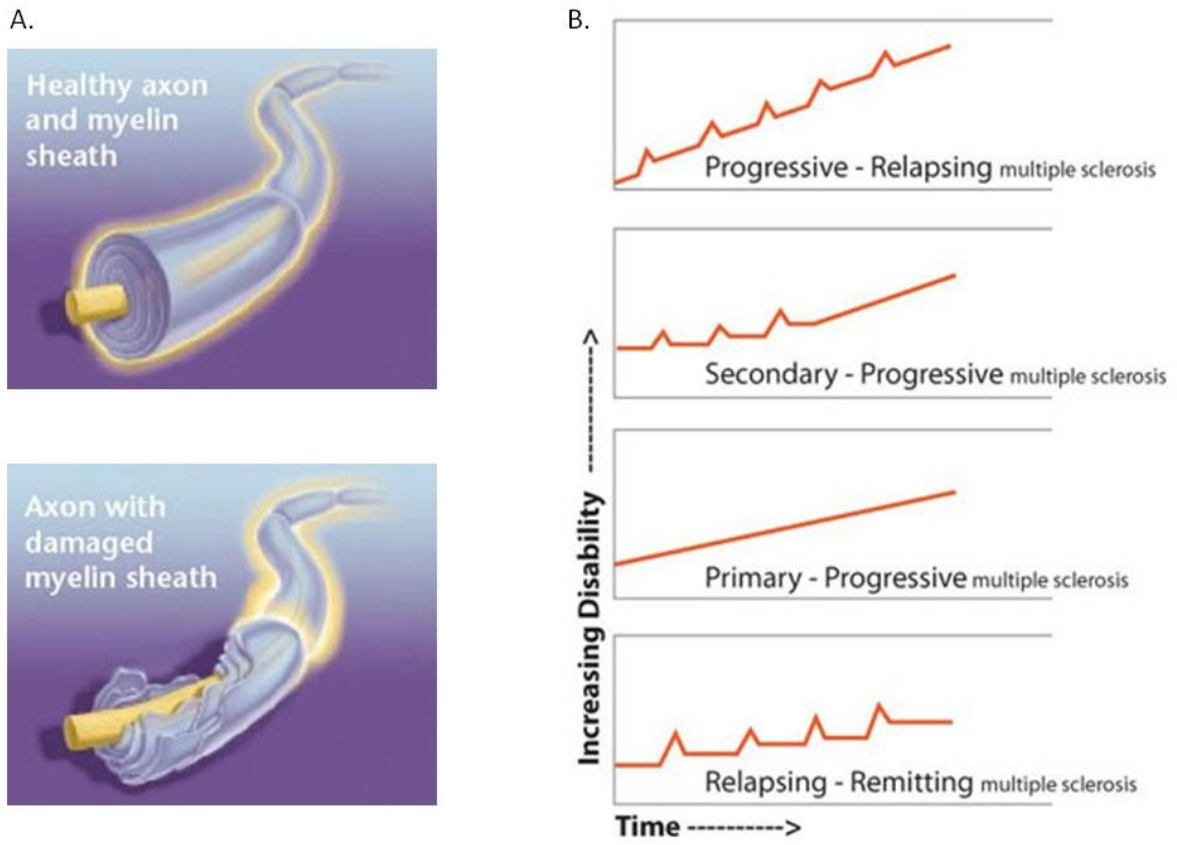

Up to now there is no known cure for MS and the only treatments available, so called disease modifying therapies (DMTs), are made for relapsing forms of MS, to prevent new attacks and disability. Acute cases can be treated with short courses of corticosteroids, which act rapidly with few adverse side effects. The same treatment can be used for acute exacerbations and to shorten the duration of MS attacks. The other FDA-approved therapeutic agents can reduce disease activity and progression in patients with relapsing forms of MS, including patients with secondary progressive MS who continue to have relapses. Most of them are immunomodulatory agents that retard the neurological damages, like interferon beta (IFN-β) or glatiramer acetate (copaxone). These two have been considered for a long time the main treatment options for RRMS, although they are only partially effective, reducing relapses by about 30% compared to placebo. Different interferon-based drugs have been developed, due to their natural functions as cytokines but, although some side effects, the main issue emerged during long

term treatment. In fact treatment with any IFNs can lead to the production of neutralizing antibodies (5). Furthermore, Shiriani and coworkers (6) did not find any significant effect on progression to long-term disability using IFN-β and this also opened the way for new compounds to prevent MS damages. In the last ten years many MS drugs became available, but what came more and more important is also the balance between benefits and possible side effects. Some examples are Mitoxantrone, a cytotoxic agent restricted to severe cases due to its cardiac toxicity and risk to develop secondary leukemia or Natlizumab, a monoclonal antibody effective in inhibiting T-cell infiltration in the brain, but also associated with potentially fatal multifocal leukoencephalopathy. The most recent compounds are focusing on the immune cell inactivation, some of them have been already used for other immune diseases and the ways of administration as well as the safety profile are important parameters to be considered.

Among them, we focused our attention on TERIFLUNOMIDE, an oral daily drug treatment marketed by Sanofi and available on 7 or 14 mg film coated tablets. Teriflunomide (trade name Aubagio), is the active metabolite of the prodrug leflunomide (Arava®), which was approved in 1998 by the US FDA for the treatment of adults with rheumatoid arthritis (7). Also known as A77 1726, it was investigated in the Phase III clinical trial TEMSO, TENERE, TOWER, TERACLES and TOPICS as a medication for multiple sclerosis (1, 3, 8-10). The registration study was completed in July 2010, with positive results. The drug was approved by the FDA on September 13, 2012 and in the EU on August 26, 2013. Immune cell activation and proliferation, which are critical for the progression of autoimmune diseases such as MS, are dependent on *de novo* pyrimidine synthesis and extensive *in vitro* studies have shown that teriflunomide is a selective and reversible inhibitor of mitochondrial dihydroorotate dehydrogenase (DHODH), the key enzyme involved in this process (11, 12). The enzyme is noncompetitively and reversibly inhibited by teriflunomide with and IC_{50} of 1.3 μM in humans and 86 nM in rats .Teriflunomide reversibly arrests cells in the G1 phase of the cell cycle, inhibiting the *de novo* pyrimidine biosynthesis within the immune system. This results in inhibition of cell proliferation and maturation, thereby preventing T cell and B cell clonal expansion and migration to the CNS as well as antibody production *in vivo* (12, 13). Mean plasma concentrations of Teriflunomide

resemble the ones detected for Leflunomide, when same dose is used. Peak plasma concentrations occur in 1 to 4 hours after oral administration and steady state occurs after approximately 3 months of treatment. Teriflunomide is highly bound to plasma proteins (> 99%), it undergoes minor metabolism, mainly mediated by hydrolysis, oxidation and conjugation reactions. The median half-life of TER is approximately 18-19 days and it is dose dependent, its elimination is mostly biliary dependent and metabolites are removed renally. The most common side effects of Aubagio® include abnormal liver test results, hair thinning or loss, diarrhea, flu, nausea, and burning or prickling feeling in the skin. Based on data in animal studies, there is also an increased risk of teratogenicity if teriflunomide is taken during pregnancy. Teriflunomide remains in the blood for a long time after stopping treatment, so this risk may continue for up to two years. Women of childbearing age must use reliable contraceptive methods and in case of pregnancy during the treatment, it is recommended the use of cholestyramine or activated charcoal to reduce the blood level of teriflunomide. Several other drugs are commercially available at the moment, but since they are just partially effective, further investigations have to be done. Furthermore, simple habits such as exercise, rest and healthful nutrition may relieve symptoms and promote a satisfactory quality of life. We also have to consider that, while the prognosis is difficult to predict and it depends on several factors, the life expectancy of MS patients is at the moment only 5 to 10 years lower than that of an unaffected population (14).

1.2 MS risk factors

MS is affecting about 2.5 million people worldwide and has been recognized across all ethnicities. It is more diffused in women than in men, with a female-male ratio of 3:1 that is significantly increasing during the last century and it usually occurs between 20 and 50 years of age with a peak around 30 years. The disease is thought to be triggered in a genetically susceptible individual by a combination of one or more environmental factors (15).

1.2.1 Genetic risks

The concept of genetic inheritance and family risk is of considerable importance to patients with MS to help them make the necessary informed medical and personal decisions. Approximately 15% of patients with MS have a positive family history of the disease, and the overall age-adjusted risk in the general population is approximately 0.3%. Recurrence among monozygotic twins is approximately 35%, which reflects the degree of genetic contribution. The estimated risk to the siblings of a proband is 3–5%, increasing to 29.5% if one or both parents have MS. Risk to the offspring of a patient with MS is 2–3% and higher if both parents have MS (20%) (16, 17). If genes were solely responsible for determining who gets MS, an identical twin of someone with MS would have a 100% chance of developing the disease; the fact that the risk is only one in three demonstrates that a complex multifactorial aetiology, including interactions of genetic and environmental factors is likely. This multifactorial aetiology is common to similar autoimmune diseases is typical, for example, rheumatoid arthritis or diabetes mellitus type I (18). Large-scale genome-wide association studies have helped to identify several genes associated with disease susceptibility, the most important of which include HLA-DRB1, IL7R (CD127), IL2R and SOCS1 (19-21). The association between MS and HLA was already described in 1970s and nowadays the associations between HLA-DR15 haplotype (the DRB1*1501 allele and the alleles with which it is in linkage disequilibrium: DQA1*0102, and DQB1*0602) and MS have been described throughout European and non-European populations with MS (22, 23). These polymorphic genes may work independently and/or interact with each other, and will exert a minor or moderate effect on the development of MS (16, 24).

1.2.2 Environmental factors – sun exposure

Epidemiological data show several interesting trends regarding MS and its distribution among different populations and ethnic groups. MS is more common among Caucasians and among people of Northern or Central European descent,

especially from Scotland or Scandinavia. By contrast, MS is less common among Hispanics, Asians, and in people of African descent. MS rarely occurs among some ethnic groups, such as Inuits, Aborigines, and Maoris. In the U.S. the prevalence of MS is higher in whites than in other racial groups. There have been also "epidemics" of MS, for example, the group of people living off the coast of Denmark after WWII, suggesting an environmental cause. Migrant studies further support the important influence of environmental factors in risk of MS. In a systematic review of such studies two consistent patterns were apparent: migrants moving from a region of high MS risk to one of lower risk had a lower-than-expected MS prevalence, particularly when migration occurred before age 15 years; migrants moving from an area of lower risk to one of higher risk tended to retain the lower MS risk of their country of origin, with no clear age-at-migration effect (25, 26). This relationship is believed to be related to sunlight or UV light exposure.

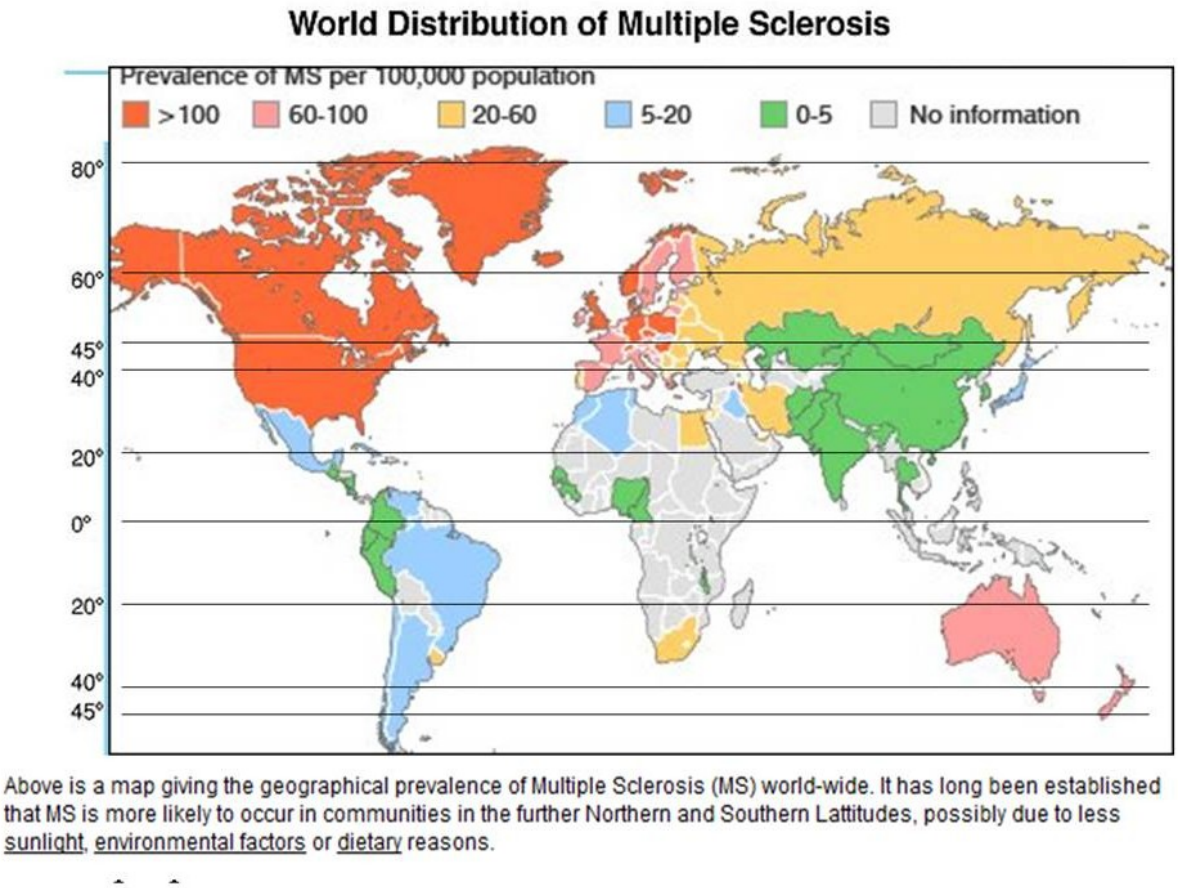

Figure 1.2. World distribution of MS patients. Adapted from a MSIF/WHO Study, published by BBC in September 2008.

In fact MS is a disease of temperate climates, its prevalence increases with distance from the equator for both hemispheres. Furthermore, this hypothesis is supported by different studies, where the average annual hours of sunlight exposure in an individual's place of birth is inversely correlated with MS development or where individuals with the highest residential and occupational solar exposure have the lowest rate of MS incidence (27, 28).

The sun emits a wide range of electromagnetic radiation, including UV (29) (100–400 nm), visible (400–800 nm) and infrared (> 800 nm) radiation. Exposure to UVR has profound effects on human health, since it can cause direct damage to DNA and this is a leading cause of skin carcinomas. UVR exposure induces immune suppression, via the inhibition of cell-mediated immunity through multiple mechanisms, thereby eliminating natural defense mechanisms against aberrant cell growth. Although its effects in skin cancer, UVR exposure has also beneficial effects on organ-specific autoimmune diseases, like in MS. Indeed, a recent study demonstrated that MS relapse rates are lower in the summer than in the winter, suggesting that decreased UV exposure may be a contributing factor in relapses (30).

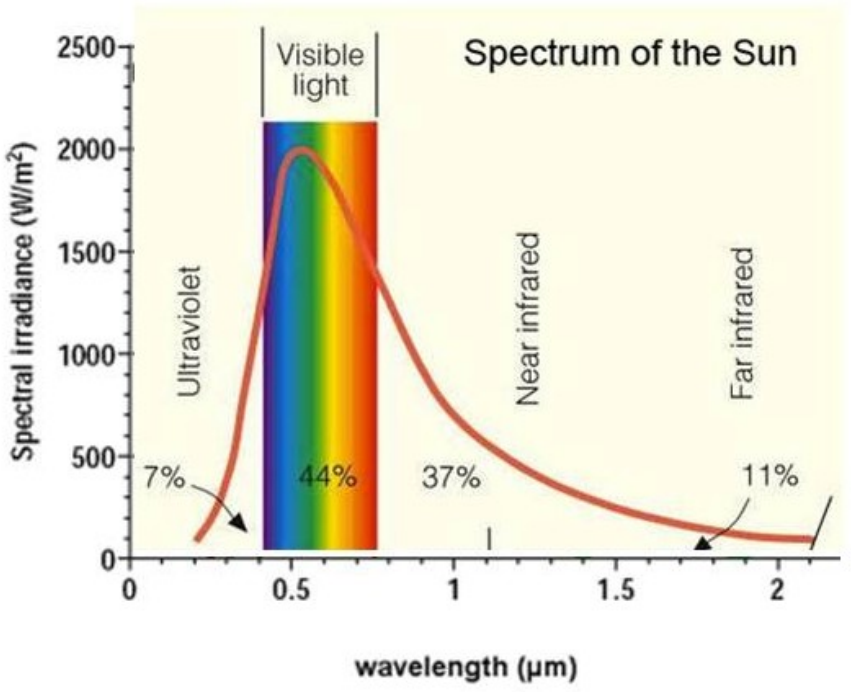

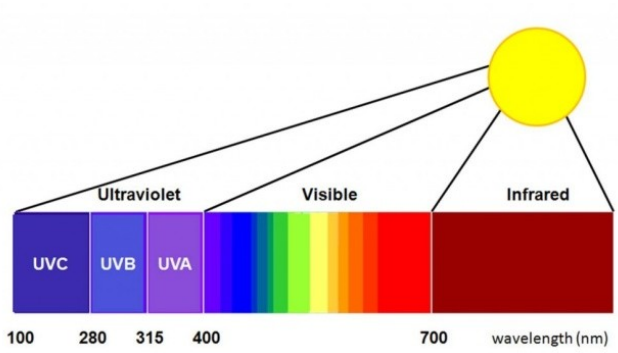

Figure 1.3. Schematic representation of the sun spectrum and the different light intensities through the wavelength pattern. © Thomson Higher Education.

Thus, although avoiding UVR exposure may reduce the risk of various skin cancers, it could inadvertently increase the risk of developing autoimmune diseases such as MS. UV irradiation is also stimulating the immune response by the production of vitamin D_3 in the skin. The cholesterol derivative 7-dehydrocholesterol is in fact converted by UVB in previtamin D, that goes through different steps in liver and kidney in order to become the active hormone 1α,25-dihydroxyvitamin D_3 [1,25$(OH)_2D_3$].

The classic biological function of 1,25$(OH)_2D_3$ is to maintain sufficient serum calcium and phosphorus levels for proper mineralization of bone and neuromuscular function. In 1970s, Goldberg also postulated a peculiar role of vitamin D_3 in MS and this was for long time the only explanation considered for the geographical distribution. Nowadays there are still groups investigating vitamin D in MS and clinical trials running, but we know that there are also publications sustaining that vitamin D is not essential or at least not enough (27, 31, 32).

1.2.3 Other potential factors

Sun exposure is not the only factor taken into consideration for MS. There is growing evidence suggesting that **hormones**, including sex hormones, can affect

and be affected by the immune system. For example, both estrogen and progesterone, two important female sex hormones, may suppress some immune activity. During pregnancy, levels of these hormones are getting very high, which may help explain why pregnant women with MS usually have less disease activity. Testosterone, the primary male hormone, may also act as an immune response suppressor. The higher levels of testosterone in men may partially account for the fact that women with MS outnumber men with MS by 3 to 1 (33).

Also **smoking** plays an important role in MS. Studies have shown that smoking increases a person's risk of developing MS and is associated with more severe disease and more rapid disease progression (16). Fortunately, the evidence also suggests that stopping smoking, whether before or after the onset of MS, is associated with a slower progression of disability.

In 2012 an international team led by U.C. Meier (34) proved that the **Epstein-Barr virus** might also contribute to the brain inflammation that occurs in MS. White matter postmortem MS tissue and control tissue were analyzed by immunohistochemistry for the expression of the proinflammatory cytokine interferon α (IFNα) and for EBV by using EBV-encoded RNA (EBER) in situ hybridization. They found high levels of interferon alpha in active MS brain lesions, as well as neighboring immune B cells latently infected by Epstein-Barr virus, in the absence of active viral infection. These findings may point to a possible mechanism for how the virus might indirectly stimulate MS disease activity.

1.3 Experimental Autoimmune Encephalomyelitis

MS is a complex disease that, despite years of extensive research and the development of several partially effective treatments, still does not have an effective cure. Researchers are performing *in vitro* as well as *in vivo* studies to mimic the disease development in laboratories, but they have only limited access to MS tissue samples. For these reasons, animal models are needed to better understand the underlying mechanisms and to test new therapeutic approaches. One of the most extensively tool used is the animal model called Experimental Autoimmune Encephalomyelitis (EAE). EAE was described and discovered in 1930s by Thomas M. Rivers, while trying to elucidate the etiology of neurological

complications that followed anti-rabies vaccinations. He performed his experiments in rhesus monkeys immunised with emulsions of normal sterile rabbit, in order to induce an inflammatory demyelinating disease in brains: 75% of the treated monkeys were showing myelin destruction with perivascular infiltrates in brains and spinal cords (7). Subsequently, EAE induction was performed using adjuvants added to brain emulsions, spinal cord homogenate, myelin preparations, or purified myelin proteins. Since then, EAE has been induced in a variety of mammal species, including mice, rats, guinea pigs, rabbits, goats, sheep, marmosets and primates CNS (35). In 1947 Wolf et al. documented that EAE resemble the human demyelinating diseases (36). EAE describes a chronic experimental demyelinating disease with an acute onset characterized by focal areas of inflammation as well as demyelination through the CNS (35). It is induced by subcutaneous injection of an adjuvant emulsified with a synthetic peptides derived from myelin proteins, like myelin oligodendrocyte glycoprotein (MOG), myelin basic protein (MBP) or proteolipid protein (PLP). There are also transgenic mice (2D2 TCR) that can develop EAE spontaneously or with minor doses of MOG (37), and EAE can also be induced by cell transfer from EAE donors to native recipients. The immunisation procedure leads to activation and expansion of peripheral antigen-specific T-cells, that pass the blood brain barrier (BBB), enter the CNS and encounter the specific myelin antigen. In general, encephalitogenic antigens are applied together with *Bordetella pertussis toxin* (PTox) and the complete Freund's adjuvant (38), made by mixing the incomplete solution with Mycobacterium tuberculosis (CFA). In fact, the antigen is emulsified in the oil emulsion of CFA, that serves as a depot, providing slow release of both the antigen and the inactivated mycobacterium. The incidence and severity of the disease induced by immunisation is enhanced by the coinjection of PTox, that induces local antigen presentation via non-specific inflammatory reaction (39). The disruption of the BBB has been considered for long time the mechanism by which PTox facilitates the EAE induction (40), but recently the promotion of autoimmune Th1 / Th2 response seems to be a better interpretation for its usage (41).

In order to address to this thesis hypotheses, the MOG induced EAE model has been used in C57BL\6J mice. Here below, a typical scoring curve, where mice are scored every day considering their disease stage. After an initial phase that follows

the first days post immunisation, the disease develops with a peak reached after approximately 14 days. There is then a remission phase, when mice are getting better, until they reach the chronic phase and their sickness stage is reaching a plateau.

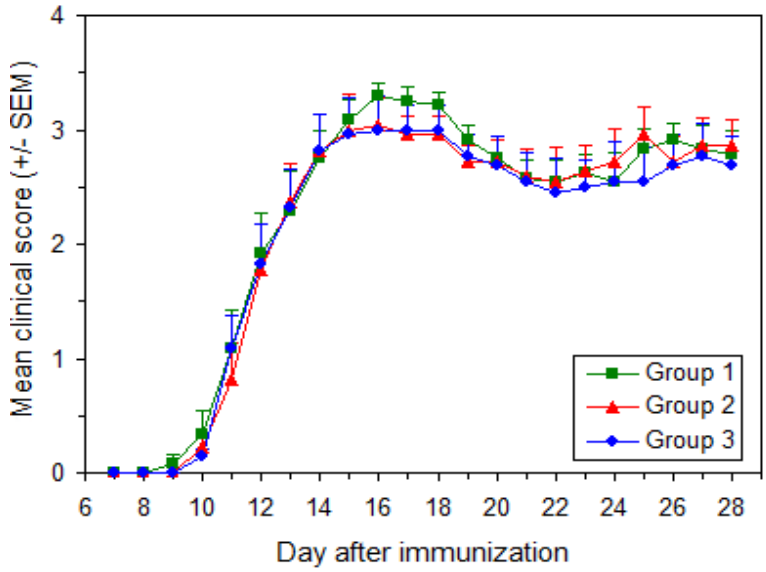

Figure 1.4. Schematic representation of a typical curve of MOG-induced EAE in C57BL/6 mice (http://hookelabs.com/products/EK-2110/).

Studies involving EAE have had an important role in identifying and delineating several aspects of the MS biology: inflammation, immune surveillance and immune-mediated tissue injury. Moreover, this experimental model has directly lead to the development of three medications approved for multiple sclerosis, glatiramer acetate, mitoxantrone and natalizumab (42). On the other hand, EAE is not the perfect model for MS since numerous therapeutic approaches that showed promising results in EAE turned out to be either ineffective or in some cases harmful in MS. Therefore other models have been proposed such as Theiler's Murine Encephalomyelitis Virus (TMEV) infection. TMEV was initially described in 1934 by Max Theiler as a filterable agent that was a known cause for paralysis in mice, but not in monkeys. It is indeed a mouse enteric pathogen, that belongs to the single-stranded RNA picornaviruses, an extremely small viruses family. This virus can be highly virulent and cause even fatal encephalomyelitis, but the strains used for MS research are less virulent and the disease caused by these strains is either mono-or biphasic. The monophasic disease consists of a transient meningo-

encephalo-myelitis, which reaches its peak in 7 days and last approximately 3 weeks. The biphasic phase consists of an initial monophasic phase followed by a chronic demyelinating stage, where most of the demyelinating lesions are in the spinal cord, similarly to EAE models (43). Unlike EAE, the disease is always chronic-progressive in susceptible mice and its pathology is more similar to human MS. With the advent of small animal MRI and MRS techniques, a growing number of investigators are trying to draw parallels between human MS and its rodent models. However, it has to be stated that there is no single animal model that can capture the entire spectrum of heterogeneity of human MS and its variety in clinical and radiological presentation. Appropriate animal models have to be selected depending on the specific research question, still considering the clearly existing limitations.

1.4 The immune system in MS

It is now generally accepted that the demyelination seen in MS is caused by an abnormal immune response mediated by T cells. Over the last 15 years, several studies have been done to investigate these cells and elucidate their role.

1.4.1 The MS immune cells

Until a few years ago, it was believed that CD4+ T helper type 1 (Th1) cells were the main effectors T cells responsible for the autoimmune inflammation. These cells are secreting interferon gamma (IFNγ) and have been found in brain lesions, in CSF and blood of MS patients as well as in EAE mice (44). More recent studies have highlighted an important pathogenic role in EAE for CD4+ T cells that secrete interleukin (IL)-17, so called T_H17 (45). Therefore, it seems that there is a bipolar mechanism involved, where IFN-γ– and IL-17–producing T cell subsets are important for promoting EAE, while IL-10 is important for EAE negative regulation (46, 47). As the capacity to define subsets of immune cells has evolved, an increased number of other subsets have been implicated as mediators of immune regulation with different potential mechanisms of action. Even a brief search

through literature provides examples of groups that focused their attention on natural killer cells (NK) (48), others on IL-17-secreting γδ T cells (45) or microglia cells (49). In addition, a role for autoimmune MOG-specific CD8+ T cells responses have also been discussed (50). Still, immune cells have to overcome the BBB, in order to induce CNS inflammation. Whether BBB dysfunction precedes immune cell infiltration or is the consequence of perivascular leukocyte accumulation remains enigmatic, but leukocyte migration per se can also modify the BBB permeability and the access to CNS. Furthermore, immune cells express inflammatory cytokines, reactive oxygen species (ROS) and enzymes like matrix metalloproteinases (MMPs), that can facilitate their migration to the CNS by influencing BBB function (51).

1.4.2 Skin cells

The single appliance of antigens is not sufficient to promote an immune reaction, but specific cells have to be present and mediate the reactive cells activation. Dendritic cells (DCs) are “professional antigen presenting cells” that play an important role in promoting activation and differentiation of naïve T cells. These DCs are also involved in EAE response, where they activate encephalitogenic T cells and result in either induction or tolerance of the disease, depending on their own activation state and the antigen uptake mechanism (52). They are normally positioned as sentinels in the periphery, ready to migrate to secondary lymphoid organs, particularly lymph nodes, in case of foreign antigens invasion. There, they encounter with naive or central memory T cells and stimulate their activation. DCs are particularly important in this thesis context, due to their ability of promoting and/or repressing immune reactions depending on the local conditions (53, 54). The skin immune system, as first barrier against external antigens, relies on a rich network of professional antigen-presenting DCs that populate the epidermis and the dermis: Langerhans cells (LCs), macrophages, mast cells and γδ T cells.

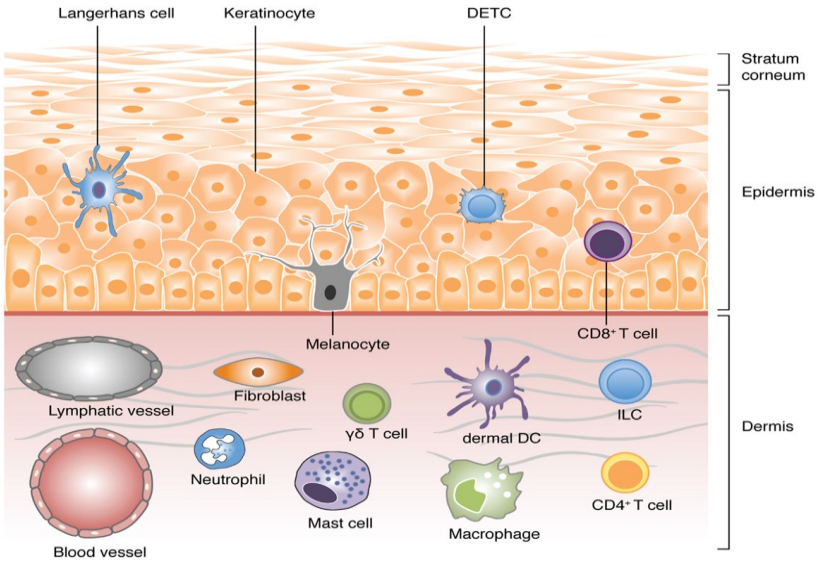

Figure 1.5. A schematic view of the different cell types populating the skin (55).

LCs got their name from Paul Langerhans, who was the first to report the presence of dendritic, non-pigmentary cells in the epidermis, regarded as intra-epidermal receptors for extracutaneous signals of the nervous system. These cells remained an enigma to dermatologists for over a century until the recognition that LCs are leukocytes that are derived from the bone marrow and are the DC population found in the epidermis (56). They are characterized by distinct endocytic vesicles, termed Birbeck granules, surface markers like CD207 (Langerin) and the presence of the epithelial cell adhesion molecule (EpCAM; CD326). The relative contributions of Langerhans cells and dermal dendritic cells in antigen uptake have been discussed for a long time, but studies in mice that exhibits Langerhans deficiencies helped to clarify their role. What has been clearly shown is that both of them can traffic to lymph nodes through afferent lymphatic vessels and their uptake capacity are crucial for the execution of their functions (57, 58). Other innate cells, such as mast cells and macrophages, also populate the dermis and respond to pathogens by secreting proteases and inflammatory cytokines and chemokines. In addition to the classical αβ T cells, the dermis also have γδ T cells, which are important for the macrophages recruitment during inflammation and for the keratinocytes survival (59).

1.5 Tryptophan and the aryl hydrocarbon receptor

The immune response can be regulated in different ways and in recent years tryptophan metabolism has received increasing attention as a potent immunosuppressive mechanism involved in the maintenance of immunological tolerance. L-tryptophan (Trp) is an essential amino acid that serves as a building block for proteins and neurotransmitters synthesis. Trp can only be synthesized by plants and microorganisms, therefore all the other organisms, that do not possess the enzymatic machinery to synthesize it from simpler molecules, have to assume it via diet. In the CNS, Trp is required for serotonin production, in pineal glands for the antioxidant melatonin and it is also involved in oxidoreductase reactions, with the synthesis of the cellular cofactor Nicotinamide adenine dinucleotide (NAD^+) as main product (60). Originally, the effects of Trp in modulating the immune system have been thought to be mediated solely by its depletion. In fact, local depletion of Trp results in starvation of the surrounding cells, which leads to the activation of the integrated stress response (ISR) pathway via the general control non-depressible kinase 2 (GCN2), causing cell cycle arrest and anergy of T-lymphocytes (61). Recent studies also focused on the Trp accumulation and showed that Trp can modulate the immune system via its metabolites. The enzymes that break down tryptophan through this pathway are found in numerous cell types, including cells of the immune system. Some of these enzymes are induced by immune activation, including the rate-limiting enzyme present in macrophages and dendritic cells, indoleamine 2,3-dioxygenase (IDO). IDO has been implicated in maternal tolerance towards allogeneic concepti, controlling autoimmune diseases and chronic infection, as well as promoting tumour immune escape (62-64). Two theories have been proposed to explain how tryptophan catabolism facilitates tolerance. One theory posits that tryptophan breakdown suppresses T cell proliferation by dramatically reducing the supply of this critical amino acid. The other theory postulates that the downstream metabolites of tryptophan catabolism act to suppress certain immune cells, probably by pro-apoptotic mechanisms (60, 65).

Several of the Trp metabolites have been demonstrated to bind, activate and mediate immune-modulation via the aryl hydrocarbon receptor (AhR). This

receptor, best known for mediating the response to xenobiotic and toxins such as 2,3,7,8-tetrachlorodibenzo-p-dioxin (TCDD), belongs to the bHLH/PAS family of transcription factors. It is normally localized in the cytosol, forming a multiprotein complex with two heat shock protein 90 chaperones (hsp90), a small protein (p23) and an immunophilin-like protein termed X-Associated Protein (XAP2). Upon binding with specific ligands, the complex dissociates and AhR migrates into nucleus. There, it forms an heterodimeric complex with the AhR Nucleus Translocating protein (ARNT), which binds to dioxin responsive elements (DRE or XRE) present in the upstream regulatory region of target genes and induces gene expression. The target genes identified include members of the cytocrome P450 family, like CYP1A1, as well as the Ahr repressor (AhRR), which acts as competitor of ARNT and regulates therefore the entire process.

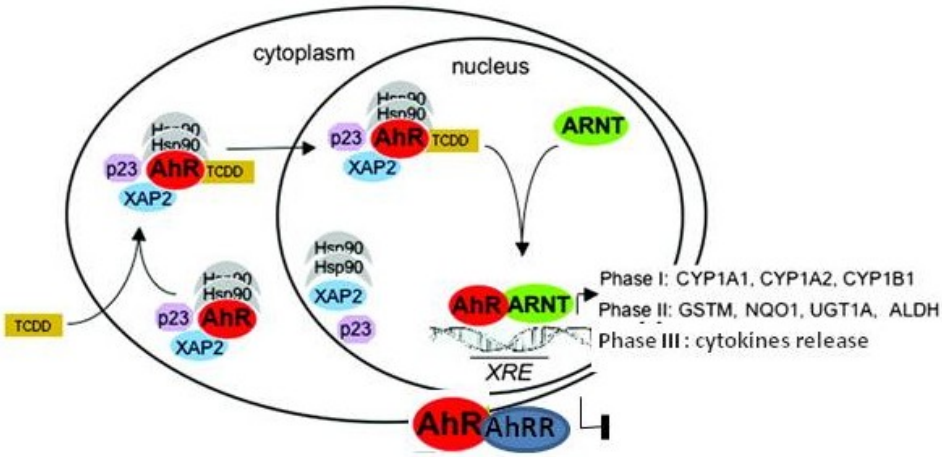

Figure 1.6. Schematic representation of the AhR activation mechanism (The aryl hydrocarbon receptor (AhR) in the regulation of cell–cell contact and tumor growth – Oxford University Press).

In the EAE context, it has been shown that the disease course can develop in different ways, depending on which ligand binds the AhR and consequently which kind of immune response is triggered. Interestingly, this twofold ligand-dependent mechanism can lead to an IL-17 upregulation, shifting the balance to a worse EAE state, or can expand the T_{reg} population, inducing IL-10 and preventing EAE (66-68). Due to its promiscuous binding site, structurally diverse synthetic and naturally ligands can bind the AhR. Among the natural ligands considered, the 6-formylindolo[3,2-b]carbazole (FICZ) has been widely studied *in vitro* by Rannug

group (69). FICZ is a photoproduct of tryptophan with high affinity ligand for the AhR, is generated by UV light and implicated in the differentiation of DCs and CD4+ T cells. The key question, whether enough Trp metabolites can be produced *in vivo* in order to activate the AhR and modulate cellular function, remains unanswered. Generation of knockout mice lacking the AhR (AhR-/-) opened the way to further investigations in different fields (70, 71).

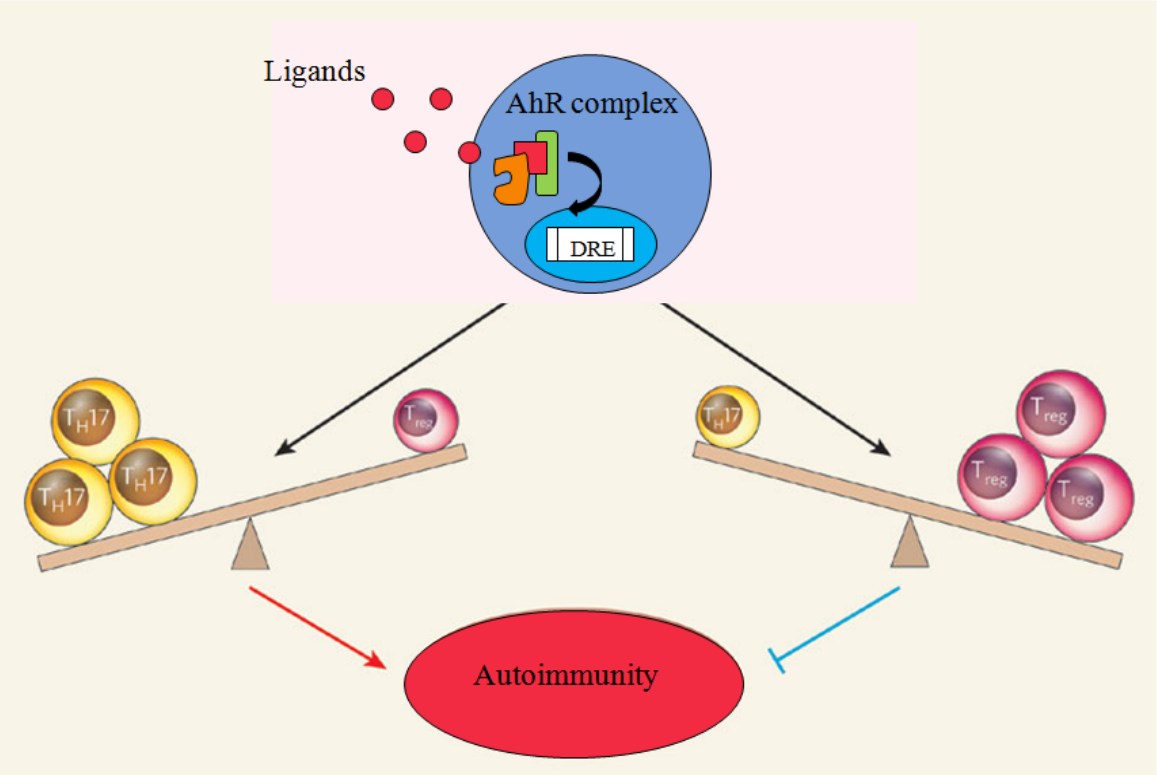

Figure 1.7. Revised schema of the T_H17 vs. T_{reg} balance in the autoimmune response. (Immunology: T cells hang in the balance. Emily A. Stevens & Christopher A. Bradfield).

1.6 Aim of this thesis

This work has been divided in two parts related to the investigation of the Aryl hydrocarbon receptor (AhR) and to its functions in a Experimental Autoimmune Encephalomyelitis context. Part 1 focuses on the beneficial effects of UVB irradiation in EAE. The aim of this project was to investigate the immunological mechanism behind the delayed onset of the disease observed in wt mice.

Following the hypothesis of an AhR involvement, we analysed the skin, as the first immunological compartment influenced by UVB. First, we wanted to identify the metabolites produced during the irradiation and possibly able to activate the AhR. We also focused our attention on the key cell populations involved, followed them during their migratory process to the lymphatic organs and analysed their interaction with other immune cells. The AhR-mediated activation of a specific T-cell population could explain the different courses of the disease observed in the mice. Finally, microarray analyses were also performed, to obtain an overview of the pathways involved in the UVB response.

Part 2 focuses on the response to the treatment of a newly approved MS drug, Teriflunomide (TER). The main purpose of this study was to investigate a possible interaction between AhR and TER, in order to gain information regarding the mechanism of action of this drug. AhR-proficient and -deficient mice were compared in their drug-response and lack of the AhR-induced morbidity and mortality of mice treated with TER. Further analyses were then necessary, to better understand the cause of death and the role of the AhR in this response.

2. Materials and methods

2.1. Reagents and media

Proliferation media was prepared in laboratory adding 10% FBS, 100 U/ml penicillin and 100 µg/ml streptomycin, 25 mM Hepes, 1 mM Sodium Pyruvate Solution, 0.1 mM Non-Essential amino acids solution and 5 x 10 M 2-mercaptoethanol to RPMI-1640 with 2 mM L-glutamine. Staining buffer for Flow Cytometry was prepared in laboratory adding 3% FBS and 2 mM EDTA to PBS. All the components were purchased by PAA Laboratories (Pasching, Austria), while FBS was purchased by Thermo Fisher Scientific Inc., Waltham, MA, USA. Tetrachlordibenzodioxin (TCDD) was kindly provided by D. Schrenk (Kaiserslautern, Germany). StayBrite D-Luciferin and FICZ were purchased by Enzo Life Sciences (Lausen, Switzerland). L-Tryptophan, FITC powder, Acetone and Dibutylpftalate were purchased by Sigma-Aldrich (Saint Louis, MO, USA).

2.2. Animals

Female between 7 and 9 weeks old C57BL/6J WT mice were purchased from Charles River Laboratory (Sulzfeld, Germany). Albino-Bl6 (B6(Cg)-Tyrc-2J/J) and AhR-/- mice (B6;129-Ahrtm1Bra/J) were initially purchased from the Jackson Laboratories (Sulzfeld, Germany) and were bred and maintained in the DKFZ animal facility. As homozygous AhR-/- female mice are infertile, homozygous males were bred with hemizygous females. A new reporter mouse strain (DRE_Luc) was created in our lab to study the AhR activation. DRE-reporter mice were generated by randomly inserting 12 repeated DRE sites into the genomic mouse DNA upstream of a click beetle red luciferase and an mCherry fluorochrome, separated by a T2A site. Several DRE sites from the literature were tested in cell cultures for lowest background and highest activation levels upon stimulation with TCDD 10 nM. The sequence GATCGCCGGGTTTGCGTGCGAT (underlined: core recognition sequence of the AhR), repeated 12 fold, proved to be

the most efficient reporter construct (72, 73). The construct was amplified in E. coli, then linearized by restriction enzyme digestion and inserted into cells by y pronuclear DNA microinjection, carried out by the Interfacultary Biomedical Faculty (IBF), University of Heidelberg, Germany. Transgenic animals were detected using standard PCR from tail biopsies (β2-Microglobulin and mCherry – Table 1). Offspring of the first litter was tested for responsiveness to TCDD and the brightest mouse strain was chosen for further breeding and experiments. Mice were crossed to albino-Bl6 mice (B6(Cg)-Tyrc-2J/J) to obtain white transgenic animals suitable for detection of bioluminescence without shaving. The AhR and the DRE_Luc litters were genotyped from tail biopsies according to standard protocols. An Applied Biosystems 2720 Thermal Cycler was used to perform PCR reaction: as suggested by the Jackson laboratory, specific primers were used (listed in Table1) and protocol was adapted using Taq DNA Polymerase kit (Qiagen, Hilden, Germany). Samples were then loaded on 1% agarose gel, results were acquired using UV-Transluminator (INTAS Science Imaging, Göttingen, Germany) and listed in Tierbase software. All mice were housed at the DKFZ animal facility under specific pathogen-free conditions and exposed to 12-h light-dark cycles. WT control mice were age- and sex matched to AhR-/- mice. All animal work was performed in accordance with the German animal protection law under the permission of the local authorities in Heidelberg and Karlsruhe.

AhR -/- mice	**AhR KO 443**	GGATTTGACTTAATTCCTTCAGC
	AhR KO 444	TCTTGGGCTCGATCTTGTGTCAG
	AhR KO 8162	TGGATGTGGAATGTGTGCGAG

DRE_Luc mice	**mCherry fwd**	ACCCAGACCGCCAAGCTGAAGGT
	mCherry rev	CTCGTTGTGGGAGGTGATGTCCA
	ß2-microgl fwd	CACCGGAGAATGGGAAGCCGAA
	ß2-microgl rev	TCCACACAGATGGAGCGTCCAG

Table 1. Primers used for genotyping AhR-/- and DRE_Luc mice.

2.3. UV irradiation procedure

Following what described by Becklund (27), we built a UV irradiation system for our experiments. The machine consisted of a box made of trespa, a laminate material used for cladding, a movable plate done with the same material and 2 plexiglas protecting panels, 6 mm thick. In the upper part of the box, four lamps UVB Broadband TL 20W / 12 (Philips, Amsterdam, Netherlands) were inserted in an housing steel luminary, they were emitting a broad band of UVR from 280 to 360 nm, where approximately 65% of the output was in the UVB range (290–320 nm). The surface area was approximately 720 x 481 mm and a sensor on the front door regulated the activation of the irradiation flux. The main switch was on the machine roof and a radiometer equipped with a 302-nm sensor was used to monitor the radiance (W/m^2) and the radiant exposure (J/m^2). The entire system was built in collaboration with LAT - Labor- und Analysen-Technik GmbH (Garbsen, Germany), lamps were purchased by Waldmann GmbH (Villingen-Schwenningen, Germany) and a Waldmann sensor was kindly borrowed by the group of Prof. Rösl (ATV / DKFZ Heidelberg).

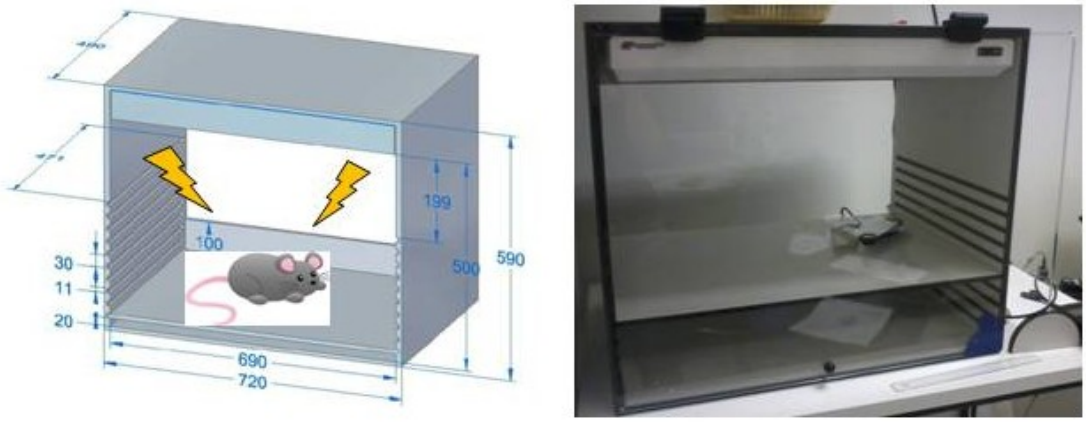

Figure 2.1. Schematic representation and final picture of the UV machine built for mice irradiation experiment.

Mice from the control and UV-treated groups were shaved with electric clippers 1 day before initiating UV therapy. UV-treated mice were irradiated in a specially designed 6-chamber Plexiglas cage to prevent mice from sheltering each other from the UVR. Because the UVB output was unequal in the different chambers, mice were rotated through the different chambers on successive days. They were irradiated starting from one week before immunisation every other day for 13 min (2.5 kJ/m^2) at a distance of 40 cm from the UV source. Same UVB dose and timing was kept for the whole duration of the experiment. Mice from control group also received a sham treatment and Bepanthen (Bepanthen®, Bayer Vital GmbH, Leverkusen, Germany) was applied on their eyes in order to protect them from UV light.

2.4. Induction of EAE

Myelin oligodendrocyte glycoprotein peptide ($MOG_{35–55}$) (MEVGWYRSPFSRVVHLYRNGK) was purchased from GenScript USA Inc. The $MOG_{35–55}$ peptide was resuspended in sterile PBS to a concentration of 4 mg/ml, then emulsified with an equivalent volume of complete Freund's adjuvant (CFA) supplemented with 5 mg/ml inactivated Mycobacterium tuberculosis H37Ra (DIFCO Laboratories, Detroit, MI, USA). EAE was induced in 8-week-old C57BL/6J female mice as described elsewhere (27). Briefly, mice were injected s.c. with 50 µl of emulsion on each side of their chest. On the day of immunisation and 48 h later, mice were injected i.p. with 200 ng of pertussis toxin (ListBiological Laboratories, Campbell, CA, USA) diluted in sterile PBS. Mice were scored daily for clinical signs of EAE using the following scale: 0, no clinical disease; 1, loss of tail tone; 2, unsteady gait; 3, hind limb paralysis; 4, forelimb paralysis; 5, death. Scoring was performed by the same individual throughout the experiment to ensure consistency.

2.5. Cells tracking from the skin to the LNs

In order to follow cells migrating from the skin to lymph nodes, two different methods were used: FITC-painting and NP injection. Mice were shaved 1 day before treatments. FITC powder (Sigma-Aldrich, Saint Louis, MO, USA) was dissolved in a 50 : 50 (v/v) mixture of acetone and dibutylphthalate to obtain a 1% FITC solution and 20 µl were applied onto the back skin of mice (74). For NP injections, 5×10^8 1µM unmodified red fluospheres (Invitrogen, Life Technologies, Darmstadt, Germany) were injected s.c. (75). 12 h later, mice were UV irradiated on their back (5 kJ/m^2) and then sacrificed after 24h. Skin and antigen-draining inguinal lymph nodes were harvested and fixed in 4% paraformaldehyde to procede with histology staining. Lymph nodes were embedded in 1% agarose gel and 35 µm slices were obtained using Vibratome machine (Leica Biosystem, Nußloch, Germany), while skins were embedded in Tissue Tek O.C.T. compound (Sakura Finetek, Germany) and sliced in 10 µm slices with Cryotome machine (Leica Biosystem, CM1950). Histology staining was performed using DAPI, Armenian hamster anti mouse-CD11c primary antibody (Abcam Antibodies, Cambridge, UK) and respectively Goat anti Armenian Hamster TRICT- or FITC-conjugated secondary Antibody (Jackson ImmunoResearch Laboratories, Inc., West Grove, PA, USA). Images acquisition was performed using a Confocal Microscope (Leica Biosystem,TCS SP5 II) and Macro programme was generated by Damir Krunic in order to quantify the NP in the LNs.

2.6. Staining procedure for Flow cytometry (FACS) analysis

Mice were sacrificed through cervical dislocation and skin from their back was removed. Epidermal and dermal layers were separated, minced and prepared as described elsewhere (76). In some cases, skin was removed from the mice and directly frozen in liquid nitrogen. Inguinal Lymph nodes were extracted, meshed through a 70 µm strainer to singularize them, using a plunger of a syringe to push them through the meshes and washed with PBS. Cells obtained from both procedures were then counted and seeded into U-bottom 96-well plate ($1x10^6$

cells/well) to proceed with staining protocols. After centrifugation, supernatant was removed and 200 µl of staining buffer were added to wash the plate. Further centrifugation was performed before resuspending the cells in 100 µl ml of staining buffer containing 1 µl of anti-mouse CD16/32 antibody, necessary to block Fc-receptors. An appropriate amount of surface staining antibodies was added in each well, followed by an incubation time of 30 min on ice in the dark. Washing steps with 200 µl ml of staining buffer and centrifugations (1600 rpm, 5 min at 4°C) were performed before proceeding with fixation/permeabilization. This last step can be slightly different if it is necessary to proceed immediately with intracellular staining procedure or if samples have to be conserved for longer time. In the first case, cells are resuspended in 200 µl BD Cytofix/Cytoperm solution (Becton, Dickinson and Company, Franklin Lakes, NJ, USA) and incubated 20 min on ice in dark, then washed 2 times with (1X) BD Perm/Wash Buffer and spun down at 1600 rpm for 5-7 min at 4°C. Cells are then resuspended in 50 µl of (1X) BD Perm/Wash Buffer containing appropriate conjugated intracellular antibodies and incubated at least 30 min on ice in dark, washed again 2 times with (1X) BD Perm/Wash Buffer and finally resuspended in 200 µl of staining buffer, wrapped in aluminium foil and kept at 4°C until acquisition. For long-term preservation, cells are fixed by resuspending in 200 µl of 4% formaldehyde for 20 min. on ice in the dark, then washed 2 times with Staining buffer and kept on ice in the dark for the next 24 h or frozen at -80˚C in 90% FBS and 10% DMSO. The antibodies used for these studies were purchased by eBioscience (San Diego, CA, USA). To analyze different immune populations, several antibodies were used (Table 2).

UV-T_{regs}	CD4-PacificBlue	CD25-FITC	FoxP3-APC	CD62L-PercPy5.5	
T-regs	CD4-PacificBlue	CD25-FITC	FoxP3-APC		
Langerhans	CD11c – PECy7	CD45 – PacificOrange	MHCII – PacificBlue	CD40-APC	EpCam-FITC
Dendritic cells	CD45-PacificOrange	CD11c- PE			

Table 2. Antibody panel used for staining immune cells of interest in skin and lymph nodes of mice.

Data were collected with a BD FACS Canto II Flow Cytometer (Becton, Dickinson and Company, Franklin Lakes, NJ, USA) and analyzed with FlowJo software (Treestar – Data Analysis Software). For skin samples, cells were sorted using a BD FACS-Aria II Cell Sorter (FACS Core Facility – DKFZ) and collected in 350 µl RLT-buffer/ beta-Mercaptoethanol (1:100 ß-Me in RLT buffer, Qiagen Hilden, Germany) for further RNA extraction.

2.7. Proliferation assay and Enzyme Linked Immunosorbent Assay (ELISA)

Mice were sacrificed through cervical dislocation 8 days after immunisation. Inguinal Lymph nodes and spleens were collected and meshed through a 70 µm strainer, ACK lysing buffer was added to remove blood cells and, after washing steps using PBS, cells were counted. $5x10^5$ cells / well were seeded in a 96 well plates U-bottom and stimulated for 48, 72 or 96h with different MOG concentrations or other stimuli like PLP and ConA as respectively negative and positive controls. After this time, proliferation plates were pulsed with 50 µCi (50 µl RPMI + ^{3}H-Thymidin) and frozen 20 h later. ^{3}H-Thymidin incorporation was measured with a MicroBeta TriLux (Perkin Elmer, Waltham, MA, USA). Elisa plates were harvested after 72 and 96 h, supernatant was transferred to 96 well plates F-bottom and frozen. Elisa assays were performed following ELISA Ready-SET-Go Kit protocols for murine IL-2, IL-6, IL-10, IL-12, IFN-g and TNF-a (eBioscience, SanDiego, CA, USA).

2.8. Tissue specimens and immunohistochemistry

At day 15 post immunisation, EAE mice were sacrificed through intracardial perfusion with PBS, spinal cords were collected and preserved in 4% paraformaldehyde for 24h and then transferred in 30% sucrose solution and kept at 4°C. Samples were then cut into pieces and embedded in paraffin using Leica EG1160 (Paraffin Embedding). Slices were obtained using Microm HM 355S (Microtome for Paraffin Slices) and let dry ON. Stainings for CD3 and MAC3 were

performed with the following protocol as standard procedure to identify immune cell invasion (CD3) or activated macrophages / microglia cells (MAC3): paraffin was removed from the slices through subsequent EtOH dilutions, then 0.2% citrate buffer pH=6 was used as antigen retrivial and endogenous Peroxidase was quenched. First Ab was applied and left incubating ON at 4°C. Next day secondary Ab was applied for 1h at RT, then ABC kit was used to stain slides for 1h. DAB staining and Hämalaun counterstaining were performed before repeating the dehidratation procedure with EtOH scale and then sliced were mounted using Eukit (Fluka, Sigma.Aldrich). Images acquisition was performed using a Cell Observer Microscope (Olympus FluoView FV1000) and Macro programme was generated by Damir Krunic in order to quantify positive cells. At day 10 post immunisation, teriflunomide and control mice were sacrificed, organs were preserved in Roti®-Histofix 4.5% (Carl Roth, Karlsruhe, Germany) and hematoxylin and eosin staining (H&E) was performed in collaboration with Prof. H-J. Gröne, Cellular and Molecular Pathology Dept., DKFZ.

2.9. Magnetic-activated cell sorting

LN cells were also sorted using CD4+ T Cell Isolation Kit and Magnetic Technology (MACS - Miltenyi Biotec, Bergisch Gladbach, Germany). Cells were resuspended in 500µl of sterile FACS buffer (PBS + 3% FBS + 2 mM EDTA), stained with 5 µl of anti-mouse CD16/32 and incubate for 15min on ice to block Fc-receptors; then 5 µl of biotinylated anti-mouse CD4 were added and incubated on ice for 30 min. After proper washing steps using sterile FACS buffer, cells were resuspended in 180 µl FACS buffer with the addition of 20 µl of anti-biotin Microbeads (Miltenyi Biotec, Germany) and incubated on ice for 20 min. Finally cells were washed with sterile FACS buffer and prepared for manual cell separation procedure. Considering the number of cells to sort, MS or LS-columns can be used. In principle, Miltenyi Biotec protocol was followed: columns were prewet with FACS buffer, cell suspension was applied onto the column through a cell strainer, column was then washed repeatedly with FACS buffer and samples were collected. Sorted cells were then resuspended in 350 µl RLT-buffer/ beta-

Mercaptoethanol (1:100 ß-Me in RLT buffer, Qiagen, Hilden, Germany) and used directly for RNA extraction or frozen at -80°C.

2.10. RNA extraction and quantitative PCR analysis

Organs from teriflunomide treated mice were snap-frozen in liquid nitrogen and then pulverized using a Mixer ball mill MM400 with a frequency of 28Hz, for 30 seconds (Retsch GmbH, Haan, Germany). Beakers were previously cooled with liquid nitrogen, so that the samples remained frozen during the procedure. RNA was then extracted using peqGOLD Total RNA Kit (PeqLAB Biotechnologie GmbH, Erlangen, Germany). RNA was also isolated from cells collected in RLT Buffer, using RNeasy Mini-Kit (Qiagen, Hilden, Germany). Briefly, one volume of 70% ethanol was added to each lysate and mixed well by pipetting, then up to 700 µl of each sample was transferred to an RNeasy Mini spin column placed in a 2 ml collection tube and centrifuged for 15 seconds at ≥8000 x g. Flow-through was discarded and same procedure was repeated after adding respectively 700 µl of buffer RW1 and 500 µl of buffer RPE adjusted with ethanol. Buffer RPE was added a second time, but centrifugation time was then extended to 2 minutes and another minute was necessary to dry the membrane. Finally each RNeasy spin column was placed in a new 1.5 ml collection tube, 30–50 µl RNase-free water were directly added to the spin column membrane and centrifugation step occurred once more for 1 min at ≥8000 x g to elute the RNA. For both procedures, RNA yield was finally measured with a NanoDrop 1000 (ThermoScientific, Darmstadt, Germany), a quantity equal to 10 µg was used to obtain cDNA, following the protocol shown in Table 1. High Capacity CDNA Reverse Transcription Kit (Applied Biosystem - Foster City, CA, USA) was used. Finally cDNA was preserved at -20°C or directly used for quantitative analyses. QRT-PCRs were performed in an ABI 7000 thermal cycler with SYBR Green PCR Mastermix (Applied Biosystems) and specific primer mixes. All the primers were designed based on the cDNA sequence of each target and housekeeping gene, spanning at least one intron to eliminate or distinguish amplified contaminating fragments from genomic DNA. PCR reactions were checked by including no-RT-controls, by omission of templates and by both melting curve and gel analysis. The

size of the amplicons was analyzed by loading the samples and a 100 bp ladder (Life Technologies) on a 2% agarose gel, which was then stained with ethidium bromide and analyzed under UV light. Standard curves were generated for each gene. Relative quantification of gene expression was determined by comparison of threshold values. All samples were analyzed in duplicate in two different dilutions. All results were normalized to GAPDH (77, 78).

Primer sequences were (5'-3' forward, reverse):

GCCTTCCGTGTTCCTACCC, CAGTGGGCCCTCAGATGC (Gapdh),

GCCCTTCCCGCAAGATGTTAT, CAGGGGTGGACTTTAATGCAA (Ahr),

CTACAGGACATTTGAGAAGGGC,AGGTCCAAAACAATCGTGATGAC (Cyp1a1),

TTGGAAATTCTTCTGTAGAGACCA,CTTCTTCAATTAGTCGAACAACAGA (Tiparp).

Component	Volume/Reaction (µL)	
	Kit with RNase Inhibitor	Kit without RNase Inhibitor
10X RT Buffer	2.0	2.0
25X dNTP Mix (100 mM)	0.8	0.8
10X RT Random Primers	2.0	2.0
MultiScribe™ Reverse Transcriptase	1.0	1.0
RNase Inhibitor	1.0	–
Nuclease-free H_2O	3.2	4.2
Total per Reaction	10.0	10.0

	Step 1	Step 2	Step 3	Step 4
Temperature (°C)	25	37	85	4
Time	10 min	120 min	5 min	∞

Table 3. Protocol followed for the conversion of RNA in cDNA using High Capacity CDNA Reverse Transcription Kit.

2.11. Microarray – Genomics Core facility, University of Heidelberg

RNA samples obtained from lymph nodes of irradiated and control mice were also used for a microarray test. Briefly, RNA was kindly checked for quality controls by

the Core Facility Microarray Unit of DKFZ, using RNA Eukaryote Total RNA Pico kit. Upon samples acceptance, a MouseWG-6 v2.0 Expression BeadChips (Illumina, San Diego, CA, USA) was used. Samples were labelled and hybridized to the microarray, all the steps were monitored and image acquisition, single chip analysis as well as normalization across all of the samples was performed. In depth analyses were performed using Ingenuity software (Qiagen, Hilden, Germany) and GSEA software (Gene Set Enrichment Analysis – Broad Institute, USA). Statistical analysis of the data were performed in collaboration with Alex Brenner and Thomas Hielscher from the Biostatistics Dept. of DKFZ.

2.12. Cloning strategy

With the aim of having a new AhR reporter mouse, different cloning strategies were developed. The protocol followed required as first step the design of specific primers, in order to insert the fragment of interest in a backbone plasmid. That was done using Geneious software and online tools offered by Sigma Aldrich. Primers were then used for a PCR amplification step, using the Phusion® HF Buffer Pack kit (New England BioLabs Inc., Ipswich, MA, USA). Successful amplicons were checked on band size, loading the PCR products and running a 1% agarose electrophoresis gel. GenEluate PCR Purification kit (Sigma Aldrich) was then used to purify the right amplicons, that still needed to be cut with specific restriction enzymes. This last step was usually performed in parallel with the backbone cut, since both reactions ran at 37°C for 1, 5 h. After further purifications, proportional amount of insert and vector were calculated for the ligation step, mediated by the T4 ligase. Products were further used to transform competent bacteria (E.Coli DH5α), which were then distributed on petri dishes previously prepared with appropriate antibiotic. The next day, grown colonies were picked and further expanded before proceeding with MINI-preparation using QIAspin mini prep Kit (Qiagen, Hilden, Germany). Products were digested, checked on gel and sent to GATC Biotech for sequencing. Results were compared with the predicted ones, using Geneious software and only the correct ones were further amplified, using NucleoBond xtraMaxi kit (MACHEREY-NAGEL GmbH & Co. KG, Düren, Germany). The products obtained were used for *in vitro* tests: cells were trasfected

with the plasmid of interest, treated with known compounds activating the AhR (i.e. TCDD) and fluorescent signal was acquired on confocal microscope.

2.13. DRE_Luc mice and Total Body Imaging

DRE_Luc mice are reporter mice generated in our laboratory as an important tool to monitor the AhR activation *in vivo*. In order to perform total body imaging, DRE_Luc mice were shaved on the back with electric clippers 1 day before starting the treatment. Mice were then irradiated at different time point and AhR activation was checked using IVIS® Lumina Imaging System. Briefly, mice were injected i.p. with 150µl StayBriteTM D-Luciferin (Enzo Life Science) diluted in PBS (30mg/ml), narcotized with Isofluorane flowing through a XGI-8 Gas Anesthesia System and imaged for 10min using IVIS machine. Data were collected and analyzed with Living Image software (PerkinElmer, Waltham, MA, USA).

2.14. High-performance liquid chromatography (HPLC) measurements

High-performance liquid chromatography was performed in collaboration with Ece Gaffarogullari at the Institute of Pharmacy and Molecular Biotechnology, Department of Chemistry (University of Heidelberg) in order to measure Teriflunomide and with Gernot Poschet from the Metabolomics Core Technology Platform, (University of Heidelberg) for the Trp and its metabolites derived from UV irradiation. Both procedures are hereby described.

Teriflunomide measurements

Standard controls and samples were prepared as shown elsewhere (79). Briefly teriflunomide was dissolved in Phosphate buffer (pH 8, 0,05 M) and used for serially dilutions, blank plasma was spiked to obtain different teriflunomide concentrated samples and fresh plasma was obtained to every treated mouse. 100µl of each sample was add to 200µl of acetonitrile and prepared for HPLC measurements. All HPLC measurements were performed. 50 µl of the samples

were injected to 5u C18 300A column (5 µm, 250 x 4.6 mm) (Phenomenex , Aschaffenburg, Germany) connected to a Agilent Series 1100 HPLC machine (isocratic 75% buffer A/B, 25 °C, 1 ml/min) with a diode array detector (Absorbance: 260 nm and 305 nm, slit width: 4 nm). Buffer A: 0.05 M sodium acetate pH 2.5 (adjusted by glacial acetic acid), Buffer B: acetonitrile. Teriflunomide was detected after 9.5 min. The data was analysed by Agilent ChemStation (Agilent Technologies, Santa Clara, CA, USA), and the calibration curve for the standard samples was generated.

Determination of tryptophan, FICZ and untargeted metabolomics

Tryptophan was extracted from homogenized skin samples with 0.5 ml of 2.4% perchloric acid in an ultrasonic ice-bath for 10 min. To prevent hydrolysis of Trp the pH was neutralized by addition of 17µl 10 M NaOH afterwards. To extract apolar metabolites (e.g. FICZ), the second aliquot was extracted with 0.5 ml of acetonitrile (ACN) first, as described above. After centrifugation for 5 min at 4°C at 16.400 g the pellet was reextracted with 0.5 ml methanol and centrifuged. Both supernatants were combined. Prior analysis, homogenates were centrifuged again for 10 min at 4°C to remove remaining cell debris. Compounds were separated by reversed phase chromatography on an Acquity HSS T3 column (100 mm x 2.1 mm, 1.7 µm) connected to an Acquity H-class UPLC system (Waters GmbH, Eschborn, Germany). For the determination of Trp, the column was heated to 42°C and equilibrated with 5 column volumes of 97% buffer A (0.1% formic acid) and 3% buffer B (0.1% formic acid in ACN) at a flow rate of 0.55 ml min-1. Clear separation of Trp from interfering compounds was achieved by increasing the concentration of buffer B in buffer A as follows: 1 min 3% B, 4 min 23% B, 4.1 min 85% B, 6 min 85% B, and return to 3% B in 2 min. To determine FICZ, the column was equilibrated with 5 column volumes of 60% buffer A and 40% buffer B and the following gradient was used: 0.5 min 40% B, 5.5 min 95% B, 7 min 95% B and return to 40% B in 2 min. Trp and FICZ were detected by fluorescence using an Acquity FLR detector (Waters). The FLR detector was set to different parameters for Trp and FICZ: excitation: 254 nm, emission: 401 nm, gain: 100 for the first and excitation: 525 nm, emission: 390 nm, gain: 1000 for the second. For quantification, ultrapure standards were used (Trp from Sigma-Aldrich, FICZ from Enzo Life Scientific). Data acquisition and processing was performed with the

Empower3 software suite (Waters). In order to perform untargeted metabolomics, metabolites were extracted from 30 mg homogenized skin samples with 0.5 ml of ACN, as previously described. 5 µl of each sample were injected onto a reverse-phase Acquity HSS T3 C18 column (Waters), using a binary Acquity UPLC system running a gradient (composition of mobile phases A and B as described above). Each sample was resolved for 10 min at a flow rate of 0.5 ml min−1. The gradient consisted of 97% A for 0.5 min, a ramp to 77% A from 0.5 min to 4.0 min, another ramp to 95% B from 4.0 to 12.0 min, a hold at 95% B until 12.5 min, then returned to 97% A from 12.5 min to 12.6 min, and hold at 97% A until 15 min. Column temperature was maintained at 40°C throughout the run and samples temperature was constantly kept at 8°C. The column eluent was introduced directly into the mass spectrometer by electrospray ionization (ESI).

Mass spectrometric analysis was performed on a Xevo qTOF G1 (Waters) operating in both positive and negative mode. The capillary voltage was set to 0.8 kV and 3 kV, and the cone voltage of 30 V and 25 V, respectively. The desolvation gas flow was set to 950 l h−1 and the temperature was set to 550°C. The cone gas flow was 30 l h−1, and the source temperature was 120°C. Accurate mass was maintained by introduction of Lock-Spray interface of Leucine-enkephalin (556.2771 [M+H]+ or 554.2615 [M−H]−) at a concentration of 4 ng µl−1 in 50% ACN and a rate of 8 µl min−1 (scan time 0.5 sec, interval 20 sec, scans to average 3). Mass signals were acquired in centroid mode from 50 to 1000 mass-to-charge ratio (m/z) in MS scanning using the MassLynx 4.1 software package (Waters). Data analysis of raw mass spectrometric data was carried out using the MarkerLynx add-on tool (Waters).

2.15. Statistical Analysis

Data are expressed as mean ± s.e.m or as boxplots designed using Sigma Plot. Analysis of significance was performed using the Student's t-test or Mann-Whitney Rank Sum Test (SigmaPlot). P values < 0.05 were considered significant. Correlations were analysed by Spearman rank correlation (Sigmaplot).

3. Results

3.1 Project 1: Benefits in multiple sclerosis treatment via UV irradiation

3.1.1. UV irradiation delays onset of EAE in wt mice, but not in AhR-/- mice

Becklund et al. (27) suggested that EAE can be suppressed by UV irradiation in a vitamin D_3 independent manner. Our hypothesis is that not vitamin D_3, but tryptophan mediates the immune response via the involvement of the AhR. Therefore we first asked whether the clinical course of EAE would have changed in the absence of the AhR. To address this question, WT and AhR deficient mice (AhR-/-) were subdivided into two groups. One group received a UV pre-treatment with a 2.5 KJ/m^2 dose administration every second day, starting from one week before immunisation, while the other group received a sham irradiation treatment. Irradiated as well as control mice were immunised with $MOG_{35–55}$ peptide and pTox, while the irradiation procedure continued every second day during the experiment time. The clinical EAE course of WT and AhR-/- mice was observed during the whole experiment. At day 15 post immunisation, 6 mice from wt groups were sacrificed and spinal cords were isolated in order to prove, via histological staining, a corresponding different T-cell invasiveness status. Experimental procedure and results are depicted in Figure 3.1.

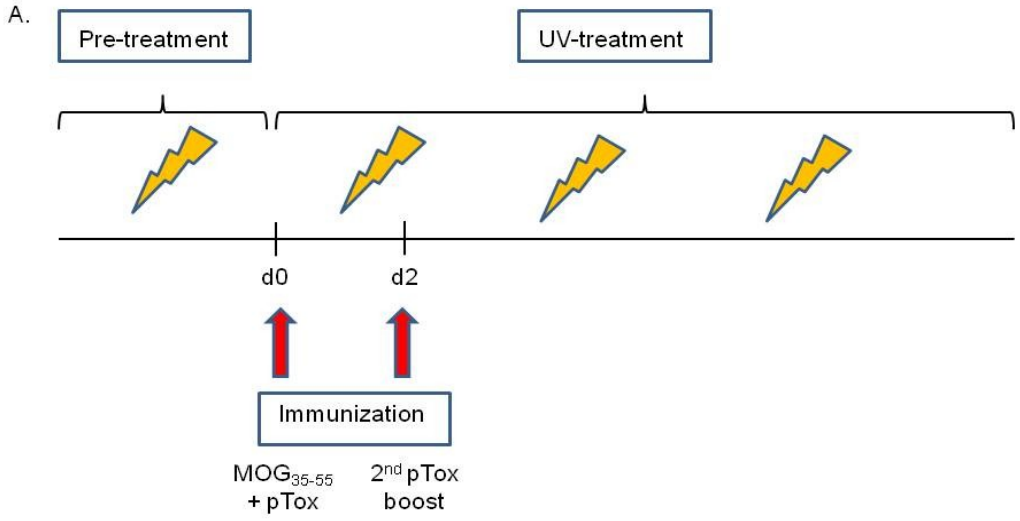

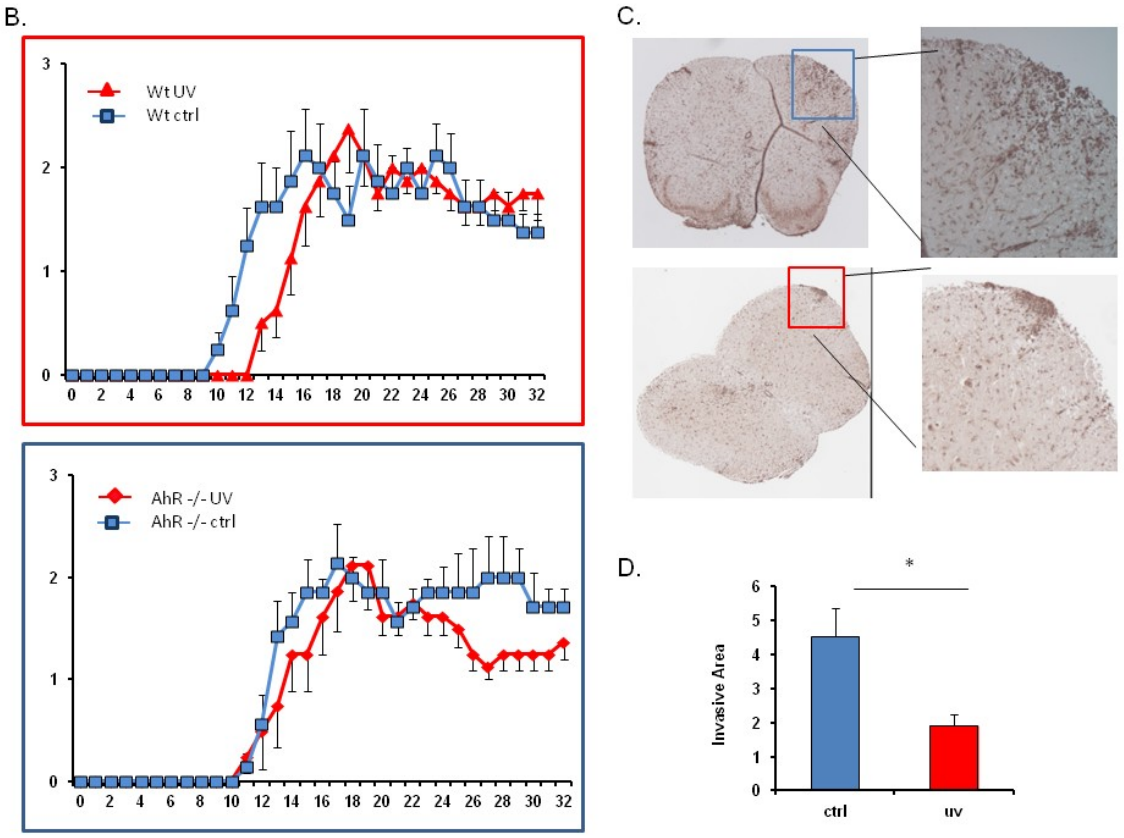

Figure 3.1. In vivo UV irradiation. A. Schema of the experimental procedure applied: mice were irradiated /sham treated every second day during the whole experiment. At day zero (d0) and day 2 (d2), mice were immunised in order to induce EAE. B. Scoring curve during the disease development for WT and AhR-/- mice. C. and D. Immune cell invasion, visualized by CD3 histological staining and quantification in spinal cords of wt mice, n = 6, * p <0,05.

3.1.2. AhR is activated by UV irradiation in a time and dose dependent manner

To support the hypothesis of an AhR involvement, we used DRE_Luc mice, reporter mice created in our laboratory and used as tool to monitor AhR activation *in vivo*. Once DREs are induced, it is possible to quantify and localize specific luminescence in the mice, which corresponds to the AhR activation. For the measurement, mice were shaven on their back, irradiated and AhR activation was measured using an IVIS system. The experiment was performed with different UV doses and the signal was measured 24h later. As seen in Fig. 3.2., the AhR activation is proportional to the UV dose the mice received and the signal is specifically located on the irradiated region. Luminescence is lost, once the skin layer is removed. Further, a time course experiment was performed with a dose of

5 kJ /m^2. Surprisingly, the signal was clearly detected as early as three hours after the irradiation.

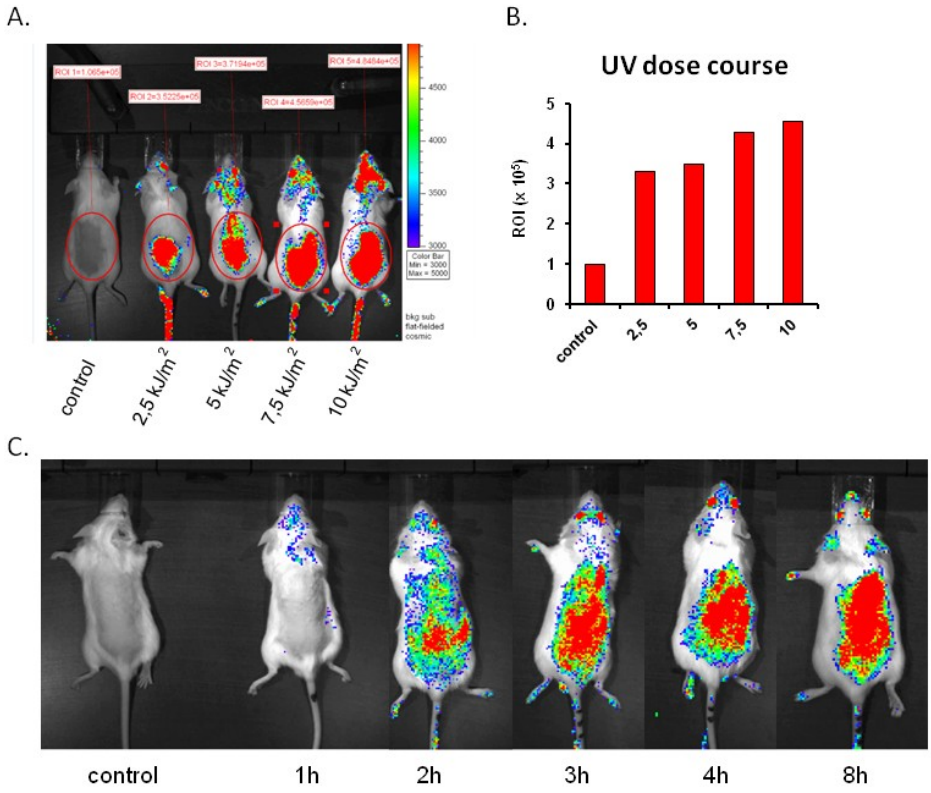

Figure 3.2. Dose and time course of DRE_Luc reporter mice. A. Luciferase intensity was measured 24h after irradiating mice with different UV doses. B. Quantification of the luciferase intensity in the ROI (red circle). C. A single dose of 5 kJ /m^2 was used for irradiating mice and the signal intensity was measured at different time point. For further experiments, measurements were done after 4h with a 5 kJ /m^2 single dose.

3.1.3. Cyp1A1 is up-regulated in the skin cells from irradiated mice

We next investigated how the skin immune compartment is modulated during UV irradiation. The skin is constituted by two layers, epidermis and dermis, where keratinocytes and immune cells are found (Fig. 1.5). In collaboration with the group of Prof. Schäkel (Skin Clinic Heidelberg), dermis and epidermis layers were separated, immune cells were isolated and stained to perform FACS-sorting. Data showed that, in the epidermis, the Langerhans cell (LC) population expressed higher levels of MHC II after UV irradiation. Vice versa, we observed a diminishing number of MHC II positive cells in the dermis layers of irradiated mice and this

decrease was more abundant in WT mice (Fig. 3.3A). These cells were subsequently utilized for RNA extraction in order to quantify gene expression. Cyp1A1 primers were used to perform quantitative PCR analyses. Results showed an increase of Cyp1A1 mRNA levels in irradiated cells, supporting an involvement of the AhR in the UV response (Fig. 3.3B).

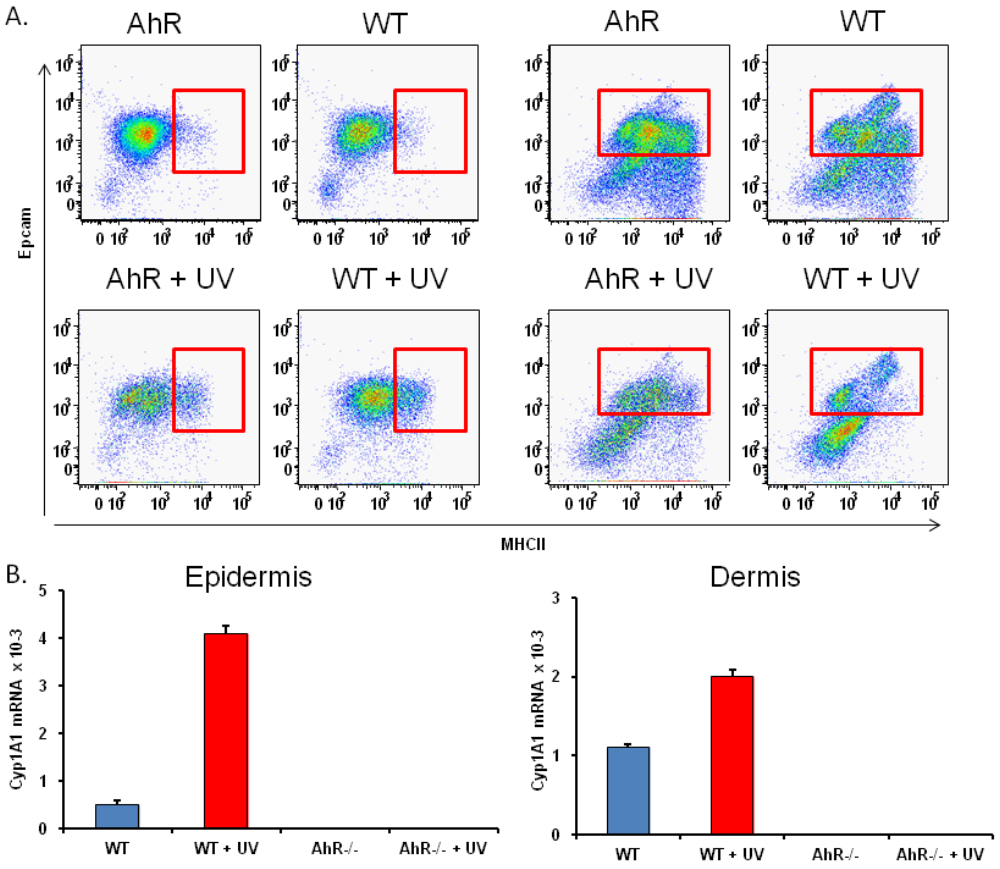

Figure 3.3. Skin analysis. A. Representation of flow cytometry analyses of epidermis and dermis samples from WT and AhR-/- mice (n=6 per group). Cells plotted are CD4+, CD25+, Epcam+ and MHCII+, markers used to stain LCs. In epidermis, UV irradiated samples showed a shift to higher MHCII+ levels. In dermis, cell subpopulations responded to irradiation treatment with higher variance than control groups. B. Cyp1A1 mRNA expression levels in the sorted cells are shown.

3.1.4. Determination of AhR activators

Once the involvement of the AhR and its UV irradiation specific activation were proved, the following step was to determine factors produced by UV irradiation that activate AhR in this specific manner. From the studies published by Rannug et. al. (80), we postulated that tryptophan and in particular its photoproduct FICZ might

be involved. *In vitro* studies were performed in collaboration with the Metabolomic Platform present in the Heidelberg University Campus, in order to optimize the FICZ detection conditions via HPLC. As described by Wincent et al. (69), a 80 µM Trp solution was prepared in dH_2O and irradiated for different time and different doses. We managed to detect a small amount of FICZ starting from a UV dose of 5,3 kJ /m^2, corresponding to 30 min irradiation time at 40 cm distance from the lamps. The chromatogram also showed that there were further compounds produced by UV irradiation, similar to FICZ and potentially comprise more hydrophobic FICZ metabolites like ICZ (Fig. 3.4A). Subsequently, *in vivo* experiments were performed using DRE_Luc mice, that were irradiated with a UV dose of 5 kJ /m^2 and sacrificed 24 h later. Furthermore, WT and AhR-/- mice were subjected to a long-term UV experiment, where they received a dose of 2.5 kJ /m^2 every second day and then sacrificed at day 8 p.i. Skin from these mice was collected, frozen and prepared for HPLC measurements. Since FICZ is a potent AhR activator, pure FICZ (Enzo Life Science) was used as standard reference in a range of 20- 500 nM, to mimic the natural amount, but no FICZ was detectable in the skin biopsies of the animals (Fig. 3.4B). Interestingly, there was a significant increase of Trp levels in the skin of long-term irradiated mice (Fig. 3.4C).

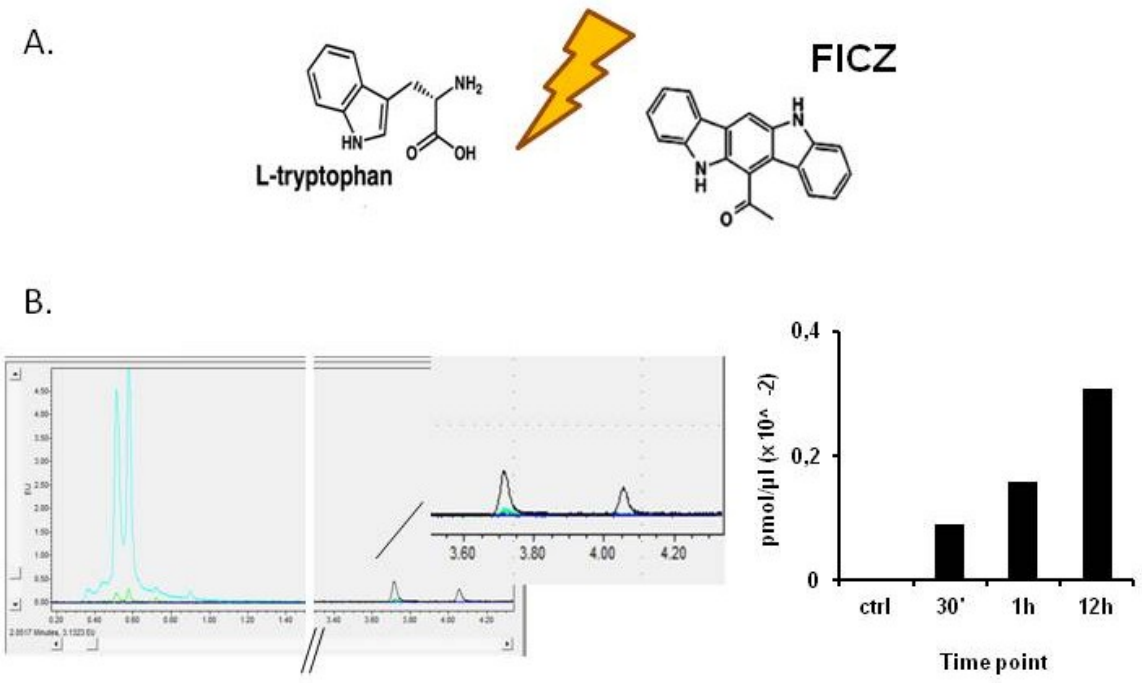

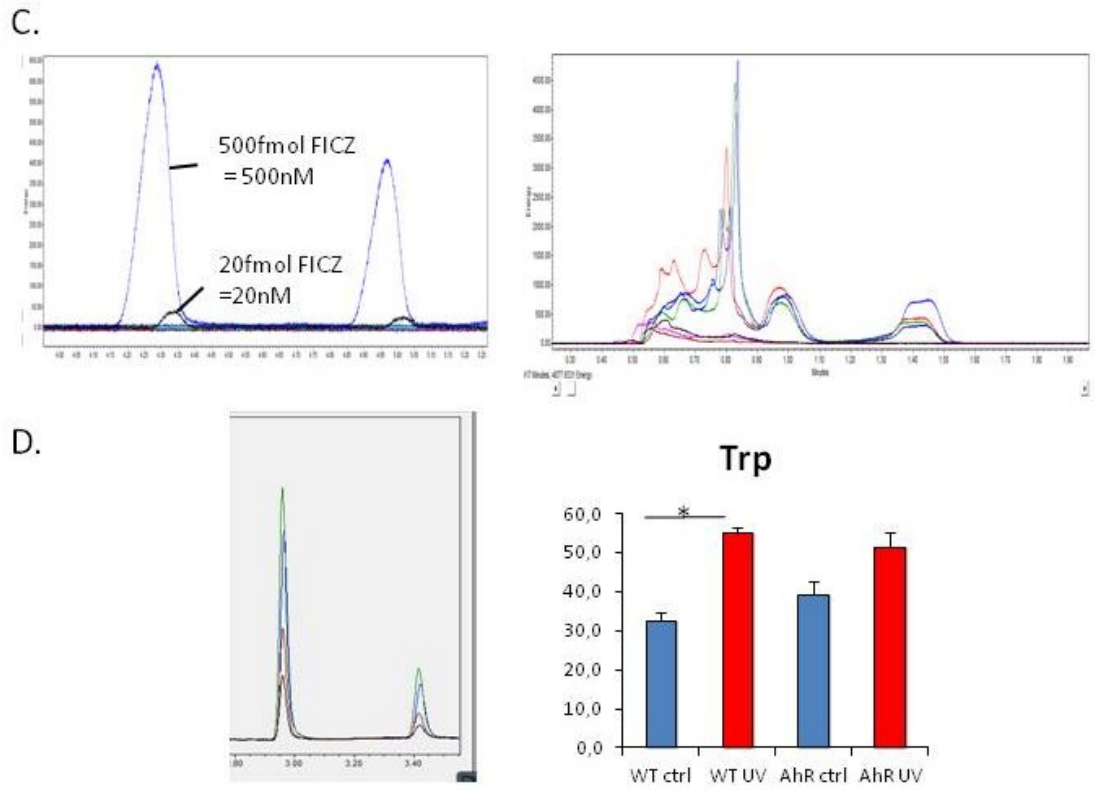

Figure 3.4. UV metabolites. A. Schematic representation of the hypothesis proposed by Rannug et al. B. *In vitro* studies to detect FICZ, water solution was irradiated for different times, HPLC measurements were performed, however no FICZ was detectable with less than 30 min of irradiation. Even after 12 h, the amount detected was still very low. C and D. Mice were irradiated for one single time or for several times (as described in 2.3). FICZ was not detectable in the skin under either condition, however Trp levels increased after irradiation. n = 6, * p <0,05.

Nevertheless, untargeted mass spectrometry was performed, looking for other candidates responsible for the AhR activation. From the skins of DRE_Luc mice, two compounds drew our attention: inosine and sulfolane (Fig. 3.5).

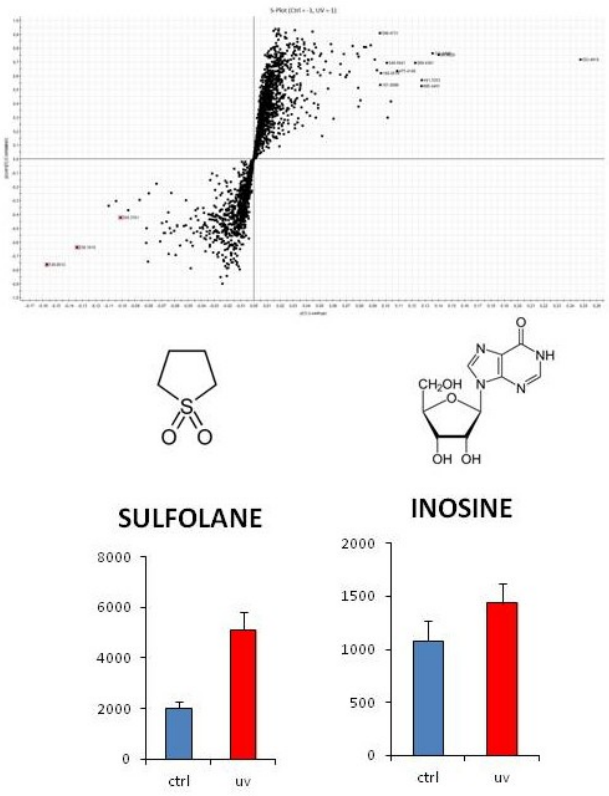

Figure 3.5. Untargeted mass spectrometry comparing mouse skins with and without UV treatment. Mass spectrometric analysis was performed on a Xevo qTOF G1 mass spectrometer operating in both positive and negative mode. Data analysis of raw mass spectrometric data was carried out using the MarkerLynx add-on tool (Waters).

Based on the signals extracted for the corresponding masses, their chemical structure and some hints from literature (80) further tests were performed. HepG2 cells stably transfected with a reporter plasmid expressing luciferase under the control of 3xDRE were treated with 5mM Sulfolane (Sigma Aldrich), 5mM Inosine (Sigma Aldrich), or DMSO and TCDD as negative and positive controls, respectively. After 24 h, the medium was removed and luciferase substrate was added. After 5 min incubation in the dark, cells were imaged using an IVIS machine and pictures were acquired at different exposure times (Fig. 3.6A). Exposure to inosine resulted in activating AhR and further investigation were performed *in vivo*, using the DRE_Luc reporter mice. Inosine was dissolved in PBS (4 µM) and injected s.c. at the back of the mice. After topical administration a luciferase signal was detected after one hour and it stayed stable for the next six hours, indicating that inosine is capable of activating the AhR in the skin (Fig. 3.6B).

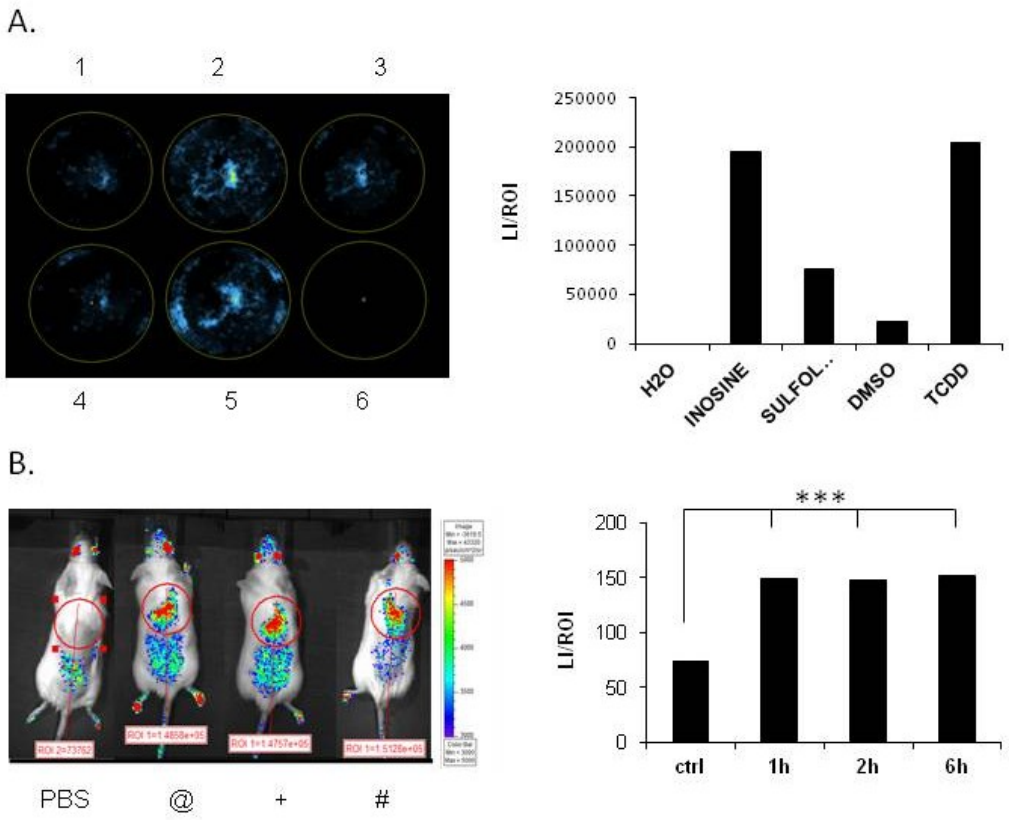

Figure 3.6. Untargeted mass spectrometry validation. A. HepG2 cells carring 3xDRE construct were treated with H2O (1), Inosine (2), Sulfolane (3), DMSO (4) or TCDD (5) and luciferase assay was performed 24 h after treatment using IVIS luminometer. Quantification analysis was performed using ImageJ, where well 6 was used for background subtraction and all the data were further normalised to the water sample. B. *In vivo* tests were performed using DRE_Luc mice. The first mouse received sham injection only with PBS while the others were injected s.c. with 200 µl of inosine 4 µM (red circle), are respectively imaged after 1h (@), 2h (+) and 6h (#). n=3 mice per group.

3.1.5. UV irradiation does not influence the cell trafficking to the lymph nodes

We then focused on the cells that are able to migrate and diffuse in the body to induce an immune response. This characteristic belongs especially to DCs and LCs. They are able to take up antigens from the skin and process them, becoming fully functional antigen-presenting cells (APCs). APCs then traffic to secondary lymphoid tissue and there they switch their functions, losing the ability to migrate, but gaining the capacity to interact with naive T-cells. We asked whether UV irradiation interferes with any of these steps. In order to address this question, experiments to follow cell trafficking were performed. A FITC solution was painted

on the back of the mice, which were UV or sham irradiated 12 h later and then sacrificed after another 24 h. Skins and LNs were preserved and analysed as described in 2.5. However, only unspecific FITC signal could be detected, because the fluorescent solution arrived to LNs mainly via lymph flow. Therefore, instead of FITC, red fluorospheres were injected s.c and tracked in a time course experiment. Red particles were detectable in LN sections from 36h post injection and co-staining with FITC-CD11c Ab confirmed that part of the fluorospheres injected have been taken up by DCs and LCs in the skin before arriving to LNs (Fig. 3.6). With the kind help of Damir Krunic from the Microscope Core Facility in DKFZ, a Macro was created in order to automatically count and quantify the amount of fluorospheres detected in LNs sections from UV irradiated or control mice. The experiments did not show a difference in the number of nanoparticle (NP) detected, suggesting that UV irradiation does not affect the migration of phagocytic cells from the skin to the secondary lymphoid organs.

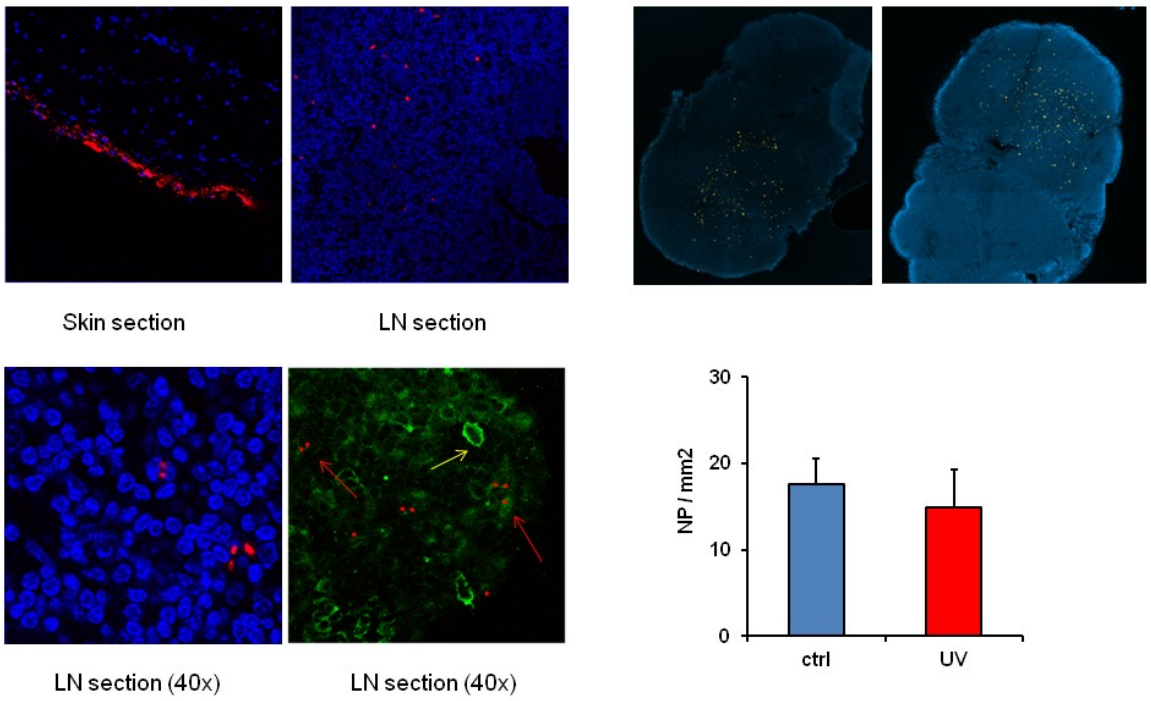

Figure 3.7. NP trafficking. Immunohistochemic pictures of skin and LN sections 36 h post red fluorosphere (NP) s.c. injecteion. DAPI is stained in blue, CD11c+ cells were stained with FITC (green). The yellow arrow indicates a CD11c+ cell, while the red arrows showed CD11c+ cells that took NP up, indicating that not all the Cd11c+ cells took NP up. On the right, representative pictures of LNs sections from irradiated and control mice, where NP are in yellow. A macro was created in order to count the NP and results are depicted in the graph. There is no significant difference between the two groups.

3.1.6. UV-Tregs

DCs and LCs travel through lymphatic vessels and, via chemotaxis, arrive to LNs, where they meet the T cells. This crucial process, called priming, requires an exchange of information between APCs and naïve T cells, it is mediated by specific molecules on the APC membrane called major histocompatibility complex (MHC), by which the T cell fate is decided. CD4+ T cells recognize the antigen-class II MHC molecule complex on the membrane of the APCs, while CD8+ T cells recognize MHC class I. The next step for our studies was therefore the analysis of the LN compartment, where DCs from the skin meet and prime the T-cells. Schwarz et al. proposed that LCs, damaged by the UV irradiation, can still migrate to LNs and prime a special kind or regulatory T-cells, called UV-T_{regs} (82, 83). These cells, generated upon UV irradiation, express the lymph node homing ligand CD62, besides the classical markers for T-regs like CD4, CD25 and FoxP3. As many other T-regs, they can inhibit immune reactions and may also harbour therapeutic potentials, as proved for contact hypersensitivity (CHS). Experiments to detect them also in our EAE context were performed. Mice were sacrificed at day 8 p.i., a LN single cell suspension was prepared and stained for FACS measurement. Stainings were performed using Abs described in Table 3. and results are shown in Fig. 3.8. Interestingly, we were able to identify UV-T_{regs} in our setting and further studies demonstrated that these cells are not present if the mice are irradiated with higher doses but for shorter time (data not shown).

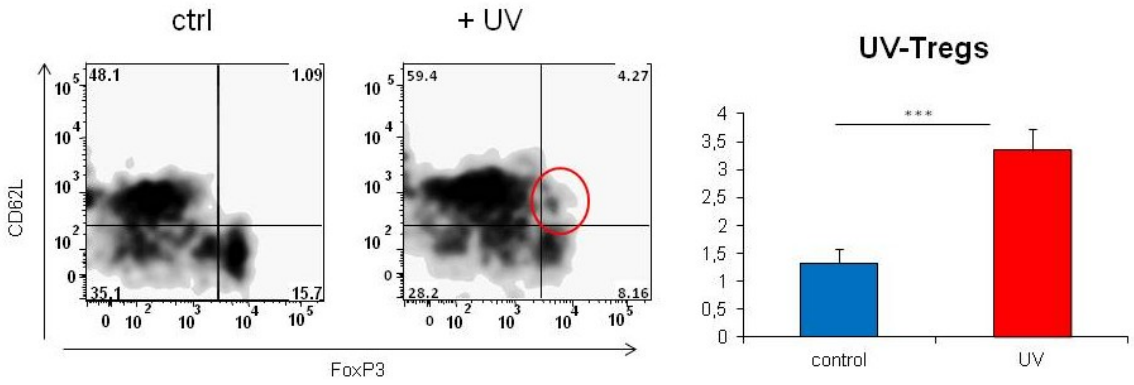

Figure 3.8. Density plots representative of an experiment to detect UV-T_{regs}. Cells were stained with CD4-PB, CD25-FITC, FoxP3-APC and CD62L-PerCpCy5.5 Abs. The population of interest is marked with a red circle. FACS analyses were performed using FlowJo, n = 6 mice per group, *** for p-value < 0,001.

Once identified, we wanted to analyse their function and understand whether they were responsible for the differential EAE onset observed in our initial studies. Therefore, proliferation assay and ELISA assay were performed, using the same experimental procedure described before. Briefly, mice from irradiated and non-irradiated groups were sacrificed 8 days p.i., inguinal draining LNs and spleens were collected to prepare single cell suspensions and counted. Cells were seeded and stimulated in triplicates for each conditions: untreated, stimulated with 1 µg/ml MOG, 5 µg/ml MOG, 10 µg/ml MOG, 20 µg/ml MOG or internal controls (PLP and ConA). *In vitro* stimulation was required to detect cells, which recognise specifically the peptide MOG and, after activation, can proliferate or release cytokines. Results are shown in Fig. 3.9.

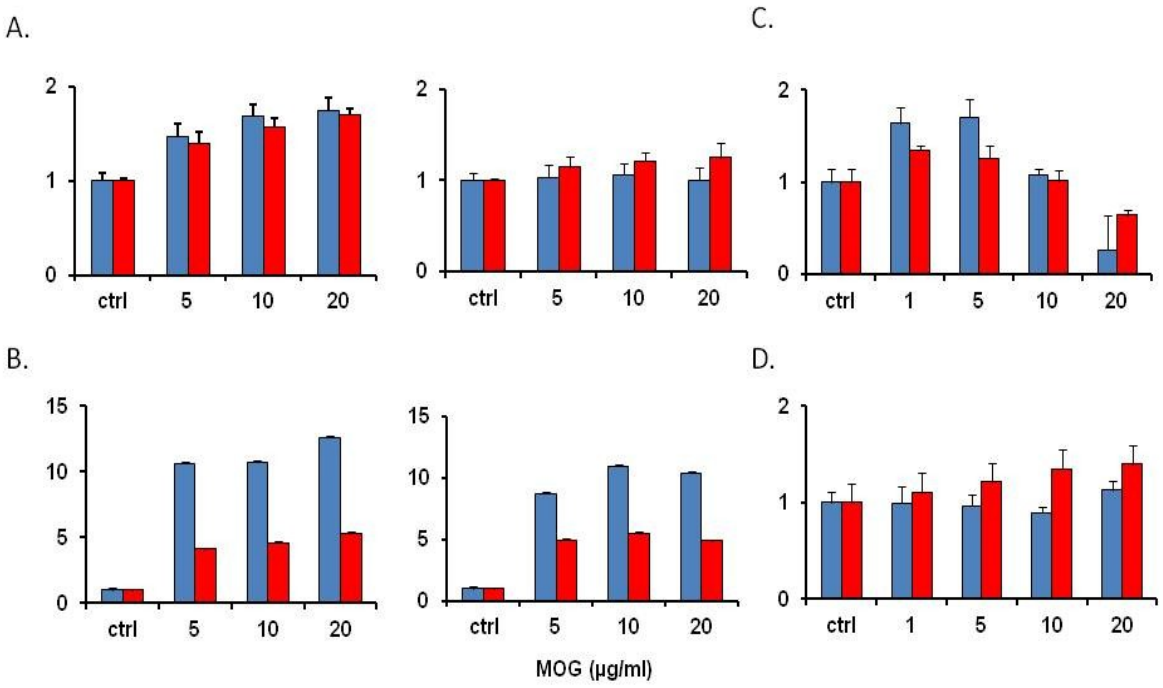

Figure 3.9. Immuno-assays in LNs. A. Analyses of proliferation assay from lymphocytes at 48 and 72 h after MOG stimulation. B. Analyses of proliferation assay from spleenocytes at 48 and 72 h after MOG stimulation. Cells were pooled from different mice (n = 9 mice per group). All data are normalised on no MOG and S.E.M is used for error bars. Red columns for UV irradiated groups, blue for control group. C and D. ELISA assay performed from same mice. IL-12 (C.) and TNF-a (D.) are the only cytokines that differed between the two groups, although not significantly.

3.1.7 Microarray, a tool to open a new prospective or to close the circle

In order to further investigate the LN compartment and to gain a broader overview of the pathways potentially activated upon UV irradiation, we performed large scale gene expression analysis. CD4+ T cells were MACS-sorted from draining LNs of irradiated and control mice, respectively, RNA was extracted, quality-checked and subjected to a MouseWG-6 v2.0 Expression BeadChips (Illumina). Two approaches were followed for the data analyses. First, all genes were plotted in a volcano plot, visualizing their fold change and the significance of this change (p-value). The 200 most significantly regulated genes were chosen and, using IPA and GSEA, the best 60 were further analysed. Pathway analysis indicated that most of these genes were involved in B cell development or in antigen response (Figure 3.10).

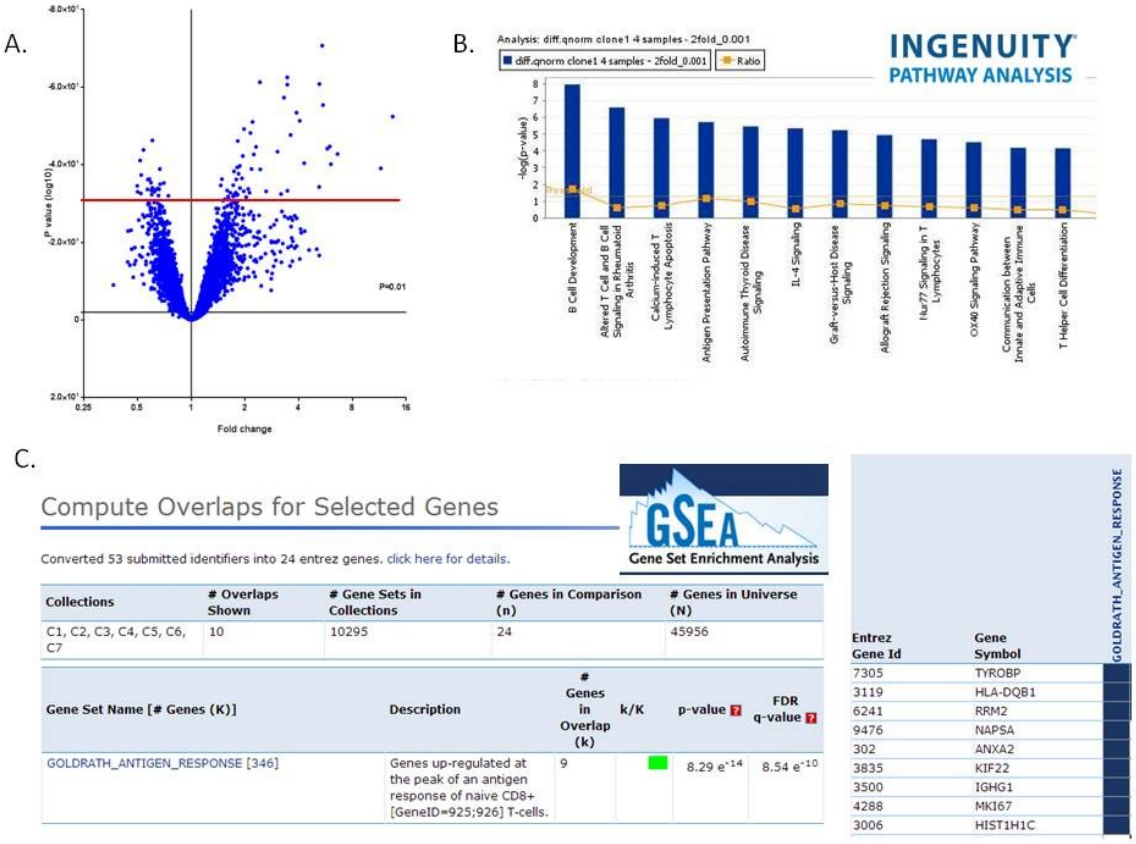

Figure 3.10. Microarray data. A. Volcano plot depicting the distribution of all measured genes, where up-regulated genes have a fold change > 1 and down-regulated < 1. Furthermore, the significance of the regulation (p-value) was considered as important parameter to set a cut-off

(above the red line) to chose candidates to proceed with in further analyses. B. Pathway analysis using Ingenuity Pathway Analysis (IPA) software from Qiagen. The most statistically significant canonical pathways are listed, blue bar height is proportional to the number of genes from the dataset matching the pathway, the orange line indicates the threshold of p value < 0.05 as calculated by Fischer's test. c) Pathway Analysis using Gene Set Enrichment Analysis (GSEA) from Broad Institute. The 60 most significantly regulated genes from the dataset were compared with all the data set collections from GSEA and the best overlap was found for 9 genes (listed on the right side). Green bar indicates high significant FDR q-value (< 0.05).

Another approach was, taking into consideration all genes listed in the raw data sheet, performing gene enrichment analysis. This tool is offered by the Broad Institute in Boston and allowed us to compare our list of genes with all the pathways present in different databases. This resulted in a list of 30 pathways strongly matching with our genes and a direct visualization of the up- and down-regulated genes in control and treated samples. Results are shown in Figure 3.11.

A.

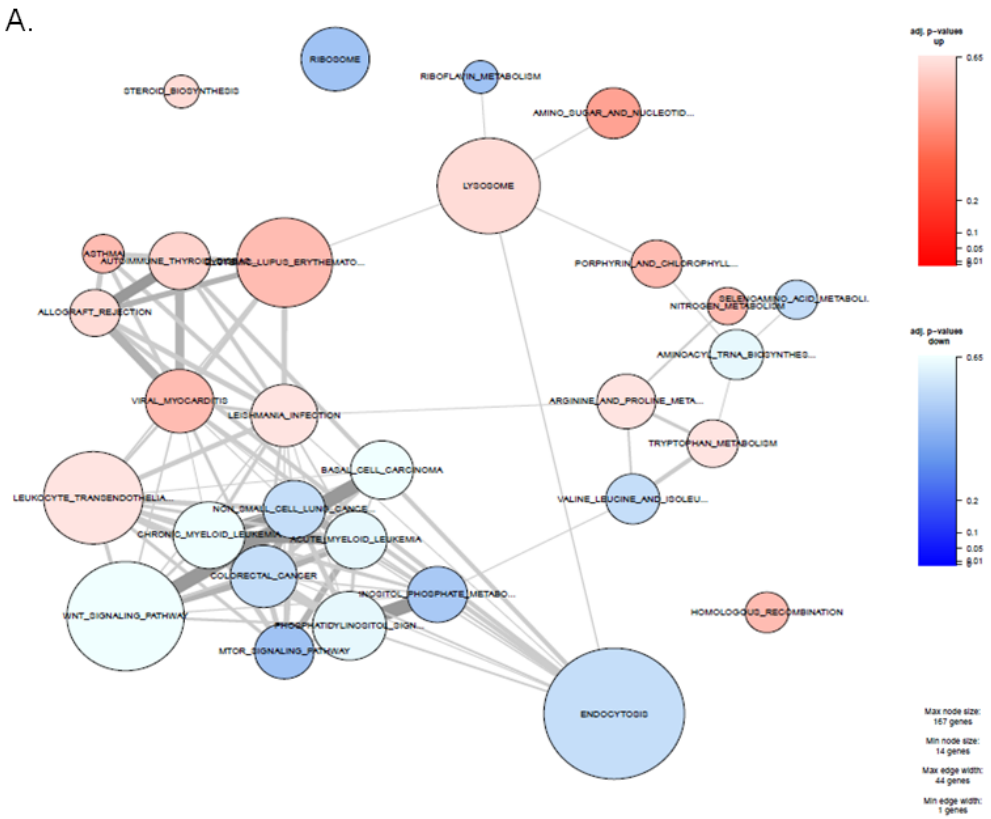

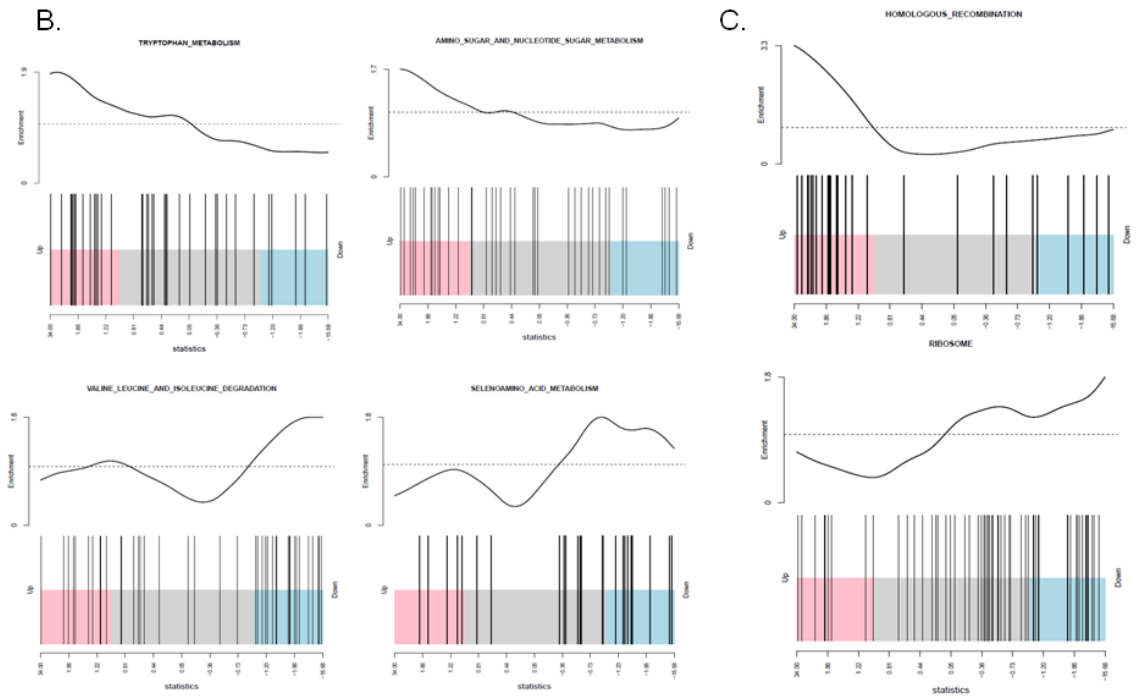

Figure 3.11. Pathway Analysis using GSEA. A. The node-edge diagram represents the best 30 pathways identified using KEGG database (*Kyoto Encyclopedia of Genes and Genomes*). Colours are proportional to the adjusted p-value of the pathways, where red stands for up-regulated and blue for down-regulated pathways. Node size is proportional to the number of genes from our database matching KEGG, where the minimum is corresponding to 14 genes and the maximum to 167. Thickness of the lines connecting the pathways is also proportional to the number of genes in common, with a minimum of 1 gene and a maximum of 44 genes. B and C. Gene set enrichment representation of the most important pathways.

3.2 Project 2: Teriflunomide metabolism is dependent on the aryl hydrocarbon receptor

3.2.1 Lethal effect of TER in AhR-/- mice

Following our initial hypothesis of an AhR involvement in the immunomodulatory response to TER as a potential AhR ligand, we immunised WT and AhR-/- mice with MOG_{35-55} peptide in order to induce EAE. Oral TER treatment (10 mg/kg/day) ameliorated disease scores and delayed the onset of disease in WT mice and in AhR-/- mice. In fact, WT mice treated with the sole methylcellulose (MC) showed paralysis signs from day 10 p.i., while the group treated with TER did not, reacting to the treatment as shown before (13). The same situation was observed in AhR-/- mice receiving control treatment, but further comparison with the corresponding TER- treated group was not possible. In fact, TER-treated AhR-/- animals lost significantly more weight than WT mice, starting from day 8 after immunisation (day 5 after start of TER treatment) and died between day 11 and 14 after immunisation (day 8 – day 11 after start of TER treatment) (Fig..3.12). The dosage was calculated according to FDA guidelines for equivalent doses in animals (U.S. Department of Health and Human Services Food and Drug Administration Center for Drug Evaluation and Research (CDER) *Estimating the Maximum Safe Starting Dose in Initial Clinical Trials for Therapeutics in Adult Healthy Volunteers*, n.d.) and similar doses had been used before for the treatment of EAE in rats (12).

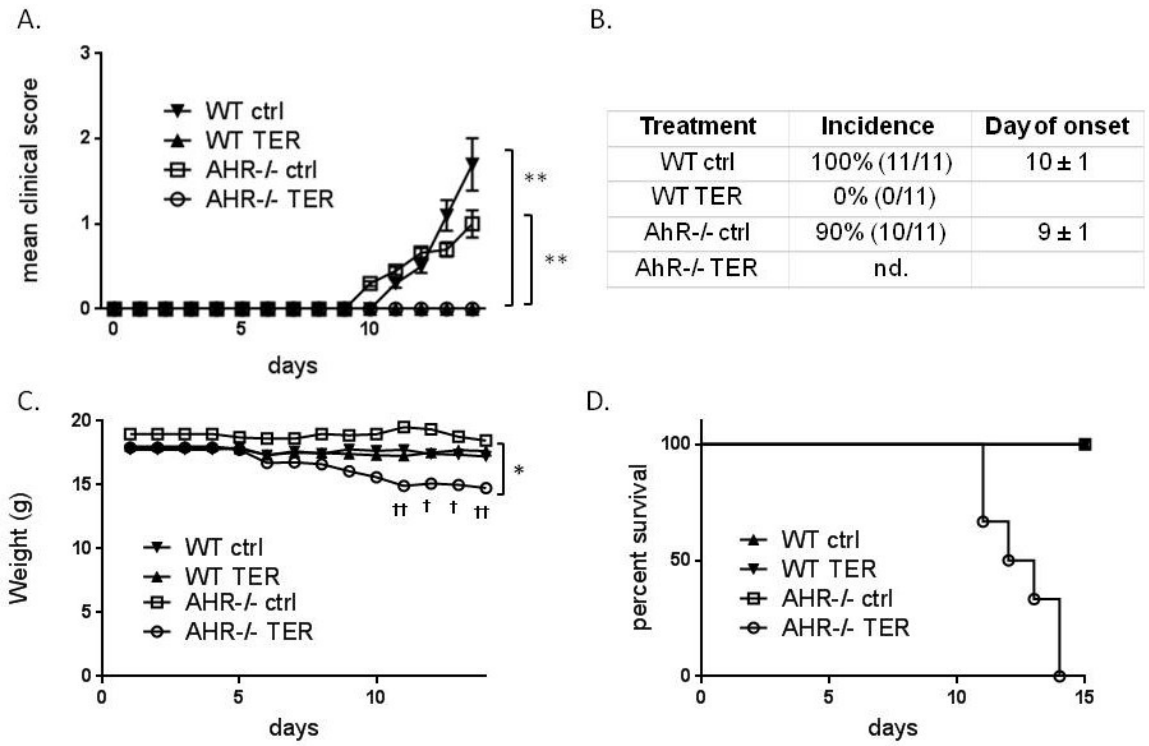

Treatment	Incidence	Day of onset
WT ctrl	100% (11/11)	10 ± 1
WT TER	0% (0/11)	
AhR-/- ctrl	90% (10/11)	9 ± 1
AhR-/- TER	nd.	

Figure 3.12. TER and EAE mice. A. EAE scoring curves of WT mice and AhR-/- mice treated respectively with TER or with a control treatment from 3 days p.i. Results from one representative experiment are shown. **p < 0.01. B. Table shows that only mice receiving control treatment were manifesting paralysis symptoms. nd. = not detectable, since mice in this group died. C. Mice were weighed daily (±SD) throughout the study to monitor disease-associated weight loss and toxicity. D. AhR-/- mice receiving TER treatment were affected by weight loss and morbidity, as shown in the Kaplan-Meier curve.

3.2.2. Histology investigations

All the mice were sacrificed by terminal blood collection, total blood and serum were then preserved for further analyses. Autopsies were also performed in order to check for macroscopic observations. A post-mortem external examination did not reveal any anomalies while, during the dissection of the animals, evident changes in the intestinal truck were present. Interestingly, only the AhR-/- mice treated with TER had darker gut compared to mice from the other groups (Fig. 3.13A) For further investigations, intestine, liver, spleen, kidneys, stomach, lungs and heart of every mouse were collected and stored either in paraformaldehyde or shocked-frozen. Histopatology analyses performed by Prof. H.J. Gröne (Fig. 3.13B) revealed gastritis (i) and enteritis (iii, iv) in the AhR-/- TER mice. At multiple sites, the villi were oedematous, the crypts demonstrated massive apoptosis and

necrotic epithelial cells were found (ii). As a consequence, the necrosis of the epithelial cells induced inflammation. In all the other organs analysed, the morphology was regular.

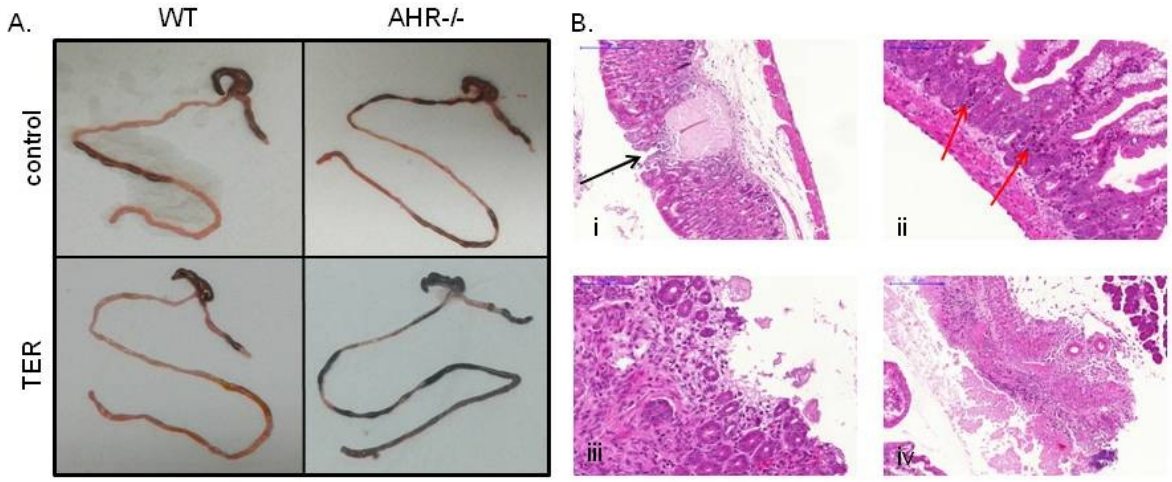

Figure 3.13. Macro and microscopic organs analyses. A. Macroscopic analysis of the intestine of treated mice. AhR-/- TER mice have visibly darker intestine. B. Histologic findings in stomach and intestine sections from AhR TER mice. i. small ulcer of the Corpus Ventriculi (black arrows - H&E staining 10x). ii. apoptotic and necrotic cells at the crypt of the mucosa (red arrows - 10x). iii and iv. representative examples of a flat (iii) and a transmural ulcer (iv) in the small intestine (20x and 10x).

3.2.3. Blood investigations

Fresh blood was preserved in coated tubes and immediately brought to the Analysis Centre of the Medical Clinic in Heidelberg. A complete blood cell count test was performed for every sample and results revealed no significant differences in most of the parameters considered. Interestingly, platelets were significantly decreasing in mice treated with TER (Fig. 3.14B) and this difference was even higher in AhR-/- mice. Serum was also tested in the same centre for GPT/ALT parameters and the values detected in AhR-/- mice treated with TER were 3 folds higher than the values detected in the other groups (Fig. 3.14C). Furthermore, HPLC measurements were performed in order to detect TER presence in mice serum (Fig. 3.14D). Serial dilutions from stocks of 500 µg/ml TER in Phosphate buffer and from blank serum spiked with 60 µg/ml TER were

used to generate a six point calibration standard curve, measuring samples at 260 nm and 305 nm. The same procedure was used for the serum collected from each mouse. A comparison of these chromatograms with the respective controls and standards guaranteed that endogenous substances did not interfere with the assay and to avoid unspecific peaks due to serum proteins. Further analyses were performed, comparing peak area ratios of the samples to internal standards. Linearity of the curve over the concentration range 0.5–250.0 µg/ml TER was determined using regression analysis. These data revealed a low TER concentration in wt mice serum, while samples from the corresponding AhR-/- mice treated with TER had 2-fold higher concentrations.

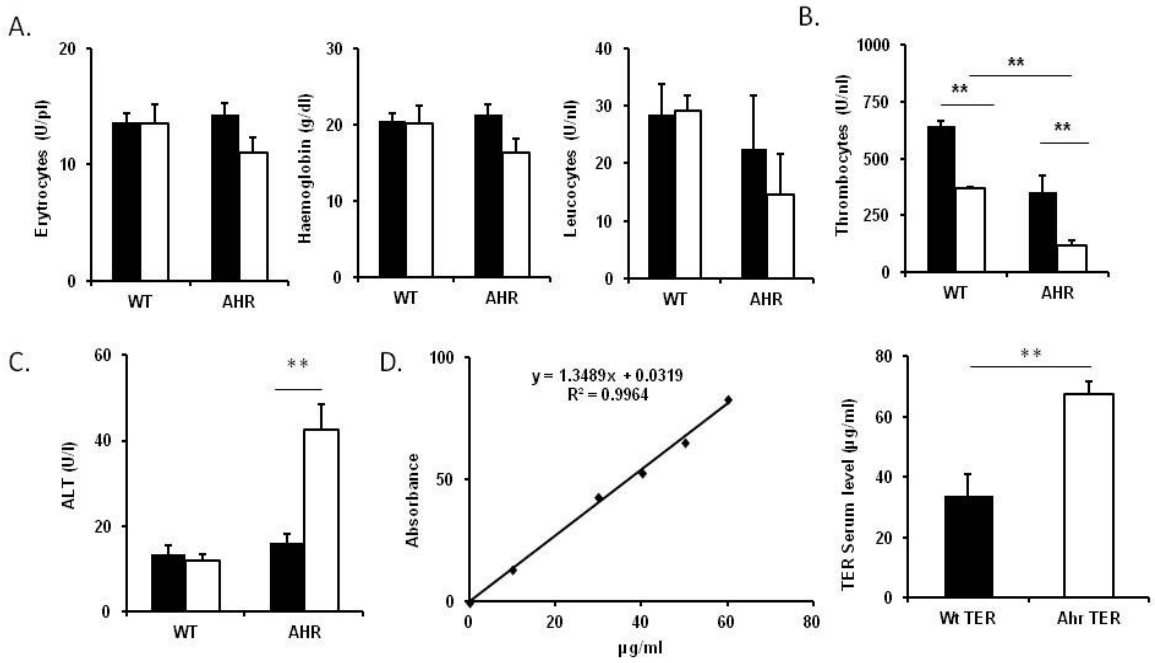

Figure 3.14. Blood tests. A. Fresh blood was collected and complete blood count was performed for every samples. Black bars indicate mice which received control treatment, white is for mice which received TER treatment. Plots show mean ± SEM; n = 3 mice per group. Results from two independent *in vivo* experiments are shown. **p < 0.01. B. Thrombocytes count was significantly lower in mice treated with TER. C. ALT values were measured in mice serum and results revealed liver toxicity in AhR-/- mice. D. HPLC analysis. Standard curves were generated using serial dilution of TER in Phosphate Buffer and of TER in blank serum from untreated mice. Serum from treated mice was collected and prepared for HPLC as described. Fig. C shows TER detection in four different groups. Plot shows mean ± SEM; n = 6 mice per group. Results from two independent *in vivo* experiments are shown. **p < 0.01.

3.2.4 TER acts via AhR

As additional investigation tool, we used DRE_reporter mice. These mice allow us to follow specific AhR activation due to their DRE coupled Luciferase construct. Upon i.p. injection of Luciferase substrate, a luciferase signal is detected only if mice received any other stimuli that induced AhR migration into the nucleous and binding to the DRE sequences. Therefore, animals were orally treated every day, as previously described for the other mice, and images were acquired using IVIS system every second day. The luciferase signal was detected only in the mice that received TER and moreover revealed an activation of AhR localized on the front side (Fig.3.15B). In order to confirm an AhR activation due to TER treatment, we investigated whether that would cause transcriptional changes in AhR responsive genes. Therefore, we performed quantitative PCR analyses using cDNA obtained from gut, liver and kidney and GAPDH was used as housekeeping gene. AhR expression was monitored in all the samples, but no difference was detected between the treated and the control ones. On the other side, TER administration significantly up-regulated expression of the cytochrome p450 member Cyp1A1 in all the organs analysed as compared to mice receiving control treatment only.

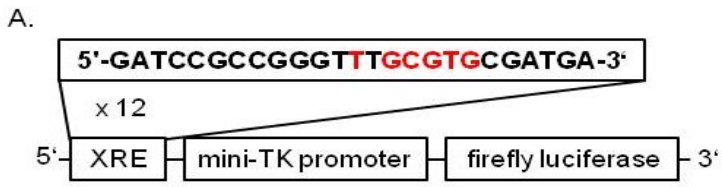

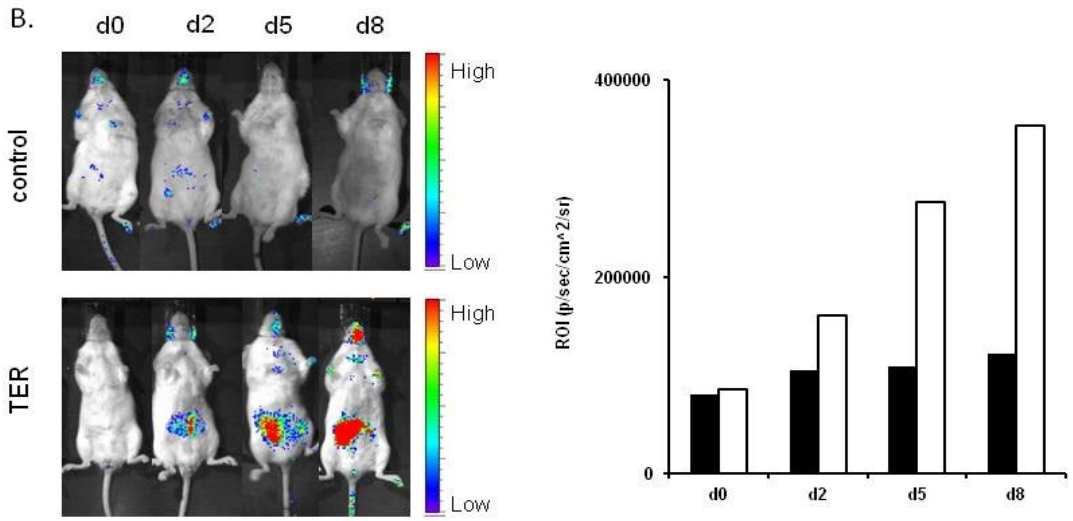

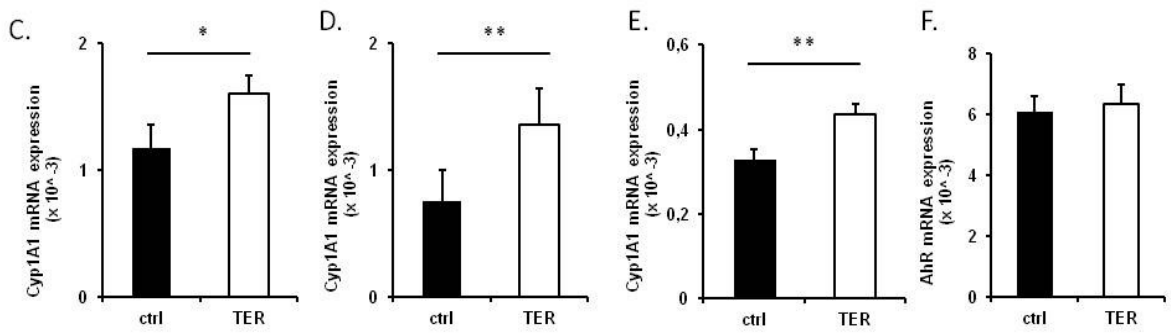

Figure 3.15. TER and AhR interaction A. DRE-reporter mice carry the construct randomly integrated in their genome. This plasmid contains 12 times repeated DRE sequences necessary for the activation of the CBG99 Luciferase cassette. B. Luciferase expression in DRE-reporter mice after treatment. Mice were orally treated and imaged over time for bioluminescence. Signal intensity correlates with the colour bar on the right. The intensity of luciferase expression is shown on the mouse: red represents high expression, violet represents low expression. Mice were imaged for several days during the treatment. On the right, quantification of the luminescent signal over time. C,D,E. mRNA expression of AhR responsive gene Cyp1A1 from treated DRE-reporter mice receiving vehicle (black bars) or TER (white bars): C. liver, D. gut and E. kidney. F. No differences in AhR expression were detectable in the organs. n= 3 mice per group, * p< 0,05, **p < 0.01.

4. Discussion and final remarks

4.1 Project 1: Benefits in multiple sclerosis treatment via UV irradiation

MS is a very complicated neurodegenerative disease and current studies are still focusing on the different aspects and factors involved. Among them, the environmental factors as well as human habits are under investigation, especially from the epigenetic point of view (84, 85). We concentrated our research on one of these factors and analysed its immunological aspects. Therefore this thesis focuses on the role of UVB irradiation in activating the immune system to react against autoimmune cells. It is a common believe, that the sun exposure increases the vitamin D_3 production in human bodies and this in turn can provide benefits in several pathologies, like diabetes, renal transplantation and even cancer (86-88). However, this is still a matter of debate for MS. A few years ago, Becklund et al. claimed that UV irradiation suppresses the disease in the murine model for MS, , irrespective of the involvement of vitamin D_3 (27). On the same line, the mechanism we want to propose has been studied in murine models and proves that UVB irradiation is beneficial in the setting of MS. Interestingly, we were able to add novel aspects by seeing the involvement of the aryl hydrocarbon receptor as the mediator of the UV-immune response. In order to prove this, we first performed a classical EAE experiment, using C57Bl6 wild type mice and mice lacking the AhR (AhR-/-). Half of them were irradiated, half received a sham treatment and while there was no influence of the UV treatment in AhR deficient mice, irradiated wt mice showed EAE symptoms four days later compared to the corresponding control group. Spinal cord stainings also confirmed a higher demyelination status in wt mice that did not receive UV. In order to confirm the involvement of the AhR, DRE_Luc mice were used. These reporter mice are an important tool in our laboratory, they carry a specific construct, which allow us to determine the AhR activity. Mice irradiated with different UV doses showed AhR activation. Importantly, this is time dependent, proved by the fact that the signal detected in the back of the mice took three hours to become specific (Fig. 3.2).

To follow this hypothesis, we analysed the skin also from the cellular point of view. Epidermis and dermis from the mice were stained for FACS measurements and we detected an increased level of MHCII+ cells (Langerhans cells) in the epidermis of UV irradiated mice. In the dermis, the situation varied more, since there was generally a lower number of cells expressing the MHC II marker and some cells subsets were even lost upon UV irradiation. To further investigate the UV effects on the skin cells, the populations indicated by the red square in Fig.3.3A were isolated via FACS-sorting, RNA was extracted and quantitative PCR analyses were performed. As shown in the results (Fig.3.6), we detected an up-regulation of the AhR-responsive gene Cyp1A1 in samples from irradiated mice. These crucial experiments strongly confirm the involvement of the AhR and its activation by UV and opened the way for further investigations on possible AhR ligands. Since a few years, our group has been investigating this receptor in the context of tumor growth, considering the amino acid tryptophan and its metabolites as important regulators (89, 90). Rannug et al. described a photoproduct of tryptophan generated by UV irradiation as a natural AhR ligand (69, 80). Our first hypothesis was then that tryptophan can be degraded by UV irradiation into 6-Formylindolo (3,2-b) carbazole (FICZ) which could in turn via activating the AhR trigger the immune response in a preventive direction, delaying the onset of disease in mice. To prove our hypothesis, optimization experiments were performed to set up the right parameters for HPLC analyses, FICZ standards were measurable even at low concentration, but traces of FICZ were found in irradiated Trp solution only after a long irradiation time. Nevertheless, HPLC analysis of the skin compartment was performed, however no FICZ was present with one single irradiation dose and not either with long-term experiments. Unexpectedly, we could detect higher Trp levels in skin of irradiated mice, both in wt as well as AhR-/- mice. The increase in Trp lead us to postulate that microorganisms on the skin surface, upon being killed by the irradiation, release substances like Trp; which might explain the elevated concentration detected. Again, DRE_Luc mice were used to address this question, but neither images nor microbiological tests from their skins did help us clarifying our hypothesis. In fact, there was no difference in Trp levels in irradiated skin following disinfection and the only bacteria detected from skin swaps from control mice were *Enterococcus gallinarum* and *Rothia sp*. (data not shown).

Hence, further analyses were required to identify other AhR activators. Untargeted metabolomic tests were performed and two components up-regulated in irradiated skins were chosen for further investigation: inosine and sulfolane. We wanted to determine their ability to activate the AhR; for this reason *in vitro* as well as *in vivo* tests were performed. First, HepG2 cells, carrying a plasmid similar to the one in DRE_Luc mice, were treated and luciferase assays showed a strong activating signal for inosine, but not for sulfolane. Then, DRE_Luc mice were used for testing the capacity of inosine to activate the AhR *in vivo*. The signal detected on the site of injection revealed that inosine can immediately bind and activate the AhR. Inosine is generated by degradation of ATP and adenosine and this reaction seems to be impaired in MS patients, where no suppressive adenosine is produced (91). In 2009, Koprowski et al. also conducted a study, treating RRMS patients with inosine (81). Despite kidney stone formation as side effect, they noticed a beneficial effect on the patients.

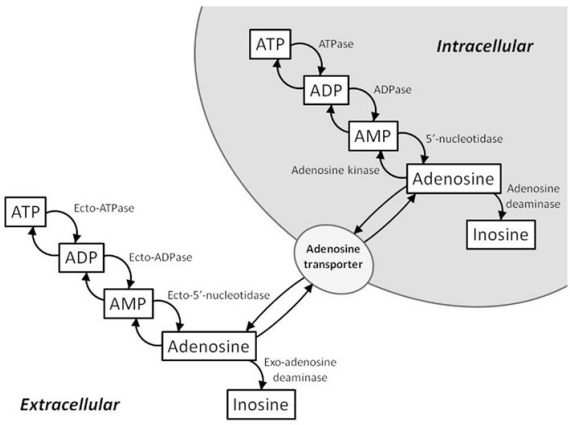

Figure 4.1. Schematic representation of the intra- and extra-cellular ATP/adenosine signaling cascades (92).

ATP is also known to regulate immune cell functions via the P2X receptor (93, 94), to influence the cytokines production on DCs (95) and to promote T_H17 differentiation in the intestinal lumen (96). Interestingly, ATP is involved in DNA repair processes, where inosine is known to have antioxidant and anti-inflammatory properties, protecting the DNA (97, 98). We can therefore speculate that in normal conditions, a balance between ATP and inosine is maintained, while in MS patients this balance is lost and less inosine is produced. With irradiation,

further inosine production is triggered and this has beneficial effects not only on the DNA repairing mechanisms, but also on the progression of MS.

ATP is broken down to adenosine and subsequently to inosine by UVB radiation, which, even if in a mild dose, leads to DNA damages to be repaired. On the other side, higher levels of inosine can mimic the healthy conditions and, via the AhR activation, delay the disease onset. We then concentrated our research on the cellular components of the AhR-mediated immune modulation in the skin. The first step is the so called “trafficking”, the ability of the APCs to internalise particles and transport them to LNs via lymphatic vessels. Therefore we wanted to track cells on their way from skin to LNs, hypothesizing that UV irradiation might impair some cells in their ability to take up particles or in their migratory skills. As a proof, we used fluorescent nanoparticles, injected them s.c in the back of the mice and performed stainings on the skin and on the draining LNs. It was possible to detect the particles on the site of the injection as well as in LNs sections from 36 h after injection. Nevertheless, confocal microscope analyses and counting of the particles that reached the LNs did not reveal any differences concerning the up-take of these particles from APCs, and neither of their migration. After the “trafficking”, cells reach the LNs and there “prime” T-cells. Thus, the next step was to analyze the LNs, looking for a different T cell profile in irradiated samples. Recently, Breuer et al. (99) claimed that the beneficial effect of UVB irradiation is mediated by tolerogenic DCs and T_{regs} and this is also reflected in a clinical trial they conducted on a small cohort of MS patients. We did not find any significant difference in DCs numbers, nor in CD8+ cells, but we detected a trend of increased T_{regs}, that was subsequently confirmed with a different staining panel. In Fig.3.8 we identify the so called UV-T_{regs}, a cell population significantly present after UV irradiation, but absent in control groups. This population is characterised by the expression of the classical T_{reg} markers (CD4, CD25 and FoxP3), and express also CD62L, a cell adhesion molecule also known as L-selectin. Schwarz et al. (83, 100) identified these cells for the first time and described them to be specifically UV dependent. Recent literature described CD62L as a ligand to discriminate among the different T_{reg} subtypes (101, 102), claiming that CD62L+ cells are more potent suppressors than the CD62L- population T_{reg} cells are more responsive to chemokine-driven migration to secondary lymphoid organs. We also wanted to investigate the role of these UV-T_{regs}, performing proliferation assays as

well as ELISAs to determine cytokine expressions. As shown in Fig.3.9, cells from the draining LNs were barely proliferating, while in the splenocytes we were able to measure higher proliferation for wt cells compared to cells derived from irradiated mice. This correlates with the reduced proliferative response described by Weill et al in case of chronic UV irradiation (103). Goudy et al also described a limited proliferation activity associated with CD62+ cells (104), while Beissert et al. claim that CD62L+ T_{reg} cells lose their migratory skills, due to their lack of other selectin markers (105). Furthermore, no real differences in the cytokine profile were measured, only IL-12 was slightly increasing in UV irradiated LNs, supporting the role of this cytokine in DNA repair and its ability to modulate TNFα (106-108). In order to further investigate the mechanism behind it, microarray analyses were performed, using RNA samples from draining LNs of irradiated and control mice. The volcano plot in Fig.3.10A described a situation in which few genes were highly up-regulated, but a lot had a significant p-value. The red line represents the cut-off line we decided to use for the screening of our candidates, considering the ones with p-value higher than 0.001. We used software analysis tools from Ingenuity (IPA) as well as from the Broad Institute (GSEA) and in both ways the pathway analyses underlined a strong involvement of the immune system in the UV response. Pathways involving B and T cells were in fact the first ones suggested by these tools. Further analyses performed with the help of bioinformatics helped us clarifying the up- and down-regulated pathways, comparing our data with different databases like KEGG, REACTOME, GENE ONTHOLOGY and BIOCARTA. The data obtained from the enrichment analysis suggested that KEGG was the most suitable database to refer to, and the node-edge diagram (Fig.3.11) allowed us to easily identify up- and down-regulated pathways. In particular we focused our attention on pathways related to amino acids metabolism. As shown in Fig 3.11A, tryptophan and amino-nucleotide sugar pathways were up-regulated, while the degradation of small amino acids like Valine, Leucine and Isoleucin was down-regulated. Interstingly, also selenoamino acid metabolism was down-regulated. All together, these data are representative of a metabolic situation in the UV irradiated cells where the mainly promoted function is cell survival. In fact, instead of degrading small amino acids in response to critical situations, sugars are utilized. Also protein synthesis is decreased in this stress setting, due to other priorities of the cells. The same situation could be

described from Fig.3.11B, where there was an up-regulation of the homologous recombination pathway in order to repair DNA damages and a down-regulation of the ribosome complex, where proteins were no longer produced due to a cell cycle arrest. As explained by Rudra and Warner in their studies in yeast (109), ribosome synthesis is a massive consumer within the economy of the cell, since it requires several elements working together. The same is true for any other organism. In case of amino acid deprivation or stress caused by diverse sources, including heat shock, free radicals or radiation, repression of ribosome synthesis can occur. This is reflected by the down-regulation of the mTOR pathway in irradiated cells. Also other studies performed in vitro described the complexity of the transcriptional profile of the UVB response. In fact, keratinocytes respond by enhancing processes involved in energy production and translation, while suppressing those related to transcription, differentiation and transport. This response can vary depending on the time passed between posing the stress factor and collecting the samples, since the cells require some time to activate the repairing mechanisms. Further, seemingly paradoxical, genes that were up- or down-regulated after the UVB dose can demonstrate an opposing direction of regulation if measured at a later time point, reflecting the recovery of UVB-damaged cellular activities (110, 111). Interestingly, another study performed in lymphoblastoid human cells revealed that most genes responded to UV, but with less than 2-fold change compared to untreated conditions, similar to the situation we found in our mice. Furthermore, not only damage-response pathways were found, but also several metabolism-related pathways which were not previously associated with the damage response in mammals, but conserved in yeast (112).

The model we want to propose is explained here below (Fig. 4.2). UVB irradiation has been proved to be beneficial for treatment of EAE in mice. On the skin surface, metabolites like inosine are produced and are able to activate the AhR present on skin APCs like DCs and LCs. These cells do not lose their ability to migrate to the draining LNs, but they bring along the activating signals necessary for priming cells in LNs as well as the “danger” message generated by the irradiation. Once there, they can induce UV-T_{regs}, inhibiting T_H17 immune response and they can also activate the response cascade necessary to repair DNA damages.

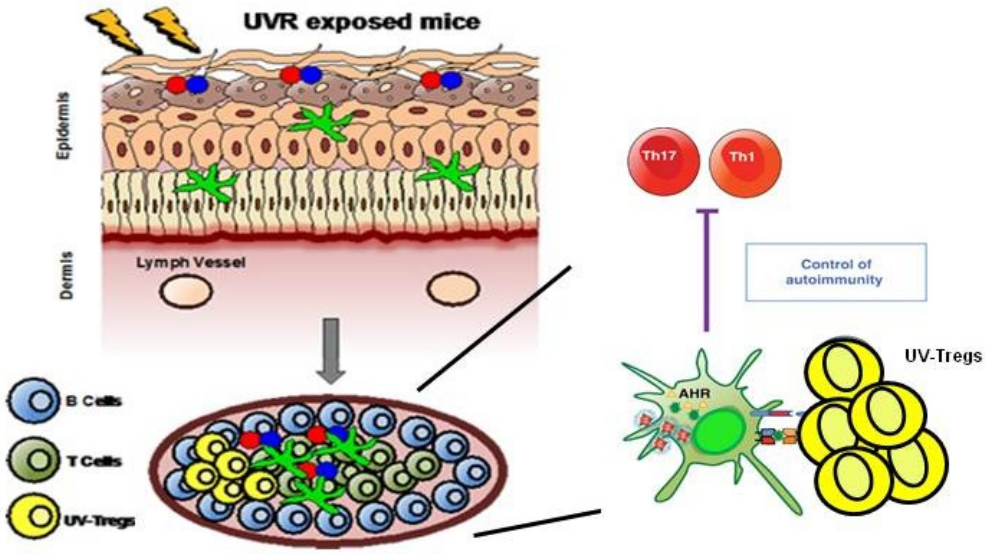

Figure 4.2 Proposed mechanism of UVB induced immune regulation in EAE. AhR on DCs is activated by products generated from UVB irradiation, like inosine. Activated DCs migrate to LNs and activate UV-T_{regs}, inhibiting T_H17 immune response (Revised from Lisa A. DeLouise, *Engineering Smart Bandage Bio Nanomaterials for Healing Skin).*

4.2 Project 2: Teriflunomide metabolism is dependent on the aryl hydrocarbon receptor

In the present study, we identified a new mechanism, where the aryl hydrocarbon receptor plays an essential role in metabolizing the drug Teriflunomide. AhR is a cytoplasmatic receptor known for mediating the response to xenobiotic and toxins, but emerging research also highlighted its role in modulating lymphocytic immune responses in the context of neuroinflammation, brain tumour immunology and inflammatory tolerance (113-117). Our group and others have identified the tryptophan metabolite kynurenine, produced in brain tumour cells via the rate-limiting enzyme tryptophan-2,3-dioxygenase, as an endogenous ligand for the AhR, promoting tumour growth and invasiveness as well as immune escape (114, 115). In the MS context, its role has been widely described as mediator of T cell differentiation (116, 117). The AhR can be activated by a variety of structurally unrelated compounds like the xenobiotics benzo[a]pyrene and 2,3,7,8-tetrachlorodibenzo-p-dioxin (TCDD) or the endogenous tryptophan photoproduct 6-formylindolo (3,2-b)carbazole (FICZ), which elicited different responses and effects (118).

On the other side, Teriflunomide is a non-competitive inhibitor of the mitochondrial enzyme dihydroorotate-dehydrogenase (DHODH), recently approved for MS treatment, due to its effect on blocking *de novo* pyrimidine synthesis and interfering in T and B immune cell proliferation. Ringheim et al. showed that TER attenuates immunopatological changes in the rat model of EAE, delaying the onset of the disease significantly (12).

A possible interaction between AhR and TER has also been considered. O'Donnell et al. showed in human and mouse hepatoma cell lines that leflunomide, but not its active metabolite TER would bind and activate the AhR. Using primary T cell cultures from WT and AhR deficient mice (AhR-/-), they showed that AhR is negligible for leflunomide and TER mediated inhibition of proliferation (119). Baban et al., using a mouse model of ischemic renal failure, showed an induction of regulatory T helper cells (T_{reg}) and a reduction of pro-inflammatory IL-17 producing T helper cells (T_H17), due to the AhR activation

mediated by leflunomide (120). These data remain speculative as both studies lacked the use of AhR-/- mice, not giving any information regarding any AhR-dependent metabolization and toxicity of TER.

Therefore, our goal was to study the interaction between the two of them, comparing deficient and proficient AhR mice in a MS context. The first step was to confirm what was shown by Ringheim et al. Immunised mice were daily treated with TER and control treatment during the course of the experiment, control groups developed the classical EAE immunopatological changes, while the TER groups had a significant delayed onset of the disease. This result demonstrated that the AhR was not a key molecule in the immunosuppressive mechanism of TER. However, AhR-/- mice lost significantly more weight and died upon TER treatment. As shown in Fig 3.13, macroscopic investigation showed that this correlated with a dark colour on the intestine of the mice. Histological analyses were then performed to identify the cause of death, which was attributed to a bleeding on the small intestine, or to an inflammation and brake of the intestinal barrier. All the other organs analysed resulted in a regular morphology. To support the histological analyses, blood tests were also performed. No significant differences were found in Hemoglobin levels nor in red or white cell counts, but there was a significant decrease of thrombocytes in TER-treated mice. This correlated with the clinical trial tests, where lower thrombocyte counts were present in the blood of TER treated patients. Tests performed on AhR deficient mice did not show any developmental problem, nor abnormal features in the animals, but a reduced thrombocyte level compared to corresponding wild types (121). Therefore we speculated that the administration of TER reduced the counts in the AhR-/- mice, possibly inducing a case of thrombocytophenia. Furthermore, Alanine aminotransferase (ALT) values and TER levels were measured in the mice serum. The first parameter, a marker for acute liver damage, was three times elevated in TER treated AhR-/- mice. The second parameter was measured via HPLC and accumulated in AhR-/- serum (Fig. 3.14C and D). Clinical trials identified liver toxicity as a possible TER side effect in human MS treatment, also correlated to the long elimination half-life of TER (122). Our studies stated that the accumulation of TER aggravated exponentially liver toxicity in case of AhR deficiency.

Another important tool used in this study were the DRE-reporter mice. As shown in Fig 3.15, their use clearly supported the other results presented before. In fact, only in mice treated with TER we detected a luminescent signal, which correlated with the AhR activation. Mice were treated every day and imaged every other day. The intensity and the amount detected increased over the time, supporting the fact that TER accumulation was taking place and it was even necessary to switch on the AhR. Another important observation regarded the localization, since the signal was not detected on the back of the mice, but only on the front side and particularly in organs involved in the metabolic processes. Information from clinical trials revealed that TER is cleared by hepatic metabolism and enterohepatic circulation (123), it is eliminated unchanged and mainly through bile, specifically 37.5% is eliminated in the feces and 22.6% in urine. Therefore, we concentrated our analyses on liver, gut and kidney, where we detected an up-regulation of Cyp1A1 mRNA expression levels. In conclusion, our data showed that an interaction between TER and AhR takes place, not to mediate an immune response, but as a step in the drug pharmacokinetic. Due to the fundamental role of the AhR for an efficient metabolism of TER, genetic AhR variants in MS patients might be considered, since they would be relevant to explain undesired side effects and toxicity of TER.

4.3 Final remarks

This work aimed to analyse the functional role of AhR in the mouse model of MS. We were able to show the importance of the AhR as a key molecule in mediating the immunosuppressive effect of UVB light as well as the metabolisation of the approved MS drug Teriflunomide.

Concerning the first project, further investigations could be performed to delineate the bacterial impact on the skin surface. It would be also interesting performing measurements of the ATP production in different conditions and deeper analyse the structural interaction between inosine and AhR. The mechanism we proposed could be further validated, moving into clinical trials, as already shown by Breuer et al. (99). A combination of phototherapy and inosine administration could be a promising therapy to reduce the degeneration status and the disability of MS patients. Moreover, underlying the importance of the AhR in the UVB immune-response, we believe that genetic tests specific for AhR would be essential for clinical purposes and for further pharmacological targeting.

With the Teriflunomide project, we proved once more the functional plasticity of the AhR. Further investigation could be performed to verify a possible interaction between the drug and AhR also on the immunological side. The identification of genetic polymorphisms is again an important parameter to consider for MS patients, in order to reduce and prevent side effects. We have to consider that TER is currently one of the three FDA-approved oral medications available for the treatment of relapsing forms of MS with fingolimod and dimethyl fumarate. While injection and IV treatments have proven to be beneficial, these newer oral agents also offer positive outcomes for patients. Numerous barriers exist, though, for these oral agents, including the unknown long-term efficacy and safety and potential side effects. Despite possible side effects, oral agents provide convenience, ease of use and the elimination of injection/IV administration-site pain. While teriflunomide is no more effective than a number of other agents that are used in the treatment of MS, it has the convenience of once a day oral

administration. Nevertheless, considering its long half-life and the possible side effects during pregnancy, it did not become a popular agent in the treatment of MS. The development of new treatments and drugs is such a dynamic process in the MS field that more and more compounds will arise in the next years.

The knowledge of genetic and environmental aspects is fundamental and a necessary background for further investigations. Undergoing studies aim to find the causes of MS and the factors which determine the disease progression. Eventually, doctors will be able to identify people at high risk for the disease and intervene with treatment at very early stages of MS, perhaps even before symptoms appear.

5. Appendix: Generation of a new AhR reporter mouse

5.1 Starting point

The DRE_Luc mice were generated to work in a bilateral way, allowing us to detect an AhR activation via luminescent signal (Luciferase) as well as via fluorescent one (mCherry). On the contrary, we never managed to detect any mCherry signal neither via FACS, nor via staining nor via 2-photon microscope imaging. Therefore the generation of a new construct and consequently of a new reporter mouse have been an important goal for this laboratory in the last years.

5.2 Monster GFP - a Qiagen helper

Since it has been proved in different ways that the Luciferase signal can be detected, we first tried to substitute CGB99 and mCherry with a different fluorochrome. We purchased a similar construct, commercially available from Qiagen (XRE Reporter), which encodes the Monster GFP gene under the control of a minimal (m)CMV promoter and tandem repeats of the XRE transcriptional response element (TRE). Therefore, a new construct with the initial 12 x DRE repetitions coupled with GFP was created and tested *in vitro,* using GL261, NIH 3T3 and Hela cells. Cells were then treated respectively with DMSO or TCDD (10 nM) 12 h after transfection and imaged in the next 24 h using a confocal microscope from the Microscope Core Facility in DKFZ. Unfortunately, the background signal detected after control treatment (DMSO) was too high and the fluorescence was also less strong than expected (Fig. 5.1B).

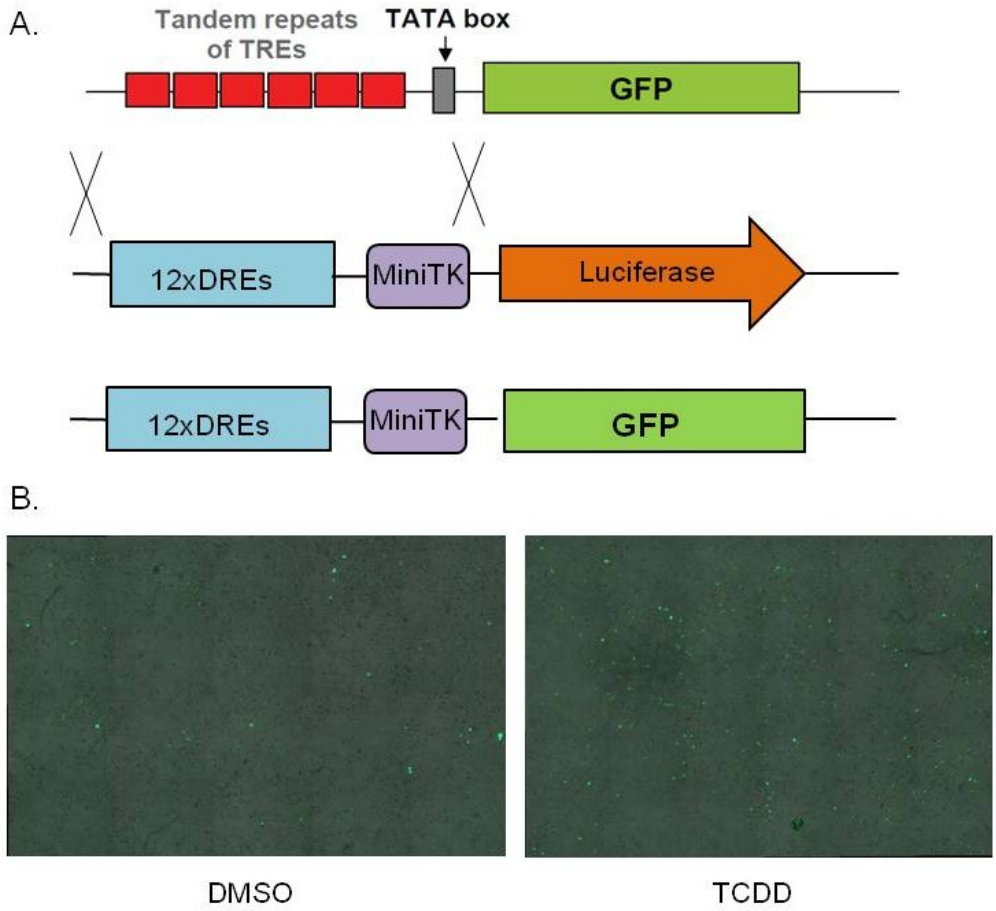

Figure 5.1. A. Schematic representation of the cloning strategy used in order to test the 12x-GFP construct. Briefly, CGB99 luciferase was substituted with a Monster_GFP purchased from Qiagen. B. Representative pictures acquired 24 h after treatment, using a Leica TCS SP5 confocal microscope.

5.3 floxCRe Brainbow – a colourful idea

Due to a high background signal with the Monster_GFP construct, we decided to try a flox-cre system. We therefore cloned the DRE repetitions in a vector kindly offered by Dr. Feyerabend (Cellular Immunology Dept., DKFZ), which contained a iCRE cassette and a stabilizing construct as described elsewhere (124, 125). Cre would be stably transcribed only in case of a DRE activation. The flox-plasmid, Brainbow-1.0, was a kind gift of Prof. Martin-Villalba (Molecular Neurobiology Dept., DKFZ) and it was used to proof Cre functionality. As shown if Fig.5.2A, once a Cre-recombinase enzyme cuts the lox sites, cells change their colour from

red to either blue or yellow. To verify our work, a co-trasfection with the Brainbow-1.0 and our new DRE-Cre construct was performed in different cell lines, cells were then treated with Kynurenic acid (KYNA) or control (NaOH) and images were acquired on a Leica TCS SP5 confocal microscope (Fig.5.2B).

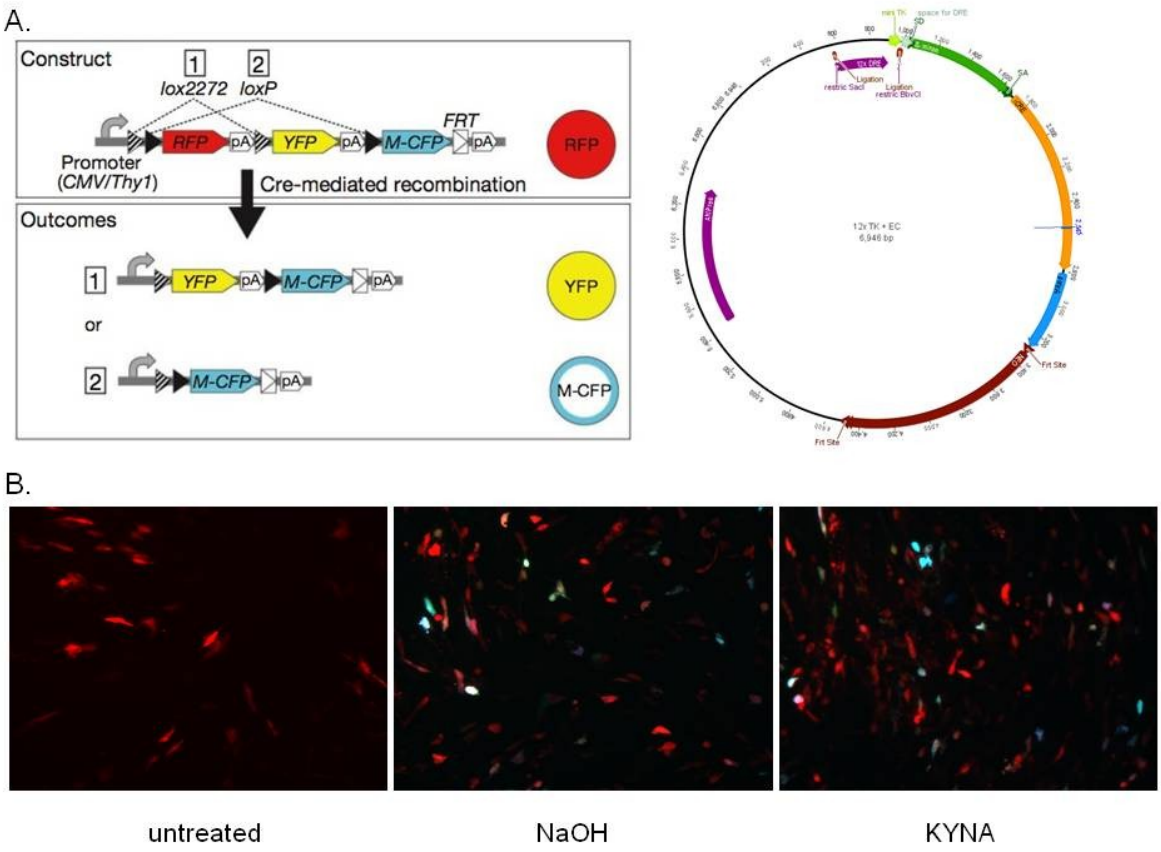

Figure 5.2. Flox-cre strategy. A.. Schematic representation of the Brainbow 1.0 construct and its functionality (Addgene- the non profit plasmid repository). On the left, plasmid map of the cre-plasmid with our additional DRE sequences. B. Pictures of co-transfected cells acquired 24h post treatment, using a Leica TCS SP5 confocal microscope.

Also in this case, the cloning procedure worked, we had high transfection efficacy (as seen in the untreated control), but a DRE activation and therefore an unspecific signal were observed even with control treatment.

5.4 Future plans

The generation of a new reported mouse is still a work in progress in our laboratory. The complexity of this construct is due to different factors. First, AhR is a promiscuous receptor and can be activated by different substances. Furthermore, there are a lot of possible variances we can try. Starting from the DRE sequences, there is a consensus binding site for the AhR, which is not consistently conserved in the DREs constructs available. In order to maintain high expression, we also have to pay attention to CpG motifs, which can be methylated and thus influence the expression level. Furthermore, promoter, cleavage sites, fluorochrome and luciferase can be substituted with different versions of the ones already present in the construct. Different collaborations have been established with Bayer GmbH and with Dr. Stefan Pusch (Neuropathology Dept., DKFZ) to perform *in vitro* tests. Currently, Dr. Edward Green is working on the optimization of the different elements described. In order to move into a murine model, we also established a collaboration with Prof. Richard Harbottle, who suggested to use Scaffold/Matrix Attachment Region (S/MAR) DNA vectors (126). We could then inject the construct into newborn mice and test directly the expression level, before generating a new strain. Once the right setup is found, the new mouse line will be generated in collaboration with the Animal Laboratory Facility of DKFZ, using the new Cas9/CRISPR system (127).

References

1. Miller AE, O´Connor P, Wolinsky JS, Confavreux C, Kappos L, Olsson TP, Truffinet P, Wang L, D'Castro L, Comi G, Freedman MS, Group TMST. 2012. Pre-specified subgroup analyses of a placebo-controlled phase III trial (TEMSO) of oral teriflunomide in relapsing multiple sclerosis. *Mult Scler* 18: 1625–32
2. Ida S. Haussleiter MBaGJ. 2009. Review: Psychopathology in multiple sclerosis: diagnosis, prevalence and treatment. *Therapeutic Advances in Neurological Disorders*
3. Goldenberg MM. 2012. Multiple Sclerosis Review.
4. Weinshenker B. 1994. Natural history of multiple sclerosis *Ann Neurology*
5. Bertolotto A, Malucchi S, Sala A, Orefice G, Carrieri PB, Capobianco M, Milano E, Melis F, Giordana MT. 2002. Differential effects of three interferon betas on neutralizing antibodies in patients with multiple sclerosis: A follow-up study in an independent laboratory. *J Neurol Neurosurg Psychiatry.* 73: 148-53
6. Shirani A, Zhao Y, Karim ME, Evans C, Kingwell E, van der Kop ML, Oger J, Gustafson P, Petkau J, Tremlett H. 2012. Association between use of interferon beta and progression of disability in patients with relapsing-remitting multiple sclerosis. *JAMA* 18
7. Osiri M, Shea B, Robinson V, Suarez-Almazor M, Strand V, Tugwell P, G. W. 2003. Leflunomide for the treatment of rheumatoid arthritis: a systematic review and metaanalysis. *j rheumatology* 30: 1182-90
8. O'Connor P, Wolinsky JS, Confavreux C, Comi G, Kappos L, Olsson TP, Benzerdjeb H, Truffinet P, Wang L, Miller A, Freedman MS. 2011. Randomized trial of oral teriflunomide for relapsing multiple sclerosis. *N Engl J Med* 365: 1293-303
9. Bar-Or A. 2014. Teriflunomide (Aubagio®) for the treatment of multiple sclerosis. *Exp Neurol*
10. Freedman MS, Wolinsky JS, Wamil B, Confavreux C, Comi G, Kappos L, Olsson TP, Miller A, Benzerdjeb H, Li H, Simonson C, O'Connor PW. 2012. Teriflunomide Multiple Sclerosis Trial Group and the MRI Analysis Center. Teriflunomide added to interferon-β in relapsing multiple sclerosis: a randomized phase II trial. *Neurology* 78: 1877–85
11. Korn T TK, Hartung HP, Jung S. 2004. Modulation of effector cell functions in experimental autoimmune encephalomyelitis by leflunomide - mechanisms independent of pyrimidine depletion. *journal of Leukocyte* 76
12. Ringheim G, Lee L, Laws-Ricker L, Delohery T, Liu L, Zhang D, Colletti N, Soos TJ, Schroeder K, Fanelli B, Tian N, Arendt CW, Iglesias-Bregna D, Petty M, Ji Z, Qian G, Gaur R, Weinstock D, Cavallo J, Telsinskas J, McMonagle-Strucko K. 2013. Teriflunomide attenuates immunopathological changes in the Dark Agouti rat model of experimental autoimmune encephalomyelitis. *Front Neurol* 4
13. Merrill JE HS, Pu SF, Liang J, Dang C, Iglesias-Bregna D, Harvey B, Zhu B, McMonagle-Strucko K. 2009. Teriflunomide reduces behavioral, electrophysiological, and histopathological deficits in the Dark Agouti rat

model of experimental autoimmune encephalomyelitis. *Journal of Neurology* 256: 89-103
14. Compston A, Coles A. 2008. Multiple sclerosis. *The Lancet* 372
15. Lublin FDR, Stephen C. 1996. Defining the clinical course of multiple sclerosis. *Neurology* 46: 907-11
16. Oreja-Guevara C, Heinz Wiendl, Bernd C. Kieseier, and , Group LAftNS. 2014. Specific aspects of modern life for people with multiple sclerosis: considerations for the practitioner. *Ther Adv Neurol Disord.* 7
17. Dwosh E, Guimond C, Sadovnick AD. 2003. Reproductive counselling in MS: a guide for healthcare professionals. *Int MS Journal*
18. Baranzini S. 2009. The genetics of autoimmune diseases: a networked perspective. *Curr Opin Immunol* 21
19. Gregory S, Schmidt S, Seth P, Oksenberg JR, Hart J, Prokop A, Caillier SJ, Ban M, Goris A, Barcellos LF, Lincoln R, McCauley JL, Sawcer SJ, Compston DA, Dubois B, Hauser SL, Garcia-Blanco MA, Pericak-Vance MA, Haines JL, Multiple Sclerosis Genetics Group. 2007. Interleukin 7 receptor alpha chain (IL7R) shows allelic and functional association with multiple sclerosis. *Nat Genet*
20. Oksenberg J, Barcellos LF, Cree BA, Baranzini SE, Bugawan TL, Khan O, Lincoln RR, Swerdlin A, Mignot E, Lin L, Goodin D, Erlich HA, Schmidt S, Thomson G, Reich DE, Pericak-Vance MA, Haines JL, Hauser SL. 2004. Mapping multiple sclerosis susceptibility to the HLA-DR locus in African Americans. *am j hum genetic*
21. Vandenbroeck K, Alvarez J, Swaminathan B, Alloza I, Matesanz F, Urcelay E, Comabella M, Alcina A, Fedetz M, Ortiz MA, Izquierdo G, Fernandez O, Rodriguez-Ezpeleta N, Matute C, Caillier S, Arroyo R, Montalban X, Oksenberg JR, Antigüedad A, Aransay A. 2012. A cytokine gene screen uncovers SOCS1 as genetic risk factor for multiple sclerosis. *genes Immunology* 13
22. Schmidt H, Williamson D., Ashley-Koch A. 2007. HLA-DR15 haplotype and multiple sclerosis: A HuGE review. *Am. J. Epidemiol.* 165
23. O'Gorman C, Lucas Robynand Taylor Bruce. 2012. Environmental Risk Factors for Multiple Sclerosis: A Review with a Focus on Molecular Mechanisms. *int j mol sci* 13
24. Burrell A, Handel A., Ramagopalan S., Ebers G., Morahan J. . 2011. Epigenetic mechanisms in multiple sclerosis and the major histocompatibility complex (MHC). *discov med* 11
25. Gale C, Martyn CN. 1995. Migrant studies in multiple sclerosis. *Prog Neurobiol.*
26. O'Gorman C, Robyn Lucas and Bruce Taylor. 2012. Environmental Risk Factors for Multiple Sclerosis: A Review with a Focus on Molecular Mechanisms. *Int j mol sci*
27. Becklund BR, Severson KS, Vang SV, DeLuca HF. 2010. UV radiation suppresses experimental autoimmune encephalomyelitis independent of vitamin D production. *Proc Natl Acad Sci U S A* 107: 6418-23
28. Freedman D, Dosemeci M, Alavanja MC. 2000. Mortality from multiple sclerosis and exposure to residential and occupational solar radiation: a case-control study based on death certificates. *occup environ med* 57
29. Gauvreau GM, Boulet LP, Schmid-Wirlitsch C, Cote J, Duong M, Killian KJ, Milot J, Deschesnes F, Strinich T, Watson RM, Bredenbroker D, O'Byrne

PM. 2011. Roflumilast attenuates allergen-induced inflammation in mild asthmatic subjects. *Respir Res* 12: 140

30. Tremlett H, van der Mei IA, Pittas F, Blizzard L, Paley G, Mesaros D, Woodbaker R, Nunez M, Dwyer T, Taylor BV, Ponsonby AL. 2008. Monthly ambient sunlight, infections and relapse rates in multiple sclerosis. *Neuroepidemiology* 31: 271-9
31. Munger K, Levin LI, Hollis BW, Howard NS, Ascherio A 2006. Serum 25-hydroxyvitamin D levels and risk of multiple sclerosis. . *JAMA* 296: 2832-8
32. Mandia D, Ferraro OE, Nosari G, Montomoli C, Zardini E, Bergamaschi R. 2014. Environmental factors and multiple sclerosis severity: a descriptive study. *Int J Environ Res Public Health.* 11: 6417-32
33. Bove R, Chitnis T. 2014 The role of gender and sex hormones in determining the onset and outcome of multiple sclerosis. *Mult Scler.* 20: 520-6
34. Tzartos J, Khan G, Vossenkamper A, Cruz-Sadaba M, Lonardi S, Sefia E, Meager A, Elia A, Middeldorp JM, Clemens M, Farrell PJ, Giovannoni G, Meier UC. 2012. Association of innate immune activation with latent Epstein-Barr virus in active MS lesions. *Neurology* 78: 15-23
35. Baxter AG. 2007. The origin and application of experimental autoimmune encephalomyelitis. *Nat Rev Immunol* 7: 904-12
36. Wolf A, Kabat EA, Bezer AE. 1947. The pathology of acute disseminated encephalomyelitis produced experimentally in the rhesus monkey and its resemblance to human demyelinating disease. *J Neuropathol Exp Neurol.* 6: 333-57
37. Bettelli E, Pagany M, Weiner HL, Linington C, Sobel RA, Kuchroo VK. 2003. Myelin oligodendrocyte glycoprotein-specific T cell receptor transgenic mice develop spontaneous autoimmune optic neuritis. *J Exp Med.* 197: 1073-81
38. Sommermann TG, O'Neill K, Plas DR, Cahir-McFarland E. 2011. IKKbeta and NF-kappaB transcription govern lymphoma cell survival through AKT-induced plasma membrane trafficking of GLUT1. *Cancer Res* 71: 7291-300
39. Rao PS, Benjamin M. . 2004. Autoimmunity: Methods and Protocols. Experimental Autoimmune Encephalomyelitis. *Methods in Molecular Medicine* 102: 363-75
40. Linthicum DS, J. J. Munoz, A. Blaskett. . 1982. Acute experimental autoimmune encephalomyelitis in mice. I. Adjuvant action of Bordetella pertussis is due to vasoactive amine sensitization and increased vascular permeability of the central nervous system. . *Cell. Immunol.* 73
41. Hofstetter HH, Carey L. Shive and Thomas G. Forsthuber. 2002. Pertussis Toxin Modulates the Immune Response to Neuroantigens Injected in Incomplete Freund's Adjuvant: Induction of Th1 Cells and Experimental Autoimmune Encephalomyelitis in the Presence of High Frequencies of Th2 Cells. *journal of immunology* 169: 117-25
42. Steinman L, Zamvil SS. 2006. How to successfully apply animal studies in experimental allergic encephalomyelitis to research on multiple sclerosis. *Ann Neurol.* 60: 12-21
43. Denica A, Aaron J. Johnsonb, Allan J. Bieberc, Arthur E. Warringtonc, Moses Rodriguezc,d, and Istvan Pirko. 2011. The Relevance of Animal Models in Multiple Sclerosis Research. *pathophysiology* 18

44. Abbott RJ, I Bolderson, P J Gruer, and R C Peatfield. 1987. Immunoreactive IFN-gamma in CSF in neurological disorders. *J Neurol Neurosurg Psychiatry.* 50
45. Fletcher JM, S J Lalor, C M Sweeney, N Tubridy, and K H G Mills. 2010. T cells in multiple sclerosis and experimental autoimmune encephalomyelitis. *Clin Exp Immunol.* 162: 1-11
46. Bettelli E, Das MP, Howard ED, Weiner HL, Sobel RA, Kuchroo VK. 1998. IL-10 is critical in the regulation of autoimmune encephalomyelitis as demonstrated by studies of IL-10- and IL-4-deficient and transgenic mice. *J Immunol.* 161: 3299-306.
47. Stevens E, Bradfield CA. 2008. Immunology: T cells hang in the balance. *Nature* 453: 46-7
48. Takahashi K, Miyake S, Kondo T, Terao K, Hatakenaka M, Hoshimoto S, et al. . 2001. Natural killer type 2 bias in remission of multiple sclerosis. . *J Clin Invest.* 107
49. Almolda B, González B, Castellano B. 2010. Activated microglial cells acquire an immature dendritic cell phenotype and may terminate the immune response in an acute model of EAE. *J Neuroimmunol.* 223: 39-54
50. Matsushita T, Koichi Yanaba, Jean-David Bouaziz, Manabu Fujimoto and Thomas F. Tedder. 2008. Regulatory B cells inhibit EAE initiation in mice while other B cells promote disease progression. *J Clin Invest.* 118: 3420-30
51. Larochelle C, Alvarez JI, Prat A. 2011 How do immune cells overcome the blood-brain barrier in multiple sclerosis? *FEBS Lett.* 585: 3770-80.
52. Miller SD, McMahon, E. J., Schreiner, B. and Bailey, S. L. 2007. Antigen Presentation in the CNS by Myeloid Dendritic Cells Drives Progression of Relapsing Experimental Autoimmune Encephalomyelitis. *Annals of the New York Academy of Sciences* 1103: 179–91.
53. Moser M. 2003. Dendritic cells in immunity and tolerance-do they display opposite functions? *Immunity* 19: 5-8
54. Hackstein H, Thomson AW. 2004. Dendritic cells: emerging pharmacological targets of immunosuppressive drugs. *Nat Rev Immunol* 4: 24-34
55. Chong SZ, Evrard M, Ng LG. 2013. Lights, camera and action: vertebrate skin sets the stage for immune cell interaction with arthropod-vectored pathogens. *Frontiers in Immunology* 4
56. Merad M, Ginhoux F, Collin M. 2008. Origin, homeostasis and function of Langerhans cells and other langerin-expressing dendritic cells. *Nat Rev Immunol.* 8: 935-47
57. Gaiser M, Lämmermann T, Feng X, Igyarto BZ, Kaplan DH, Tessarollo L, Germain RN, Udey MC. 2012. Cancer-associated epithelial cell adhesion molecule (EpCAM; CD326) enables epidermal Langerhans cell motility and migration in vivo. *Proc Natl Acad Sci U S A* 109: E889-97.
58. Sparber FT, C. H. ; Hermann, M; Romani,N and Stoitznera, P. 2010. Langerhans cells and dermal dendritic cells capture protein antigens in the skin: Possible targets for vaccination through the skin. *immunobiology* 215: 770-9
59. Ilkovitch D. 2011. Role of immune-regulatory cells in skin pathology. *J Leukoc Biol. Jan* 89: 41-9.
60. Moffett JR, Namboodiri MAA. 2003. Tryptophan and the immune response. *Immunol Cell Biol* 81: 247-65

61. Munn DH, Sharma MD, Baban B, Harding HP, Zhang Y, Ron D, Mellor AL. 2005. GCN2 kinase in T cells mediates proliferative arrest and anergy induction in response to indoleamine 2,3-dioxygenase. *Immunity* 22: 633-42
62. Opitz C, Litzenburger UM, Opitz U, Sahm F, Ochs K, Lutz C, Wick W, Platten M. 2011. The Indoleamine-2,3-Dioxygenase (IDO) Inhibitor 1-Methyl-D-tryptophan Upregulates IDO1 in Human Cancer Cells. *PLoS One* 6
63. Opitz CA WW, Steinman L, Platten M. 2007. Tryptophan degradation in autoimmune diseases. *Cell Mol Life Sci* 64: 2542-63
64. Platten M, Ho PP, Youssef S, Fontoura P, Garren H, Hur EM, Gupta R, Lee LY, Kidd BA, Robinson WH, Sobel RA, Selley ML, Steinman L. 2005. Treatment of autoimmune neuroinflammation with a synthetic tryptophan metabolite. *Science* 310: 850-5
65. Munn DH, Zhou M, Attwood JT, Bondarev I, Conway SJ, Marshall B, Brown C, Mellor AL. 1998. Prevention of allogeneic fetal rejection by tryptophan catabolism. *Science* 281: 1191-3
66. Nguyen N, Hanieh H, Nakahama T, Kishimoto T. 2013. The roles of aryl hydrocarbon receptor in immune responses. *Int Immunology* 25: 335-43
67. Ho P, Steinman L. 2008. The aryl hydrocarbon receptor: a regulator of Th17 and Treg cell development in disease. *Cell Res.* 18: 605-8
68. Quintana F, Murugaiyan G, Farez MF, Mitsdoerffer M, Tukpah AM, Burns EJ, Weiner HL. 2010. An endogenous aryl hydrocarbon receptor ligand acts on dendritic cells and T cells to suppress experimental autoimmune encephalomyelitis. *Proc Natl Acad Sci U S A* 107
69. Wincent E BJ, Mohammadi Bardbori A, Alsberg T, Luecke S, Rannug U, Rannug A. 2012. Inhibition of cytochrome P4501-dependent clearance of the endogenous agonist FICZ as a mechanism for activation of the aryl hydrocarbon receptor. *Proc Natl Acad Sci U S A.* 109: 4479–84
70. Gonzalez F, Fernandez-Salguero, P. 1998. The aryl hydrocarbon receptor studies using the AHR-null mice. *Drug Metabolism and Disposition* 26: 1194-8
71. Nakahama T, Kimura A, Nguyen NT, Chinen I, Hanieh H, Nohara K, Fujii-Kuriyama Y, Kishimoto T. 2011. Aryl hydrocarbon receptor deficiency in T cells suppresses the development of collagen-induced arthritis. *Proc Natl Acad Sci U S A* 108: 14222-7
72. Lusska A, Shen E, Whitlock JP, Jr. 1993. Protein-DNA interactions at a dioxin-responsive enhancer. Analysis of six bona fide DNA-binding sites for the liganded Ah receptor. *J Biol Chem* 268: 6575-80
73. Wu L, Whitlock JP, Jr. 1992. Mechanism of dioxin action: Ah receptor-mediated increase in promoter accessibility in vivo. *Proc Natl Acad Sci U S A* 89: 4811-5
74. Ramelli G, Fuertes S, Narayan S, Busso N, Acha-Orbea H, So A. 2010. Protease-activated receptor 2 signalling promotes dendritic cell antigen transport and T-cell activation in vivo. *Immunology* 129: 20-7
75. Gerner MY, Mescher MF. 2009. Antigen processing and MHC-II presentation by dermal and tumor-infiltrating dendritic cells. *J Immunol* 182: 2726-37
76. Jensen KB, Driskell RR, Watt FM. 2010. Assaying proliferation and differentiation capacity of stem cells using disaggregated adult mouse epidermis. *Nat Protoc* 5: 898-911

77. Litzenburger UM, Opitz CA, Sahm F, Rauschenbach KJ, Trump S, Winter M, Ott M, Ochs K, Lutz C, Liu X, Anastasov N, Lehmann I, Hofer T, von Deimling A, Wick W, Platten M. 2014. Constitutive IDO expression in human cancer is sustained by an autocrine signaling loop involving IL-6, STAT3 and the AHR. *Oncotarget* 5: 1038-51
78. Carraro G, Albertin G, Forneris M, Nussdorfer GG. 2005. Similar sequence-free amplification of human glyceraldehyde-3-phosphate dehydrogenase for real time RT-PCR applications. *Mol Cell Probes* 19: 181-6
79. Chan V, Charles BG, Tett SE. 2004. Rapid determination of the active leflunomide metabolite A77 1726 in human plasma by high-performance liquid chromatography. *J Chromatography B* 803: 331-5
80. Bergander L, Wahlstrom N, Alsberg T, Bergman J, Rannug A, Rannug U. 2003. Characterization of in vitro metabolites of the aryl hydrocarbon receptor ligand 6-formylindolo[3,2-b]carbazole by liquid chromatography-mass spectrometry and NMR. *Drug Metab Dispos* 31: 233-41
81. Markowitz CE, Spitsin S, Zimmerman V, Jacobs D, Udupa JK, Hooper DC, Koprowski H. 2009. The treatment of multiple sclerosis with inosine. *J Altern Complement Med* 15: 619-25
82. Schwarz T. 2008. 25 years of UV-induced immunosuppression mediated by T cells-from disregarded T suppressor cells to highly respected regulatory T cells. *Photochemistry and Photobiology* 84: 10-8
83. Schwarz A, Maeda A, Schwarz T. 2007. Alteration of the migratory behavior of UV-induced regulatory T cells by tissue-specific dendritic cells. *J Immunol* 178: 877-86
84. Sawcer S, Hellenthal G, Pirinen M, Spencer CC, Patsopoulos NA, et al. 2011. Genetic risk and a primary role for cell-mediated immune mechanisms in multiple sclerosis. *Nature* 476: 214-9
85. Link J, Kockum I, Lorentzen AR, Lie BA, Celius EG, Westerlind H, Schaffer M, Alfredsson L, Olsson T, Brynedal B, Harbo HF, Hillert J. 2012. Importance of human leukocyte antigen (HLA) class I and II alleles on the risk of multiple sclerosis. *PLoS One* 7: e36779
86. Klampfer L. 2014. Vitamin D and colon cancer. *World J Gastrointest Oncol* 6: 430-7
87. Courbebaisse M, Alberti C, Colas S, Prie D, Souberbielle JC, Treluyer JM, Thervet E. 2014. VITamin D supplementation in renAL transplant recipients (VITALE): a prospective, multicentre, double-blind, randomized trial of vitamin D estimating the benefit and safety of vitamin D3 treatment at a dose of 100,000 UI compared with a dose of 12,000 UI in renal transplant recipients: study protocol for a double-blind, randomized, controlled trial. *Trials* 15: 430
88. Nasri H, Behradmanesh S, Maghsoudi AR, Ahmadi A, Nasri P, Rafieian-Kopaei M. 2014. Efficacy of supplementary vitamin D on improvement of glycemic parameters in patients with type 2 diabetes mellitus; a randomized double blind clinical trial. *J Renal Inj Prev* 3: 31-4
89. Platten M, Litzenburger U, Wick W. 2012. The aryl hydrocarbon receptor in tumor immunity. *Oncoimmunology* 1: 396-7
90. Platten M, Wick W, Van den Eynde BJ. 2012. Tryptophan catabolism in cancer: beyond IDO and tryptophan depletion. *Cancer Res* 72: 5435-40
91. Kleinewietfeld M, Hafler DA. 2014. Regulatory T cells in autoimmune neuroinflammation. *Immunol Rev* 259: 231-44

92. Chikahisa S, Sei H. 2011. The role of ATP in sleep regulation. *Front Neurol* 2: 87
93. Khakh BS, North RA. 2006. P2X receptors as cell-surface ATP sensors in health and disease. *Nature* 442: 527-32
94. Salmi M, Jalkanen S. 2005. Cell-surface enzymes in control of leukocyte trafficking. *Nat Rev Immunol* 5: 760-71
95. Schnurr M, Toy T, Shin A, Wagner M, Cebon J, Maraskovsky E. 2005. Extracellular nucleotide signaling by P2 receptors inhibits IL-12 and enhances IL-23 expression in human dendritic cells: a novel role for the cAMP pathway. *Blood* 105: 1582-9
96. Atarashi K, Nishimura J, Shima T, Umesaki Y, Yamamoto M, Onoue M, Yagita H, Ishii N, Evans R, Honda K, Takeda K. 2008. ATP drives lamina propria T(H)17 cell differentiation. *Nature* 455: 808-12
97. Gudkov SV, Shtarkman IN, Smirnova VS, Chernikov AV, Bruskov VI. 2006. Guanosine and inosine display antioxidant activity, protect DNA in vitro from oxidative damage induced by reactive oxygen species, and serve as radioprotectors in mice. *Radiat Res* 165: 538-45
98. Buckley S, Barsky L, Weinberg K, Warburton D. 2005. In vivo inosine protects alveolar epithelial type 2 cells against hyperoxia-induced DNA damage through MAP kinase signaling. *Am J Physiol Lung Cell Mol Physiol* 288: L569-75
99. Breuer J, Schwab N, Schneider-Hohendorf T, Marziniak M, Mohan H, Bhatia U, Gross CC, Clausen BE, Weishaupt C, Luger TA, Meuth SG, Loser K, Wiendl H. 2014. Ultraviolet B light attenuates the systemic immune response in central nervous system autoimmunity. *Ann Neurol* 75: 739-58
100. Maeda A, Beissert S, Schwarz T, Schwarz A. 2008. Phenotypic and functional characterization of ultraviolet radiation-induced regulatory T cells. *J Immunol* 180: 3065-71
101. Fu S, Yopp AC, Mao X, Chen D, Zhang N, Chen D, Mao M, Ding Y, Bromberg JS. 2004. CD4+ CD25+ CD62+ T-regulatory cell subset has optimal suppressive and proliferative potential. *Am J Transplant* 4: 65-78
102. Zhang X, Chang Li X, Xiao X, Sun R, Tian Z, Wei H. 2013. CD4(+)CD62L(+) central memory T cells can be converted to Foxp3(+) T cells. *PLoS One* 8: e77322
103. Weill FS, Cela EM, Ferrari A, Paz ML, Leoni J, Gonzalez Maglio DH. 2011. Skin exposure to chronic but not acute UV radiation affects peripheral T-cell function. *J Toxicol Environ Health A* 74: 838-47
104. Goudy KS, Johnson MC, Garland A, Li C, Samulski RJ, Wang B, Tisch R. 2011. Reduced IL-2 expression in NOD mice leads to a temporal increase in CD62Llo FoxP3+ CD4+ T cells with limited suppressor activity. *Eur J Immunol* 41: 1480-90
105. Beissert S, Schwarz A, Schwarz T. 2006. Regulatory T cells. *J Invest Dermatol* 126: 15-24
106. Schwarz A, Stander S, Berneburg M, Bohm M, Kulms D, van Steeg H, Grosse-Heitmeyer K, Krutmann J, Schwarz T. 2002. Interleukin-12 suppresses ultraviolet radiation-induced apoptosis by inducing DNA repair. *Nat Cell Biol* 4: 26-31
107. Majewski S, Jantschitsch C, Maeda A, Schwarz T, Schwarz A. 2010. IL-23 antagonizes UVR-induced immunosuppression through two mechanisms: reduction of UVR-induced DNA damage and inhibition of UVR-induced regulatory T cells. *J Invest Dermatol* 130: 554-62

108. Werth VP, Bashir MM, Zhang W. 2003. IL-12 completely blocks ultraviolet-induced secretion of tumor necrosis factor alpha from cultured skin fibroblasts and keratinocytes. *J Invest Dermatol* 120: 116-22
109. Rudra D, Warner JR. 2004. What better measure than ribosome synthesis? *Genes Dev* 18: 2431-6
110. Takao J, Ariizumi K, Dougherty, II, Cruz PD, Jr. 2002. Genomic scale analysis of the human keratinocyte response to broad-band ultraviolet-B irradiation. *Photodermatol Photoimmunol Photomed* 18: 5-13
111. Lee KM, Lee JG, Seo EY, Lee WH, Nam YH, Yang JM, Kee SH, Seo YJ, Park JK, Kim CD, Lee JH. 2005. Analysis of genes responding to ultraviolet B irradiation of HaCaT keratinocytes using a cDNA microarray. *Br J Dermatol* 152: 52-9
112. Rieger KE, Chu G. 2004. Portrait of transcriptional responses to ultraviolet and ionizing radiation in human cells. *Nucleic Acids Res* 32: 4786-803
113. Bessede A, Gargaro M, Pallotta MT, Matino D, Servillo G, Brunacci C, Bicciato S, Mazza EM, Macchiarulo A, Vacca C, Iannitti R, Tissi L, Volpi C, Belladonna ML, Orabona C, Bianchi R, Lanz TV, Platten M, Della Fazia MA, Piobbico D, Zelante T, Funakoshi H, Nakamura T, Gilot D, Denison MS, Guillemin GJ, DuHadaway JB, Prendergast GC, Metz R, Geffard M, Boon L, Pirro M, Iorio A, Veyret B, Romani L, Grohmann U, Fallarino F, Puccetti P. 2014. Aryl hydrocarbon receptor control of a disease tolerance defence pathway. *Nature* 511: 184-90
114. Opitz CA, Litzenburger UM, Sahm F, Ott M, Tritschler I, Trump S, Schumacher T, Jestaedt L, Schrenk D, Weller M, Jugold M, Guillemin GJ, Miller CL, Lutz C, Radlwimmer B, Lehmann I, von Deimling A, Wick W, Platten M. 2011. An endogenous tumour-promoting ligand of the human aryl hydrocarbon receptor. *Nature* 478: 197-203
115. Pilotte L, Larrieu P, Stroobant V, Colau D, Dolusic E, Frederick R, De Plaen E, Uyttenhove C, Wouters J, Masereel B, Van den Eynde BJ. 2012. Reversal of tumoral immune resistance by inhibition of tryptophan 2,3-dioxygenase. *Proc Natl Acad Sci U S A* 109: 2497-502
116. Quintana FJ, Basso AS, Iglesias AH, Korn T, Farez MF, Bettelli E, Caccamo M, Oukka M, Weiner HL. 2008. Control of T(reg) and T(H)17 cell differentiation by the aryl hydrocarbon receptor. *Nature* 453: 65-71
117. Veldhoen M, Hirota K, Westendorf AM, Buer J, Dumoutier L, Renauld JC, Stockinger B. 2008. The aryl hydrocarbon receptor links TH17-cell-mediated autoimmunity to environmental toxins. *Nature* 453: 106-9
118. Guyot E, Chevallier A, Barouki R, Coumoul X. 2013. The AhR twist: ligand-dependent AhR signaling and pharmaco-toxicological implications. *Drug Discov Today* 18: 479-86
119. O'Donnell EF SK, Koch DC, Kopparapu PR, Farrer D, Bisson WH, Mathew LK, Sengupta S, Kerkvliet NI, Tanguay RL, Kolluri SK. 2010. The anti-inflammatory drug leflunomide is an agonist of the aryl hydrocarbon receptor. *PLoS One*
120. Baban B, Liu JY, Mozaffari MS. 2012. Aryl hydrocarbon receptor agonist, leflunomide, protects the ischemic-reperfused kidney: role of Tregs and stem cells. *Am J Physiol Regul Integr Comp Physiol* 303: R1136-46
121. Lindsey S JJ, Woulfe D, Papoutsakis ET. 2014. Platelets from mice lacking the aryl hydrocarbon receptor exhibit defective collagen-dependent signaling. *j Thromb Haemost.* 12: 383-94

122. Oh J, O'Connor PW. 2014. Teriflunomide in the treatment of multiple sclerosis: current evidence and future prospects. *Ther Adv Neurol Disord* 7: 239-52
123. Warnke C, Meyer zu Hörste G, Hartung HP, Stüve O, Kieseier BC. 2009. Review of teriflunomide and its potential in the treatment of multiple sclerosis. *Neuropsychiatr Dis Treat* 5: 333-40
124. Schlenner SM, Madan V, Busch K, Tietz A, Laufle C, Costa C, Blum C, Fehling HJ, Rodewald HR. 2010. Fate mapping reveals separate origins of T cells and myeloid lineages in the thymus. *Immunity* 32: 426-36
125. Luche H, Nageswara Rao T, Kumar S, Tasdogan A, Beckel F, Blum C, Martins VC, Rodewald HR, Fehling HJ. 2013. In vivo fate mapping identifies pre-TCRalpha expression as an intra- and extrathymic, but not prethymic, marker of T lymphopoiesis. *J Exp Med* 210: 699-714
126. Wong SP, Harbottle RP. 2013. Genetic modification of dividing cells using episomally maintained S/MAR DNA vectors. *Mol Ther Nucleic Acids* 2: e115
127. Wang H, Yang H, Shivalila CS, Dawlaty MM, Cheng AW, Zhang F, Jaenisch R. 2013. One-step generation of mice carrying mutations in multiple genes by CRISPR/Cas-mediated genome engineering. *Cell* 153: 910-8

List of Abbreviations

Ab	Antibody
ACK	Ammonium-Chloride-Potassium Lysing Buffer
AhR	Aryl Hydrocarbon Receptor
ALT	Alanine transaminase
APC	Allophycocyanin
APCs	Antigen presenting cells
ATP	Adenosine triphosphate
B cell	Bursa of Fabricius-derived lymphocyte
BBB	Blood-brain-barrier
CFA	Freund's adjuvant (CFA)
CHS	contact hypersensitivity
CMV	Cytomegalovirus
CNS	Central nervous system
ConA	Concanavalin A
CSF	Cerebrospinal fluid
Cyp1A1	Cytocrome P 450, family 1, member A1
DCs	Dendritic cells
dH_2O	Distilled water
DHODH	Dihydroorotate dehydrogenase
DMSO	Dimethyl sulfoxide

DNA	Deoxyribonucleic acid
DRE	Dioxin responsive elements
EAE	Experimental autoimmune encephalomyelitis
EBV	Epstein-Barr-virus
EDTA	Ethylenediaminetetraacetic acid
ELISA	Enzyme Linked Immunosorbent Assay
FACS	Fluorescence-activated cell sorting
FBS	Fetal bovine serum
FDA	Food and Drug Administration
FICZ	6-Formylindolo(3,2-b)carbazole
FITC	Fluorescein isothiocyanate
FoxP3	Forkhead box P3
GAPDH	Glyceraldehyde 3-phosphate dehydrogenase
GCN2	General control non-derepressible 2
GFP	Green fluorescent protein
H_2O_2	Hydrogen peroxide
HLA	Human leukocyte antigen
HPLC	High performance liquid chromatography-mass spectrometry
i.p.	Intraperitoneal
IC_{50}	Half maximal inhibitory concentration
IDO	indoleamine 2,3-dioxygenase
IFNγ	Interferon-γ
IL	Interleukin

KYNA	Kynurenic Acid
LCs	Langerhans cells
LNs	Lymph nodes
MACS	Magnetic-activated cell sorting
MBP	Myelin basic protein
MC	Methylcellulose
MHC	Major histocompatibility complex
MOG	Myelin oligodendrocyte glycoprotein
MRI	magnetic resonance imaging
MS	Multiple sclerosis
NAD^+	Nicotinamide adenine dinucleotide
NaOH	Sodium hydroxide
NK	Natural killer
o/n	Overnight
p.i.	Post-immunisation
PBS	Phosphate-buffered saline
PCR	Polymerase chain reaction
PE	Phycoerythrin
PerCP	Peridinin chlorophyll protein
PLP	Proteolipid protein
PPMS	Primary-progressive MS
PRMS	Progressive-relapsing MS
PToX	Pertussis toxin

RNA	Ribonucleic acid
ROI	Region of Interest
RPMI	Roswell Park Memorial Institute
RRMS	Relapsing-remitting multiple sclerosis
s.c.	Subcutaneous
S.E.M.	Standard error of the mean
SLE	Systemic lupus erythematosus
SPMS	Secondary progressive MS
T cell	Thymus-derived lymphocyte
TCDD	2,3,7,8-Tetrachlorodibenzo-p-dioxin
TCR	T cell receptor
TDO	Tryptophan dioxygenase
TER	Teriflunomide
TER	Teriflunomide
TGFα	Transforming growth factor-α
TGFβ	Transforming growth factor-β
T_H0	Naïve CD4+ T cells
T_H1	T helper type 1
T_H17	T helper type 17
TMEV	Theiler's Murine Encephalomyelitis Virus
TNFα	Tumour necrosis factor-α
$T_{reg(s)}$	Regulatory T cell(s)
tRNA	Transfer ribonucleic acid

Trp	Tryptophan
UV(B)	Ultraviolet radiation type B
wt	Wild-type